

# **Wall Slip of Polydisperse Linear Polymer Melts**

Seyed Mostafa Sabzevari

A Thesis  
In the Department  
of  
Mechanical and Industrial Engineering

Presented in Partial Fulfillment of the Requirements  
For the Degree of  
Doctor of Philosophy (Mechanical Engineering) at  
Concordia University  
Montreal, Quebec, Canada

August 2015

Copyright © Seyed Mostafa Sabzevari, 2015

**CONCORDIA UNIVERSITY**  
**SCHOOL OF GRADUATE STUDIES**

This is to certify that the thesis prepared

By: **Seyed Mostafa Sabzevari**

Entitled: **Wall Slip of Polydisperse Linear Polymer Melts**

and submitted in partial fulfillment of the requirements for the degree of

**Doctor of Philosophy (Mechanical Engineering)**

Complies with the regulations of the University and meets the accepted standards with respect to originality and quality.

Signed by final examining committee

_____	Chair
_____ Dr. Lynden Archer _____	External Examiner
_____ Dr. Nick Vigilio _____	External to Program
_____ Dr. Lyes Kadem _____	Examiner
_____ Dr. Martin Pugh _____	Examiner
_____ Dr. Paula M. Wood-Adams _____	Thesis Supervisor

Approved by

\_\_\_\_\_  
Chair of Department or Graduate Program Director

\_\_\_\_\_ 2015

\_\_\_\_\_ Dean of Faculty

# ABSTRACT

## Wall Slip of Polydisperse Linear Polymer Melts

Seyed Mostafa Sabzevari, Ph.D.

Concordia University, 2015

Polymeric products are an integrated component of our everyday life and the importance of optimizing manufacturing processes for higher output and lower waste is a necessity. A crucial factor here is our knowledge of the liquid-solid boundary condition in the flow of molten polymers. In contrast to small molecule fluids, polymer melts slip on solid substrates sometimes to significant extents. Polymer slip has been under investigation over the past few decades, however detailed knowledge of the extent of slip of polydisperse polymers typical of industrial applications has not yet been fully achieved. This study brings into focus the effect of molecular weight distribution on polymer slip.

We perform a systematic study of the effect of molecular weight distribution on polymer slip by examining binary and ternary mixtures of monodisperse polymers. Three different experimental techniques are used to cover different aspects of our objective.

Steady state slip of polybutadiene (PBD) mixtures on a silicon wafer in planar Couette flow is first examined. Using a microfluidic geometry, confocal microscopy and particle image velocimetry are used to measure unidirectional velocities across the flow channel. It is shown that slip dynamics at the onset and within the transition to the strong slip regime are significantly affected by the incorporation of weakly entangled polymer chains. Both size and content of short chains are substantially important in slip dynamics. Among ternary mixtures with a fixed weight average molecular weight ( $M_w$ ), those with the minimum content of intermediate chains (the lowest number average molecular weight,  $M_n$ ) exhibit the largest slip lengths. This means that a binary mixture of short and long chains of two distinct separate molar modes are most effective in promoting slip.

Polymer slip has long been related to the surface enrichment of short chains. Enrichment theories include thermodynamic segregation mechanisms as well as the shear induced fractionation mechanism. In line with our previous experiments, we examine the

short chain surface enrichment of polybutadiene mixtures after strong slip in simple shear. After strong slip, a hazy debris of polymer remains behind on the steel substrates. Experiments show that the debris from all binary and ternary polybutadiene mixtures undergoing strong slip is enriched with the short chain constituent. We develop a simple disentanglement induced enrichment model in agreement with previous slip theories that predicts our experimental data very well.

We also examine slip of thin polystyrene (PS) films dewetting from fluorinated and silanized silicon wafers. We first show that the sacrificial mica substrate, used very often in a two-step film preparation procedure in thin film studies, significantly affects the polymer slip length after the film is transferred onto a nonwetting substrate. We show that a highly entangled monodisperse PS exhibits different flow dynamics and slip length depending on whether its air or buried interface with mica is placed on the nonwetting substrate, and whether the film has been pre-annealed. We find that the buried interface shows reduced slip length compared to the air interface. The discrepancy between the two interfaces is molecular weight dependent and undetectable in unentangled polymers.

We next show that slip of highly entangled PS chains on nonwetting substrates is affected by the incorporation of short chains of molecular weights,  $M$ , below the polymer critical molecular weight,  $M_c$ :  $M < M_c$ . Among PS mixtures of the same  $M_w$  those with a higher content of short chains (lower  $M_n$ ) are likely to exhibit larger slip lengths. We show that such slip enhancement effect in binary mixtures of long and short chains is only effective when the long chain content,  $\phi_L$ , is dominant ( $\phi_L > 0.5$ ).

While the polymer slip mechanism on different substrates can be different depending on the density of adsorbed chains – disentanglement versus detachment – the consequence of the incorporation of short chains seems to be similar, i.e., slip is promoted when small amounts of short chains are added to a highly entangled polymer. In this aspect, both size and content of short chains matter. This finding has practical implications in polymer processing and is useful for developing new slip models. Furthermore, the disentanglement induced surface enrichment phenomenon is a new approach in the investigation of extrudate surface instabilities and die drool.

Dedicated to

*Sima and Taranom*

## Acknowledgements

I would like to express my deepest appreciation to my supervisor Dr. Paula Wood-Adams for her continuous guidance, generosity, support, and kindness. Paula has given me brilliant comments and ideas throughout this entire research. This thesis have not been possible without her remarkable support and guidance.

Thanks to colleagues and staffs Imam Khadimul, Vahid Shaygan, Sina Chaeichian, Ehsan Rezabeigi, Heng Wang, Dan Juras, and Henry Szczawinski at Concordia University who trained me on certain experimental setups and made a friendly environment for work.

Special thanks to Dr. Itai Cohen, Dr. Lynden Archer, Rajesh Mallavajula, Jesse Silverberg, Brain Leahy, Jeanette Nguyen, Lena Bartell, Xiang Cheng and Yen-Chih for their kind hospitality during my stay at Cornell University in Ithaca.

I would like to thank Dr. Satu Strandman, Dr. Julian Zhu, Mohammad Savoji, and Pierre Tremblay at Polytechnique de Montreal who helped me on my GPC experiments.

Many thanks to Dr. Karin Jacobs, Dr. Joshua McGraw, Sabrina Haefner, Antoine Bridet and all other friends in Dr. Jacobs' lab at Saarland University who trained and helped me on my dewetting experiments and provided me with a friendly environment during my stay in Saarbrücken.

Thanks to my dear friends at Concordia University Ali and Mohamadreza Gholizadeh, Miad Moaref, Hamid R. Hooshangi, S. Sajjad Mirvalad, and S. Javad Mirvalad who provided me mental support during this period.

My special appreciation goes to my lovely wife Sima who supportively stood by me during this entire thesis and provided me with a warm and delightful environment. And the last, not the least, thanks to my parents and family back in Iran for their continuous support during the long far-away years...

## Contributions of Authors

The results of this work are presented in chapters 3 to 7. Chapters 3 and 4 are presented in form of unaltered published journal articles. Chapter 6 is a manuscript that has been submitted for journal publication. Chapters 5 and 7 are under preparation to be submitted for journal publication.

**Chapter 3:** ‘Wall Slip of Bidisperse Linear Polymer Melts’, S. Mostafa Sabzevari, Itai Cohen, and Paula M. Wood-Adams, *Macromolecules*, 2014, 47, 3154–3160.

All experimental work, data analysis, and manuscript write-up was done by the author S. Mostafa Sabzevari. Dr. Itai Cohen allowed the author to access his laboratory in the physics department at Cornell University for conducting velocimetry experiments. He also mentored the author during experiments and revised the article before submission. Dr. Paula Wood-Adams mentored and supervised the author throughout the entire research. She revised and modified the article before submission.

**Chapter 4:** ‘Wall Slip of Tridisperse Polymer Melts and the Effect of Un-Entangled versus Weakly-Entangled Chains’, S. Mostafa Sabzevari, Itai Cohen, and Paula M. Wood-Adams, *Macromolecules*, 2014, 47, 8033–8040.

All experimental work, data analysis, and manuscript write-up was done by the author S. Mostafa Sabzevari. Dr. Itai Cohen allowed the author to access his laboratory in the physics department at Cornell University for conducting velocimetry experiments. He also mentored the author during experiments and revised the article before submission. Dr. Paula Wood-Adams mentored and supervised the author throughout the entire research. She revised and modified the article before submission.

**Chapter 5:** ‘Disentanglement Induced Surface Enrichment of Short Polymer Chains in Simple Shear Flow with Slip’, S. Mostafa Sabzevari, Paula M. Wood-Adams; *under preparation for journal publication*.

All rheometry experiments, data analysis, and manuscript write-up was done by the author S. Mostafa Sabzevari. GPC experiments were outsourced. Dr. Paula Wood-Adams mentored and supervised the author throughout the entire research. She revised and modified the article before submission.

**Chapter 6:** ‘Sacrificial Mica Substrates Influence the Slip Boundary Condition of Dewetting Polymer Films’, S. Mostafa Sabzevari, Joshua D. McGraw, Karin Jacobs, Paula M. Wood-Adams; *under review in Polymer*.

All experimental works, data analysis, and manuscript write-up was done by the author S. Mostafa Sabzevari. Dr. Joshua McGraw trained and supervised the author during experiments and data analysis. He revised and formatted the article before submission. Dr. Karin Jacobs allowed the author to access her laboratory in the experimental physics department at Saarland University for conducting dewetting and atomic force microscopy experiments. She revised the article before submission. Dr. Paula Wood-Adams mentored and supervised the author throughout the entire research. She revised and modified the article before submission.

**Chapter 7:** ‘Effect of Short Chains on Slip of Thin Polystyrene Films on Nonwetting Substrates’, S. Mostafa Sabzevari, Joshua D. McGraw, Karin Jacobs, Paula M. Wood-Adams; *under preparation for journal publication*.

All experimental works, data analysis, and manuscript write-up was done by the author S. Mostafa Sabzevari. Dr. Joshua McGraw trained and supervised the author during experiments and data analysis. He revised and formatted the article before submission. Dr. Karin Jacobs allowed the author to access her laboratory in the experimental physics department at Saarland University for conducting dewetting and atomic force microscopy experiments. She revised the article before submission. Dr. Paula Wood-Adams mentored

and supervised the author throughout the entire research. She revised and modified the article before submission.

# Table of Contents

List of Figures .....	xiv
List of Tables .....	xix
Abbreviation .....	xx
Nomenclature .....	xxii
1. Chapter 1 .....	1
1.1. Introduction .....	1
1.2. Thesis Structure .....	3
2. Chapter 2 .....	5
Literature Review .....	5
2.1. Introduction .....	5
2.2. Slip and Polymer Flow Instabilities .....	6
2.3. Slip Characterization .....	8
2.4. Slip Mechanisms .....	10
2.5. Critical Factors Influencing Polymer Wall Slip .....	12
2.5.1. Effect of Substrate Properties on Polymer Wall Slip .....	13
2.5.1.1. Ideal Surfaces .....	13
2.5.1.2. Semi-ideal Surfaces .....	14
2.5.1.3. Non-ideal Surfaces .....	16
2.5.1.4. Adsorbed Chains versus End-grafted Chains .....	16
2.5.1.5. Surface Roughness .....	17
2.5.1.6. Substrate Composition: Low- versus High-energy Surfaces .....	18
2.5.2. Effect of Polymer Characteristics on Wall Slip .....	19

2.5.2.1. Low Molecular Weight Polymers, Branched Polymers, and Polymer Solutions .....	20
2.5.2.2. Critical Stress Likely to be Independent of Molecular Weight .....	20
2.5.2.3. Slip Length Increases with Molecular Weight .....	20
2.5.2.4. Polymer Molecular Weight Distribution .....	21
2.6. Wall Slip and Surface Enrichment of Short Chains in Polydisperse Polymers .....	23
2.7. Slip in Dewetting of Thin Polymer Films .....	26
2.7.1. Dewetting Mechanisms .....	27
2.7.2. Dewetting Dynamics .....	28
2.7.3. Rim Morphology of Dewetting Hole/Front.....	30
2.8. Theoretical Disentanglement Models Predicting Slip.....	33
2.8.1. Brochard and de Gennes Scaling Model .....	33
2.8.2. Later Disentanglement Slip Models .....	37
2.8.3. Limitations of Slip Models.....	41
3. Chapter 3 .....	43
Wall Slip of Bidisperse Linear Polymer Melts: .....	43
3.1. Introduction .....	44
3.2. Materials and Experiments.....	46
3.3. Results and Discussion.....	50
3.4. Conclusion.....	60
4. Chapter 4.....	62
Wall Slip of Tridisperse Polymer Melts and the Effect of Un-Entangled versus Weakly-Entangled Chains: .....	62
4.1. Introduction .....	63
4.2. Materials and Experiments.....	66

4.3. Results and Discussion.....	69
4.4. Conclusion.....	79
5. Chapter 5.....	81
Disentanglement Induced Surface Enrichment of Short Polymer Chains in Simple Shear Flow with Slip.....	81
5.1. Introduction.....	82
5.2. Materials and Experiments.....	85
5.3. Results and Discussions.....	86
5.4. Conclusion.....	92
6. Chapter 6.....	93
Sacrificial Mica Substrates Influence the Slip Boundary Condition of Dewetting Polymer Films.....	93
6.1. Introduction.....	94
6.2. Materials and Experiments.....	96
6.3. Results and Discussion.....	98
6.4. Conclusion.....	105
7. Chapter 7.....	106
Effect of Short Chains on Slip of Thin Polystyrene Films on Non-wetting Substrates.....	106
7.1. Introduction.....	107
7.2. Materials and Experiments.....	109
7.3. Results and Discussion.....	111
7.4. Conclusion.....	120
8. Chapter 8.....	122
Conclusions and Contributions.....	122

8.1. Conclusions .....	122
8.2. Contributions .....	126
References .....	128
Appendix A .....	133
A.1. Plane parallelism in Couette flow shear cell .....	133
A.2. Velocity profiles of PBD mixtures at different shear rates .....	133
Appendix B .....	142
B.1. Debris collection .....	142
B.2. Additional examples of the molecular weight distribution (MWD) of the debris versus bulk samples for bimodal mixtures of PBD(19k) and PBD(277k) .....	142
Appendix C .....	146
C.1. Fitting models for calculation of $b$ .....	146
C.2. Additional evidence of discrepancies between the air and buried interfaces for high molecular weight polymers .....	148
C.3. Rim profiles of ternary PS mixtures examined in Chapter 7 .....	149

## List of Figures

Figure 2.1. A schematic of different boundary conditions that may occur during simple shear (partially adapted from ref [25]).	9
Figure 2.2. A schematic of the three slip regimes in a log-log plot of slip velocity versus shear rate (adapted from ref [21]).	15
Figure 2.3. Optical image of several dewetting holes of a thin film (200 nm) of PS on Teflon-coated (AF2400) silicon substrate at 150 °C after 30 minutes.	27
Figure 2.4. Evolution of a dewetting hole of a thin film (200 nm) of PS on Teflon-coated (AF 2400) silicon substrate at 150 °C.	29
Figure 2.5. AFM micrograph of a portion of a dewetting hole of PS: $M_w = 490$ kg/mol on AF 2400 coated silicon wafer; vertical view (top) and isotropic view (bottom).	31
Figure 2.6. Rim height profiles of dewetting holes ( $\sim 24$ $\mu\text{m}$ ) between two monodisperse PSs: PS(28k) with $M_w = 28$ kg/mol and PS(490k) with $M_w = 490$ kg/mol placed on AF 2400. The profiles were characterized by AFM.	31
Figure 2.7. (a) A schematic of slip velocity versus surface shear stress for a melt flowing on a grafted surface and (b) slip length versus slip velocity (Adapted from ref [29]).	36
Figure 3.1. Velocity of nanoparticles $V(z)$ of binary sample L74 at different values of $z$ as labeled (units are in $\mu\text{m}$ ) as a function of time $t$ . Steady-state velocity was ensured at long times. Dashed lines indicate steady-state values.	49
Figure 3.2. Normalized velocity profiles of binary sample L74 at nominal shear rates $\dot{\gamma}_n$ as labeled (units are in $\text{s}^{-1}$ ). The vertical axis is the distance $z$ from the stationary plate (silicon wafer) normalized by the gap $h$ and the horizontal axis is the velocity of nanoparticles $V(z)$ normalized by the moving plate (cover glass, $z = 1$ ) velocity $V_0$ .	49
Figure 3.3. Slip velocity of L90 on cover glass $v_s^b$ versus moving plate velocity $V_0$ . Solid circles are experimental data whereas solid diamonds are estimated data-points by interpolation/extrapolation through linear regression (dashed line).	50
Figure 3.4. a) Complex viscosity $\eta^*(\omega)$ , b) storage modulus $G'(\omega)$ , and c) loss modulus $G''(\omega)$ as a function of angular frequency $\omega$ of binary 4k/195k PBD mixtures.	52
Figure 3.5. Slip velocity vs. shear stress of monodisperse PBDs on silicon wafer. The dashed line is an extrapolation of the weak slip regime of the 195k sample to guide the reader's eye.	53
Figure 3.6. Friction coefficient vs. stress of monodisperse PBDs (solid symbols) and their binary mixtures (open symbols) on silicon wafer.	54

Figure 3.7. Slip velocity of binary 195k/4k PBDs (solid symbols) and their monodisperse constituents (open symbols) versus shear stress. The dashed line is an extrapolation of the slip of the 4k sample to guide the reader’s eye.....	55
Figure 3.8. Friction coefficient versus true shear rate of binary 195k/4k PBDs (solid symbols) and their monodisperse constituents (open symbols).....	57
Figure 3.9. Slip length of binary 195k/4k PBDs versus shear stress.....	59
Figure 3.10. Slip length of binary 195k/4k PBDs versus weight fraction of 195k chains.....	59
Figure 4.1. GPC chromatograms of two ternary PBD samples: W_Mn_17 containing 4k, 88k, and 195k (solid line) and U_Mn_5 containing 1k, 88k, and 195k (dashed line).....	67
Figure 4.2. Complex viscosity versus angular frequency of W_Mn_17 and W_Mn_61 compared to U_Mn_5 and U_Mn_40.....	69
Figure 4.3. Linear viscoelastic properties, storage $G'$ and loss $G''$ moduli, as a function of the angular frequency $\omega$ of samples with different $M_n$ as labeled (kg/mol): (a-b) set W containing 4k chains, and (c-d) set U containing 1k chains.....	70
Figure 4.4. Slip velocity as a function of shear stress of ternary PBDs containing weakly-entangled chains on silicon wafer (set W). The data for the binary sample W_Mn_14, containing 4k and 195k chains only, from Ref. 43 are included for the sake of comparison.....	71
Figure 4.5. Friction coefficient versus shear stress (a) and slip velocity (b) of ternary PBDs containing weakly-entangled chains over silicon wafer (set W) calculated from the data in Figure 4.4 using $k_f = \sigma/v_s$ . The data for the binary sample W_Mn_14, containing 4k and 195k chains only, are reproduced from Ref. [108] and included for the sake of comparison between ternary and binary samples.....	74
Figure 4.6. Slip velocity as a function of shear stress of ternary PBDs containing un-entangled chains on silicon wafer (set U).....	75
Figure 4.7. Friction coefficient versus shear stress (a) and slip velocity (b) of ternary PBDs containing un-entangled chains on silicon wafer (set U).....	76
Figure 4.8. Slip velocity versus shear stress of W_Mn_17 and W_Mn_61 compared to U_Mn_5 and U_Mn_40.....	77
Figure 5.1. (a) Bulk and debris material after strong slip of PBD and (b) schematic of polymer slip in the SPR shear cell.....	86
Figure 5.2. GPC chromatograms of bulk and debris samples of binary (a-d) and ternary (e and f) PBD mixtures.....	87

Figure 5.3. Schematic of the simple disentanglement induced enrichment model.....	90
Figure 5.4. Concentration of short chains in the debris layer plotted versus that of the bulk. Experimental data are compared to model predictions: (a) binary mixtures and (b) ternary mixtures. The solid line represents bulk composition. ....	91
Figure 6.1. Schematic of the sample preparation undertaken in this study. A polystyrene (PS) film is spin coated onto a mica substrate. Annealing above the polymer glass transition, $T_g$ , results in differences between the air/PS interface (i-aPS) and the mica/PS interface (i-mPS). After placing these interfaces in contact with a hydrophobic substrate (DTS schematically indicated, native SiO <sub>2</sub> layer not shown), it is possible to detect differences between i-aPS and i-mPS through dewetting of the polymer film on a hydrophobic substrate. ....	95
Figure 6.2. (a) Optical microscopy of dewetting PS(465k) films (yellow online) with annealed i-aPS in contact with DTS (white) and (b) with annealed i-mPS in contact with DTS. The initial radii (top row) are the same, and the time interval between top and bottom rows are the same. (c) For similar films, contact line radius, $R$ , as a function of time. For comparison, unannealed i-aPS and i-mPS data sets are shown, which, within the expected variance, are consistent with the annealed i-aPS dewetting sample. ....	99
Figure 6.3. (a) Rim profiles of PS(465k) dewetting from DTS at similar hole radius, cf. Figure 6.1b). (b) Slip length of PS(465K) on DTS at $T_d = 150$ °C for the profiles shown in (a), from rim profile analysis as described in [127]......	100
Figure 6.4. (a) Height profiles of PS rims formed during dewetting from DTS: PS(10k) at dewetting temperature $T_d = 105$ °C; PS(51k) at $T_d = 120$ °C with vertical profile shifts of 100 nm; and PS(130k) at $T_d = 140$ °C, 140 nm shift; PS(465k) at $T_d = 150$ °C, 230 nm shift. All films were annealed on mica prior to transfer (see text for details). (b) Slip lengths extracted from the rim profiles shown in a) for i-aPS and i-mPS (cf. Fig. 1).....	101
Figure 6.5. Slip length ratios obtained for bidisperse dewetting PS films composed of weight fraction, $\phi$ , of $M_w = 488$ kg/mol PS and weight fraction, $1-\phi$ , of $M_w = 28$ kg/mol. Inset: height profiles of PS rims formed during dewetting from AF 2400. Profiles for $\phi = 0.9$ are vertically shifted by 150 nm for clarity.....	102
Figure 7.1. a) Normalized height profiles of PS dewetting rim on AF 2400: PS(28k) with $h_0 = 120$ nm, hole radius $R = 5.9$ $\mu\text{m}$ and $T_d = 120$ °C, and PS(490k) with $h_0 = 172$ nm, hole radius $R = 6.8$ $\mu\text{m}$ and $T_d = 150$ °C; b) the best fit to experimental data for PS(28k); and c) the best fit to experimental data for PS(490k). ....	112
Figure 7.2. Slip length versus molecular weight of monodisperse PSs on AF 2400. The solid line represents the best fit: $b \propto M^2$ in contrast to the theoretical $b \propto M^3$ shown by the dashed line. The dotted line drawn at $M < M_c \sim 35$ kg/mol is a guide to eye representing the constant slip length at the weak slip regime. ....	114

Figure 7.3. Temporal evolution of dewetting holes in thin films ( $\sim 150$  nm) of  $M_w$ -fixed mixtures (set#2) on AF 2400 at  $T_d = 150$  °C. The legend indicates the value of  $M_n$ . ..... 115

Figure 7.4. Slip length of  $M_w$ -fixed mixtures (set#2) on AF 2400 as a function of  $M_n$  at different dewetting temperatures. The solid line is to guide the reader's eye. .... 116

Figure 7.5. a) Slip length of set #3, PS(LMW)-PS(490k) binary mixtures ( $\phi_{PS(490k)} = 0.90$  in all samples) on AF 2400 versus the molecular weight of the LMW component, MLMW; the dotted line shows  $M = M_c$ . b) Slip length versus  $M_n$  for two sets of fixed  $M_w$  mixtures. .... 117

Figure 7.6. Slip length  $b$  versus  $\phi_{PS(490k)}$  for two sets of binary mixtures: PS(28k)-PS(490k) and PS(86k)-PS(490k) on AF 2400. Pure PS(490k) is distinguished with a different symbol. .... 118

Figure A.1. Schematic of Couette flow shear cell used for slip velocity measurements.. 133

Figure A.2. Normalized velocity profiles of PBD 4k, PBD 195k and their binary mixtures: (a)-(f). For each sample, velocity profile measurements were carried out at different shear rates ( $\dot{\gamma}_n = V_0/h$ ) as labeled. Shear rate unit is ( $s^{-1}$ ). The dashed line in all graphs represents the nominal velocity profile according to the theory for simple shear. .... 136

Figure A.3. Normalized velocity profiles of ternary mixtures with a fixed  $M_w = 143.5$  kg/mol and varying  $M_n$  (set W in Chapter 4) containing PBD 4k, 88k and 195k: (a)  $M_n = 17$  kg/mol, b)  $M_n = 21$  kg/mol, (c)  $M_n = 43$  kg/mol, (d)  $M_n = 61$  kg/mol. For each sample, velocity profile measurements were carried out at different shear rates ( $\dot{\gamma}_n = V_0/h$ ) as labeled. Shear rate unit is ( $s^{-1}$ ). The dashed line in all graphs represents the nominal velocity profile according to the theory for simple shear. .... 138

Figure A.4. Normalized velocity profiles of ternary mixtures with fixed  $M_w = 143.5$  kg/mol and varying  $M_n$  (set U in Chapter 4) containing PBD 1k, 88k and 195k: (a)  $M_n = 5$  kg/mol, b)  $M_n = 17$  kg/mol, (c)  $M_n = 28$  kg/mol, (d)  $M_n = 40$  kg/mol. For each sample, velocity profile measurements were carried out at different shear rates ( $\dot{\gamma}_n = V_0/h$ ) as labeled. Shear rate unit is ( $s^{-1}$ ). The dashed line in all graphs represents the nominal velocity profile according to the theory for simple shear. .... 140

Figure B.1. MWD of bulk versus debris samples for 3 bimodal mixtures of PBD(19k) and PBD(277k): (a)-(c). .... 144

Figure B.2. MWD of bulk versus debris samples for 2 bimodal mixtures of PBD(19k) and PBD(277k): (a) and (b). .... 145

Figure B.3. MWD of bulk and debris samples of pure PBD(277k) and its mixtures with 10 and 20 wt% of PBD(19k). In this graph, results of pure PBD(277k) and PBD(277k)-PBD(19k)/(90-10 wt%) are shifted by $\text{Log } a = 1.5$ , and $0.75$ , respectively.....	145
Figure C.1. Rim profiles of dewetting holes for thin films of PMMA ( $M = 173 \text{ kg/mol}$ ) on DTS for $6 \mu\text{m}$ -diameter holes. The dewetting temperature is $190 \text{ }^\circ\text{C}$ . Before dewetting, all samples were annealed on mica at $150 \text{ }^\circ\text{C}$ for 2 h.....	148
Figure C.2. Slip length as a function of the content of long chains for binary mixtures of PS 28k-490k on AF 2400. Thin films are pre-annealed on mica and dewetting was done using air (i-aPS) and buried (i_mPS) interfaces as explained in Chapter 6.....	148
Figure C.3. Rim profiles of dewetting holes for thin films of PS mixtures with a fixed $M_w = 315 \text{ kg/mol}$ and varying $M_n$ (as labeled) on AF 2400.....	149
Figure C.4. Rim profiles of dewetting holes for thin films of a PS mixture with $M_w = 315 \text{ kg/mol}$ and $M_n = 20 \text{ kg/mol}$ on AF 2400 at three different dewetting temperatures.....	149

## List of Tables

Table 3.1. Molecular characteristics of monodisperse PBDs .....	47
Table 3.2. Molecular characteristics of binary PBD mixtures.....	48
Table 4.1. Basic characteristics of monodisperse PBDs.....	68
Table 4.2. Molecular weight and composition of PBD mixtures .....	68
Table 5.1. Molecular weight and composition of PBD mixtures: bulk versus debris* ....	88
Table 7.1. Polymer mixtures and dewetting temperatures examined in this work.....	111
Table C.1. List of dewetting experiments used in Chapter 7. Highlights show different fitting models used for each sample.....	147

## Abbreviation

MW	Molecular Weight
MWD	Molecular weight distribution
PBD	Polybutadiene
PE	Polyethylene
HDPE	High density polyethylene
LDPE	Low density polyethylene
LLDPE	Linear low density polyethylene
PDMS	Polydimethylsiloxane
PTFE	Polytetrafluoroethylene
PMMA	Polymethylmethacrylate
PS	Polystyrene
PI	Polyisoprene
THF	Tetrahydrofuran
DCM	Dichloromethane
GPC	Gel permeation chromatography
SPR	Sliding plate rheometer
AFM	Atomic force microscopy
LVE	Linear viscoelastic region
SAOS	Small amplitude oscillatory shear
SAM	Self-assembled monolayer
OTS	Octadecyltrichlorosilane
DTS	Decyltrichlorosilane

i-aPS	air interface of PS film in contact with mica
i-mPS	buried interface of PS film in contact with mica
Ca	Capillary number
MD	Molecular dynamics
Si	Silicon wafer
SiO <sub>2</sub>	Silicon dioxide

## Nomenclature

$PI$	Polydispersity index
$M$	Molar mass (g/mol)
$M_n$	Number average molecular weight (g/mol)
$M_w$	Weight average molecular weight (g/mol)
$M_z$	Z-average molecular weight (g/mol)
$M_e$	Molecular weight between entanglements (g/mol)
$M_c$	Critical molecular weight (g/mol)
$M_i$	Molecular weight of component $i$ in the mixture (g/mol)
$w_i$	Weight fraction of component $i$ in the mixture (%)
$N$	Degree of polymerization
$N_w$	Weight average degree of polymerization
$N_e$	Degree of polymerization between entanglements
$N_i$	Degree of polymerization of component $i$ in the mixture
$P$	Degree of polymerization of mobile chains
$Z$	Degree of polymerization of grafted/adsorbed chains
$a$	Monomer length (nm)
$\nu$	Grafting/ adsorbed density ( $1/m^2$ )
$\nu(Z)$	Number distribution of grafting chains with different chain lengths
$\nu_c$	Critical grafting/adsorbed density ( $1/m^2$ )
$d$	Distance between grafting points (m)
$D$	Coil diameter of grafted chains (nm)
$D^*$	Critical coil diameter of grafted chains (nm)

$R_0$	Coil size of grated chains (nm)
$R_g$	Radius of gyration (nm)
$R_p$	Radius of gyration of bulk mobile chains with $P$ -mers (nm)
$R_{g,l}$	Radius of gyration of long chains (nm)
$R_{g,m}$	Radius of gyration of intermediate chains (nm)
$R_{g,s}$	Radius of gyration of short chains (nm)
$kT$	Product of the Boltzmann constant, $k$ , and temperature, $T$
$n$	Portion of chains pulled out of interfacial layer by bulk flow
$Re$	Reynolds number
$\eta$	Steady state shear viscosity (Pa.s)
$\eta_0$	Zero shear viscosity (Pa.s)
$\eta_m$	Monomer viscosity (Pa.s)
$\eta^*$	Complex viscosity (Pa.s)
$G'$	Elastic shear modulus (kPa)
$G''$	Viscous shear modulus (kPa)
$G''_{max}$	Maximum viscous shear modulus (kPa)
$G_e$	Plateau modulus (kPa)
$G_0$	Constant modulus (kPa)
$G_N(\varphi)$	Plateau modulus in the mixture (kPa)
$G_r$	Struglinski-Graessley parameter
$\tau_{rx}$	Shear stress at the wall along flow direction $x$ in capillary flow (kPa)
$r$	Radial coordinate
$\gamma_e$	Effective strain

$f$	Creation rate of entanglements
$g$	Loss rate of entanglements
$\sigma$	Shear stress (kPa)
$\sigma^*$	Critical shear stress at the onset of the transition to the strong slip regime (kPa)
$\sigma_1$	Shear stress corresponding to the first characteristic velocity $v_{s1}$ (kPa)
$\omega$	Angular velocity (rad/s)
$\omega_c$	Angular velocity where $G'(\omega) = G''(\omega)$ (rad/s)
$\tau_d$	Disentanglement relaxation time (s)
$\tau_0$	Relaxation time (s)
$\dot{\gamma}$	Shear rate (1/s)
$\dot{\gamma}_n$	Nominal shear rate (1/s)
$\dot{\gamma}_T$	True shear rate (1/s)
$\dot{\gamma}^*$	Critical shear rate at the onset of the transition to the strong slip regime (1/s)
$\dot{\gamma}_T^*$	Critical true shear rate at the onset of the transition to the strong slip regime (1/s)
$v_s$	Slip velocity ( $\mu\text{m/s}$ )
$v_s^t$	Slip velocity at the top plate ( $\mu\text{m/s}$ )
$v_s^b$	Slip velocity at the bottom plate ( $\mu\text{m/s}$ )
$v_s^*$	Critical slip velocity at the onset of the transition to the strong slip regime ( $\mu\text{m/s}$ )
$v_{s1}$	First characteristic slip velocity in Brochard and de Gennes slip model ( $\mu\text{m/s}$ )

$v_{s2}$	Second characteristic slip velocity in Brochard and de Gennes slip model ( $\mu\text{m/s}$ )
$V^{**}$	Critical velocity at the onset of the strong slip regime ( $\mu\text{m/s}$ )
$V_0$	Shear cell moving plate velocity ( $\mu\text{m/s}$ )
$V(z)$	Polymer velocity along flow direction at the distance $z$ from the wall ( $\mu\text{m/s}$ )
$z$	Vertical direction normal to the wall
$x$	Flow direction
$k_f$	Friction coefficient (GPa.s/m)
$k_m$	Monomeric friction coefficient (GPa.s/m)
$k_{f0}$	Friction coefficient at the weak slip regime (GPa.s/m)
$k_{f\infty}$	Friction coefficient at the strong slip regime (GPa.s/m)
$K$	Coil stiffness (N/m)
$b$	Slip length ( $\mu\text{m}$ )
$b^*$	Critical slip length corresponding to $v_s^*$ ( $\mu\text{m}$ )
$b_0$	Slip length at the weak slip regime (nm)
$b_\infty$	Slip length at the strong slip/full slip regime ( $\mu\text{m}$ )
$b_c$	Critical slip length at the onset of stick-slip instabilities ( $\mu\text{m}$ )
$b_{i\text{-aPS}}$	Slip length of PS film on a nonwetting surface when its air interface in contact with mica is used ( $\mu\text{m}$ )
$b_{i\text{-mPS}}$	Slip length of PS film on a nonwetting surface when its buried interface in contact with mica is used ( $\mu\text{m}$ )
$\alpha$	Power factor
$h$	Gap size/film thickness ( $\mu\text{m}$ )

$\phi_{N,b}$	Volume fraction of $N$ -mer chains in the bulk (%)
$\phi_{N,d}$	Volume fraction of $N$ -mer chains in the debris (%)
$\phi_{s,d}$	Volume fraction of short chains in the debris (%)
$\phi_{s,0}$	Volume fraction of short chains in the bulk (%)
$\phi_{m,0}$	Volume fraction of intermediate chains in the bulk (%)
$\theta_N$	Relative excess of $N$ -mer chains in the debris with respect to the bulk
$\phi_L$	Volume fraction of long chains (%)
$\phi, \varphi$	Volume fraction (%)
$A$	van der Gucht Universal prefactor
$U_e$	Energy contribution of energetic-entropic factors in Archers' segregation theory
$t$	Time (s)
$\gamma$	Surface tension (mN/m)
$\gamma_S$	Surface tension of the solid (mN/m)
$\gamma_L$	Surface tension of the liquid (mN/m)
$\gamma_{SL}$	Solid-liquid interfacial surface tension (mN/m)
$S$	Speeding parameter (mN/m)
$V_d$	Dewetting velocity ( $\mu\text{m/s}$ )
$V_{d,f}$	Final dewetting velocity before the film is cooled down ( $\mu\text{m/s}$ )
$\Gamma$	Inverse decay length ( $1/\mu\text{m}$ )
$\kappa$	Redon prefactor of the dewetting velocity for thick films
$R, R(t)$	Hole radius in dewetting films ( $\mu\text{m}$ )
$r$	Radial distance to the contact line of holes in dewetting films ( $\mu\text{m}$ )

$h$	Rim height of holes in dewetting films (nm)
$w$	Rim width of holes in dewetting films ( $\mu\text{m}$ )
$h_c$	Critical thickness of polymer films (mm)
$k^{-1}$	Capillary length (mm)
$\rho$	Density ( $\text{g}/\text{m}^3$ )
$g$	Gravitational constant ( $\text{m}/\text{s}^2$ )
$\theta_e$	Equilibrium contact angle ( $^\circ$ )
$\theta_r$	Receding contact angle ( $^\circ$ )
$C_v$	Prefactor characterizing the flow field near the contact line
$T$	Temperature ( $^\circ\text{C}$ )
$T_g$	Glass transition temperature ( $^\circ\text{C}$ )
$T_d$	Dewetting temperature ( $^\circ\text{C}$ )

# 1. CHAPTER 1

## 1.1. Introduction

In contrast to the common no-slip boundary condition of small-molecule fluids, highly entangled polymer melts, typical of industrial polymers, exhibit a great deal of slip during flow on solid substrates. From a practical point of view, the slip boundary condition can be beneficial or detrimental depending on the application. In polymer processing, slip is beneficial where i) it reduces the required power for a certain flow rate of fluid by lowering the wall shear stress and ii) it expands the margins within which defect-free and smooth-surface products can be produced. Slip is detrimental i) if high shear mixing is desired, ii) in rheometry where accurate measurement of rheological properties requires ideal experimental conditions, and iii) in painting and coating applications where spreading and stability of polymer films are of critical importance.

Thorough understanding of the polymer-wall boundary condition is therefore crucial in many aspects. It allows us to correctly characterize material properties, optimize processing and manufacturing processes, design and produce high-performance lubricants, and improve surface finishes of polymeric products. Of course, another important advantage of having this knowledge is to improve the corresponding theories to obtain more accurate model predictions. Accurate models allow for more efficient material and process design.

Design and use of an application-tailored boundary condition requires a detailed knowledge of chemical and physical characteristics of both substrate and polymer. All polymers slip on solid substrates to some extent. On an adsorbing wall, some polymer chains adsorb onto the substrate surface. Other polymer chains moving with the bulk flowing above the interface are entangled with the adsorbed chains. It is the density of adsorbed chains and their entanglements with bulk chains that control the polymer-wall boundary condition. Due to these entanglements, the polymer slip on adsorbing walls is strongly shear stress dependent. On a non-adsorbing wall, on the other hand, mobile chains are directly in contact with the substrate surface and chains are not adsorbed onto the wall.

Polymer slip in the absence of adsorbed chains is shear stress dependent and it is the chain-wall friction coefficient that controls the slip velocity in this case.

Slip of polymers on non-adsorbing walls is called *true slip* due to adhesive failure between polymer chains and the substrate. Slip on adsorbing walls, however, is due to polymer cohesive failure at a distance about one or a few molecular size above the interface. The wall slip in this case is called *apparent slip*. Some of the most important factors contributing to polymer slip include the substrate and polymer surface energies, substrate roughness, polymer chemistry, polymer molecular weight and molecular weight distribution (MWD), and polymer chain architecture. Among the variety of factors affecting the polymer-wall boundary condition, the effect of polymer MWD has only been sparsely explored in previous studies. The main objective in the present work is to study the effect of MWD on slip of linear polymer melts on substrates of different surface energies. This may help us to expand our knowledge on both true and apparent slip.

To this end, we systematically investigate the effect of MWD using narrowly distributed polymers and their binary and ternary mixtures on different substrates. We use particle image velocimetry experiments to directly investigate wall slip of linear polybutadiene, PBD, on silicon wafers. We also examine dewetting of polystyrene, PS, on fluorinated and silanized silicon wafers which allows for the investigation of wall slip on low surface energy substrates.

Wall slip of polydisperse polymers has long been related to the surface segregation of short chains. Surface segregation in polydisperse linear polymers is the enrichment of short chains at the surface/interface region which can significantly affect slip characteristics. To address this subject, we design rheometry and dewetting experiments that allow us to look into the segregation phenomenon and its potential role in polymer slip.

Our objectives in the present work can thus be summarized as follows:

- ❖ to investigate the effect of MWD on polymer slip on substrates with different surface energies
- ❖ to elaborate on the effect of surface enrichment of short chains on polymer slip

## 1.2. Thesis Structure

The present manuscript consists of 8 chapters. Chapter 1 gives a brief introduction to the subject and summarizes the thesis structure. Chapter 2 gives a comprehensive literature review on wall slip of polymer melts including the critical factors in polymer slip, slip mechanisms, slip in the dewetting of thin polymer films, and theoretical models. The remainder of the thesis includes 5 chapters presenting the research results in a manuscript-based format. A short summary of the content of manuscripts is following.

In Chapter 3, we investigate apparent slip behavior of linear monodisperse and bidisperse polybutadienes flowing on silicon wafer. Monodisperse PBDs and their binary mixtures are examined at steady state during simple shear flow using particle image velocimetry and confocal microscopy. Slip velocity is obtained by image processing. A wide range of shear rates is examined to obtain a comprehensive picture of the slip velocity at different slip regimes. Viscoelastic properties of the materials are also measured by small amplitude oscillatory shear (SAOS) tests using a rotational rheometer. Complex viscosity is chosen as an estimation of the steady-state shear viscosity to calculate the shear stress in the slip studies. Slip velocity, slip length and critical shear stress at the onset of the transition to the strong slip regime are presented as main slip characteristics.

Chapter 4 is a follow up to Chapter 3 in which we examine wall slip of tridisperse linear PBD on silicon wafer. The objective is to investigate whether and how the short chain content of a polydisperse mixture affects polymer wall slip on an adsorbing surface. To this end, tridisperse mixtures with a fixed weight average molecular weight,  $M_w$ , and varying number average molecular weight,  $M_n$ , are prepared from narrowly distributed monodisperse PBD samples. In addition, two sets of ternary mixtures with different compositions including either unentangled or weakly entangled chains are examined. Slip behavior at steady state is examined at different shear rates and results are presented in the same manner as that of Chapter 2.

In Chapter 5, we investigate the molecular weight distribution of the interfacial layer below the plane of slip of linear highly entangled PBDs on stainless steel. We examine the surface enrichment of short chains in bidisperse and tridisperse PBD mixtures using gel

permeation chromatography, GPC. Experiments are done after the strong slip of samples in simple shear flow using a sliding plate rheometer. On stainless steel, a thin hazy debris of polymer remains on the substrate at shear rates above the critical shear rate for the onset of the strong slip regime. We believe that this debris represents the interfacial layer of polymer sample below the plane of slip in contact with the solid substrate. We collect this debris and measure its MWD using GPC. The technique allows us to characterize the short chain surface enrichment without the need for chain labeling. Results are presented as GPC chromatographs. A simple disentanglement induced enrichment model is introduced.

In Chapter 6, we use dewetting experiments to investigate the effect of a sacrificial mica substrate, used during a two-step film preparation procedure in polymer surface studies, on wall slip of thin polymer films. We examine flow dynamics and rim morphology of the dewetting hole of thin polystyrene films on hydrophobized silicon wafers using optical and atomic force microscopy, AFM. Slip properties, accessed using hydrodynamic models, are obtained as a function of the film preparation and annealing protocol before transfer to the main testing substrate. Discrepancies between air-polymer and mica-polymer interfaces are presented as a function of PS molecular weight.

Chapter 7 is a follow up study to Chapter 6 in which we investigate the effect of MWD on slip of polymers dewetting from fluorinated or silanized substrates. Binary and ternary mixtures of monodisperse polystyrene are systematically examined. Slip length obtained from the rim profile analysis of dewetting holes is the main slip characteristics accessed in this chapter.

Chapter 8 gives the summary of the work as well as concluding remarks.

## **2. CHAPTER 2**

### **Literature Review**

#### **2.1. Introduction**

In fluid dynamics, it has been conventionally accepted that there exists a no-slip boundary condition at the fluid /solid interface in which the fluid velocity is zero relative to the substrate past which it flows. The zero interfacial velocity implies that fluid molecules in the immediate vicinity of the fluid/solid interface are stuck to the solid surface and hence the condition, for this reason, may be called the stick boundary condition. The concept dates back to the age of Stokes in 19<sup>th</sup> century and it was generally accepted based on its agreement with experimental results on Newtonian liquids although the accuracy of the hypothesis at the microscopic scale remains doubtful [1].

In general, the no-slip boundary condition holds for simple fluids with small molecules. Violations may be observed in extreme cases such as flow on extremely smooth surfaces, when the surface is highly nonwetting, or where the flow channel has dimensions on the order of molecular sizes [2]. For complex fluids such as polymers, the boundary condition is highly influenced by physical and chemical characteristics of both substrate and polymer. The flow of polymer requires wall shear stresses orders of magnitude larger than those in simple fluids which may cause adhesive- or cohesive failure at or near the fluid/solid interface. This may consequently generate the slip boundary condition.

The high shear stress required for polymer flow originates from the entangled nature of polymer chains. The higher the molecular weight, the more entangled is the polymer exhibiting characteristics sometimes significantly different with those of low molecular weight polymers. Shear-dependent viscosity, non-linear viscoelasticity, long relaxation times, strain hardening extensional viscosity, normal force difference, and interfacial slip are some of the most important aspects of the rheological behavior of high molecular weight chains.

From the practical point of view, industrial polymers are commonly high molecular weight signifying the importance of the corresponding characteristics such as interfacial slip in flow problems. Slip is important in extrusion-based polymer processing techniques. In the past, many extrudate surface distortions and flow instabilities were intuitively related to the polymer interfacial slip. The link between slip and extrusion instabilities comes from the coincidence that highly entangled molten polymers exhibit macroscopic slip [3] and extrusion instabilities both at sufficiently high shear stresses. Much of the interest in polymer slip studies therefore comes from the impression that slip plays an important role in the presence of polymer surface distortions and flow instabilities. It is worth mentioning that polymer flow instabilities occur at very small Reynolds numbers ( $Re < 1$ ) and are governed by mechanisms entirely different with those applicable to flow instabilities of simple fluids at higher Reynolds.

The slip literature generally includes two areas of discussion: i) the correlation between slip and polymer flow instabilities and ii) wall slip characterization and parameters influencing polymer slip. Although the focus of our work is to investigate the effect of polymer molecular weight distribution on the slip behavior, mostly including the later subject, we briefly review both topics in order to enlighten issues around the problem.

## **2.2. Slip and Polymer Flow Instabilities**

Wall slip of high molecular weight polymers have long been related to extrusion instabilities [2]. During extrusion, highly entangled linear polymers may show a sequence of different instabilities as the flow rate is gradually increased. Instabilities start with a periodic low-amplitude high-frequency surface distortion termed as shark-skin at a moderately high level of shear stress (proportional to the polymer plateau modulus). Before shark-skin, the extrudate surface is smooth and glossy [4]. At higher shear stresses, the extrudate surface goes through a period of oscillatory flow with alternating shark-skin and smooth regions. The instability is commonly referred to as stick-slip and causes pressure oscillation under speed-controlled conditions. Stick-slip may only occur for certain combinations of polymer and die material or above a critical molecular weight [5]. In

pressure-controlled systems, the stick-slip behavior is replaced by flow discontinuity known as spurt [5,6]. At still higher stresses, there is a short period of steady flow with relatively smooth extrudate surface followed by a volumetric distortion called gross melt fracture. Extrusion instabilities are commonly known as the melt fracture [2,4,7].

The relationship between polymer slip and extrusion instabilities was originally established based on the observations that several slip features coincided with the occurrence of product surface distortions at about the same shear stresses. The most significant slip features observed during flow of polymers in different geometries are as follows:

- Change in the slope of flow curve in capillary or slit dies: a slight decrease in the slope of shear stress versus shear rate at the point where shark-skin is visually observed is usually attributed to weak interfacial slip [2,5-12] although viscous shear thinning has to be considered before making any conclusion.
- Flow discontinuity under stress-controlled conditions in capillary or slit dies: discontinuity in the flow curve above a critical shear stress which usually gives a sudden increase in the extrudate throughput (spurt) may indicate macroscopic slip [6,7,13].
- Pressure oscillations under speed-controlled conditions in capillary or slit dies: pressure oscillation in upstream flow is associated with stick-slip dynamics [6,13,14].
- Gap dependent measurements in torsional parallel plate rheometers [16,17] or sliding plate rheometers [5,14,15] as well as tube diameter dependent measurements in capillary flows [4,6,7,9,10,13]. Slip velocity can be indirectly quantified using these measurements. In situations where apparent viscosity is gap dependent, smaller gaps require higher shear rates to give the same shear stress compared to larger gaps.

The outstanding outcome of early polymer slip experiments was that the die material and roughness significantly affect flow instabilities. The primary intuitive impression of researchers from initial studies was that instabilities are caused by adhesive failure between

the polymer and substrate, and hence improving adhesion should delay or eliminate extrusion defects. However, further results were controversial. Experiments showed that shark-skin and stick-slip distortions of linear low-density polyethylene (LLDPE) observed using a stainless steel die were replaced by smooth extrudate surfaces when the die was replaced with a fully polished brass die [18]. Furthermore, the corresponding flow curve showed significantly lower stresses in case of brass. The conclusion was that slip, and not adhesion, is in fact the true factor suppressing flow instabilities which can be obtained through the change of the die material [2,7,18]. Smooth surfaces and fluorinated dies were particularly found to promote slip, and hence, eliminate or reduce instabilities to a significant extent. The finding that slip suppresses extrusion instabilities shifted the focus of researchers towards the characterization of interfacial slip and a new era of slip studies began.

### **2.3. Slip Characterization**

Early slip studies mostly involved indirect measurements of slip providing general understanding of the relation between macroscopic slip and flow instabilities. More direct methods for quantifying slip including fringe pattern fluorescence recovery after photobleaching (FPRAP) [19] and particle image velocimetry (PIV) [16] first used in the early 90s allowed scientists to more thoroughly characterize slip behavior at the microscopic level. Such measurements showed microscopic slip occurs at stresses below the value at which surface distortions become visible [2] and therefore several slip regimes may exist.

Later on, it was shown that different slip regimes exist for the flow of polymers on adsorbing surfaces: weak slip at low velocities, prior to the onset of instabilities, and strong slip at higher velocities as instabilities emerge [19-21]. There is a transitional margin between the two slip regimes which may correspond to the stick-slip behavior. The slip mechanisms in different slip regimes are qualitatively different and will be discussed later in this chapter.

Slip is usually characterized by the slip velocity,  $v_s$ , and/or the slip length,  $b$ , which is defined as the distance from the interface at which the velocity profile extrapolates to zero (Figure 2.1). A third parameter to characterize slip is the critical shear stress for the onset of the strong slip. Except for a few [8,22], the majority of slip studies using a variety of polymers and die materials showed that macroscopic slip occurs above a critical shear stress,  $\sigma^*$ , proportional to the polymer plateau modulus,  $G_e$ , as :  $\sigma^* \propto G_e$  [6,7,9,10,13,15,21,23,24].

Figure 2.1 shows a schematic of a variety of boundary conditions that may occur during simple shear. These boundary conditions are classified based on the place where the slip plane is located: i) at the polymer-solid interface (true slip) or ii) at a small distance ( $z_0$ ) above the solid surface (apparent slip). An important parameter to be considered in practical applications is the ratio of the slip length to gap size  $b/h$  varying from 0, no-slip, to  $\infty$ , full slip. Slip becomes macroscopically significant once  $b$  is comparable to  $h$ .

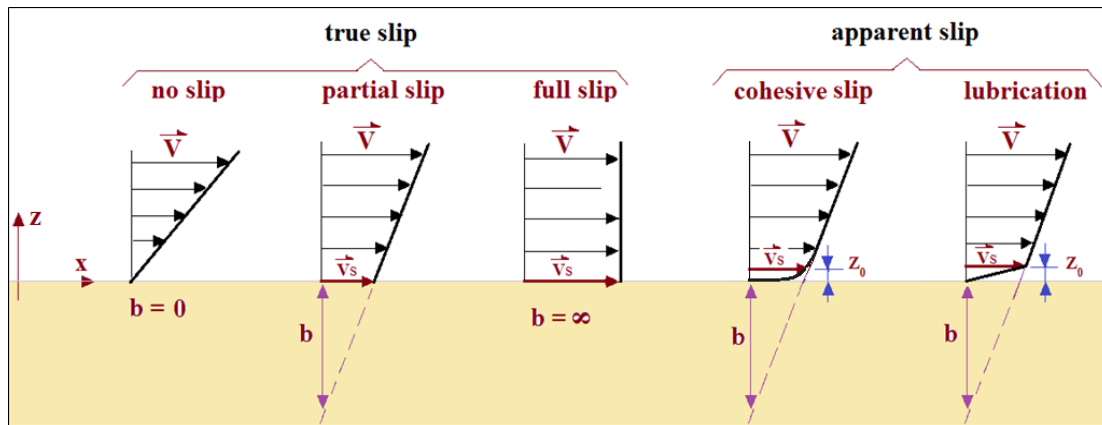


Figure 2.1. A schematic of different boundary conditions that may occur during simple shear (partially adapted from ref [25]).

In Figure 2.1, partial slip and full slip are contradictory to the traditional no-slip boundary condition since the velocity of the layer of fluid in the immediate vicinity of the interface is non-zero. On the other hand, the no-slip boundary condition still holds in apparent slip by cohesive failure or the lubrication mechanism since the relative velocity

of fluid in contact with the solid surface is zero. The velocity profile in bulk however extrapolates to a finite slip length.

As shown in Figure 2.1, the slip length in simple shear is obtained by the extrapolation of the velocity profile to zero and thus can be defined as:

$$b = \frac{v_s}{\left. \frac{dv}{dz} \right|_{z=0}} \quad (2.1)$$

where the denominator is the shear rate at the fluid-solid interface,  $\dot{\gamma}|_{z=0}$ , in case of true slip. We note that the denominator has to be modified to  $\dot{\gamma}|_{z=z_0}$  for the case of apparent slip. When slip occurs, the shear stress,  $\sigma$ , at the slip plane may be defined as the product of the slip velocity and friction coefficient,  $k_f$  [26]. On the other hand, the wall shear stress is the product of the fluid viscosity,  $\eta$ , and shear rate at the wall:  $\sigma = \eta \dot{\gamma}|_{z=0}$ . The slip length in Equation 2.1 can therefore be written as  $b = \eta/k_f$  using these relationships. The latter relation introduces the slip length as the ratio of the fluid viscosity to friction coefficient signifying the importance of interfacial interactions.

During polymer flow, interfacial interactions are affected by physical and chemical properties of both the substrate and polymer. The substrate surface composition, surface energy, and surface roughness all affect slip [14]. Polymer molecular weight, molecular weight distribution, chain architecture, chemical composition and surface energy all influence wall slip. We review the role of each of these parameters in slip but first it is crucial to review the different slip mechanisms.

## 2.4. Slip Mechanisms

Interfacial slip as opposed to the no-slip boundary condition requires adhesive failure right at the interface. This literally necessitates the ideal condition of a smooth and non-adsorbing surface. In reality, however, most surfaces are non- or semi-ideal and therefore a few or even many polymer chains may be adsorbed to the solid surface.

Two major slip mechanisms have been recognized for the flow of polymers on adsorbing surfaces: slip by i) desorption/detachment [27,28] and ii) disentanglement [29-34]. In the desorption mechanism, before slip some chains are attached to the solid surface and there is no distinct relative movement between the adsorbed and bulk chains compared to chains in the rest of the bulk. Above a critical shear stress, the adsorbed chains become detached from the substrate and are carried away by the bulk. The critical shear stress at the onset of macroscopic slip was found to follow a linear relationship with the work of adhesion between low and high density polyethylenes and stainless steel die with and without fluoropolymer coatings [28]. Slip dynamics in this mechanism are believed to be highly affected by the rate of adsorption/desorption of chains to/from the solid surface under flow conditions [35].

The alternative slip mechanism on adsorbing surfaces is cohesive failure between the polymer bulk and the layer of chains adsorbed onto the solid surface [29]. In this mechanism, it is always assumed that the force required for disentanglements is less than that of desorption, i.e., adsorbed chains are strongly attached to the solid surface to an extent that cohesive failure can precede the adhesive failure. Slip dynamics in the disentanglement mechanism are governed by the number of entanglements between the adsorbed and mobile chains as well as the surface density of adsorbed chains [30,34]. Above a critical slip velocity, mobile chains disentangle from those adsorbed to the solid surface and strong slip occurs. Apparent slip due to cohesive failure occurs at a distance of about one or a few molecular sizes away from the interface and does not therefore contradict the no-slip boundary condition.

Both slip mechanisms have been subjects of interest in the literature. The disentanglement slip mechanism, however, has attracted more attention [29-39]. The basic idea was first hypothesized by Bergem in 1976 [40] and a remarkable scaling law theory was developed by Brochard-Wyart and de Gennes in 1992 [29]. The theory soon became widely supported and many experimental results from previous slip studies were found consistent with it [16,19,21]. In real conditions, it is likely however that both mechanisms occur simultaneously and some recent theories have tried to incorporate both mechanisms into one model [37,38].

There is also a slip mechanism particularly applicable to polymer solutions and polymers containing fluoropolymer additives. The so-called lubrication mechanism is similar to flow of two-phase systems [14,41]; a stress-induced low-viscosity layer forms in the vicinity of the interface by the diffusion/migration of additives or low molecular weight species towards the interface. The mechanism is not entirely distinct from the disentanglement mechanism. Another similar mechanism has been proposed for the slip of polymers with glass transition temperatures,  $T_g$ , above the room temperature, in particular for polyethylene, PE [6,9,10]. In this case, slip occurs due to the presence of an interfacial low-viscosity structured layer formed on the solid surface. Wall slip hence occurs due to the cohesive failure between the bulk and interfacial layer.

There have also been models suggesting that polymer wall slip is an outcome of a type of bulk instability known as a constitutive instability [5,42-44]. According to the Doi-Edwards tube model, the shear stress – strain rate curve is non-monotonous, passing through a maximum followed by a minimum as the strain rate increases. The non-monotonicity as a result is believed to induce a bulk mechanical instability during steady shear; this was considered to be the source of spurt flow and hence macroscopic slip. There is now no doubt however that polymer slip is an interfacial phenomenon that occurs in the immediate vicinity of the interface and therefore nothing to do with the constitutive instability [35].

## **2.5. Critical Factors Influencing Polymer Wall Slip**

There are a variety of factors that can affect polymer slip on solid surfaces. This may include substrate surface roughness, relative surface energy of the substrate and polymer, substrate and polymer chemistry, polymer molecular weight, molecular weight distribution, chain microstructure, and chain architecture. In the following section, we review the effect of each factor on polymer wall slip in more detail.

### 2.5.1. Effect of Substrate Properties on Polymer Wall Slip

Substrates may be categorized into ideal, semi-ideal, and non-ideal surfaces according to the density of adsorbed chains onto the wall. A change in the density of adsorbed chains can occur by surface roughness or surface energy. An ideal surface by definition is smooth and non-adsorbing. A substrate with a low density of adsorbed chains - where only a few polymer chains are adsorbed to its surface - is called semi-ideal (polymers on silanized or fluorinated substrates). Non-ideal surfaces are those with a high density of adsorbed chains (a highly clean glass surface is an example of non-ideal substrates). Slip behavior significantly varies by the type of the substrate over which polymers flow. Following is a brief summary of the literature on the effect of substrate on adsorbed chains density and on polymer wall slip.

#### 2.5.1.1. Ideal Surfaces

On an ideal surface, the friction coefficient at the slip plane is only a function of the monomer viscosity,  $\eta_m$ , and monomer size,  $a$ , as:  $k_f = \eta_m/a$  which is equivalent to that of the flow of monomers,  $k_m$ , on the wall  $k_f = k_m$ . This was first argued by Brochard and de Gennes in their well-known slip theory of 1992 [29]. On the other hand according to polymer reptation theory, the polymer viscosity can be written as  $\eta = \eta_m(N^3/N_e^2)$  where  $N$  and  $N_e$  are the degree of polymerization and number of monomers between the entanglements, respectively. The slip length of polymers on ideal substrates called infinite slip length,  $b_\infty$ , hence becomes:

$$b_\infty = \frac{\eta}{k_f} = a \left( \frac{N^3}{N_e^2} \right) \quad (2.2)$$

which is a polymer property and independent of the interfacial friction coefficient [26]. In ideal conditions, slip is due to adhesive failure and slip length is extremely large on the order of a few hundred microns. The velocity field in infinite slip becomes close to plug flow although the exact shape strongly depends on the ratio of slip length to the size of the

flow channel. A fully plug flow may be observed in polymer thin films with thicknesses in range of a few hundred nanometers flowing over ideal surfaces.

It is experimentally very difficult to reach ideal conditions however. In a microfluidic study, Mhetar and Archer investigated the slip of highly entangled PBDs on smooth perfluorosilane-treated silica surfaces [16]. Stick-slip was not observed at any level of stress and a large and constant value of  $b$  was obtained independent of the shear stress but still an order of magnitude lower than the corresponding  $b_\infty$  from Equation 2.2. The discrepancy was attributed to weak van der Waals interactions between chains and surface resulting in a friction coefficient significantly higher than that of the flow of monomers. Similar results were found in thin film studies by Bäumchen and coworkers [45]. Using dewetting of thin PS films on silanized and fluorinated silicon wafers, the authors found very large slip lengths still an order of magnitude smaller than those predicted by the Brochard and de Gennes theory.

#### 2.5.1.2. Semi-ideal Surfaces

The slip of highly entangled polymers on semi-ideal surfaces is of significant importance practically. Three distinct slip regimes have been reported both experimentally [19,21,46] and theoretically [29,30]: weak slip, transitional region, and strong slip. Leger and coworkers [21,46] extensively studied the wall slip of highly-entangled monodisperse polydimethylsiloxane (PDMS) on different low surface energy substrates: i) a fully dense octadecyltrichlorosilane OTS monolayer [21] and ii) OTS monolayer with a few artificially grafted PDMS chains (OTS+PDMS) [46]. It was shown that the shear flow of PDMS on fully dense OTS monolayer and OTS+PDMS surfaces exhibits three distinct slip regimes in accord with the slip model of Brochard and de Gennes. Schematic of the three slip regimes in a log-log plot of slip velocity versus shear rate - adapted from ref [21] - is shown in Figure 2.2.

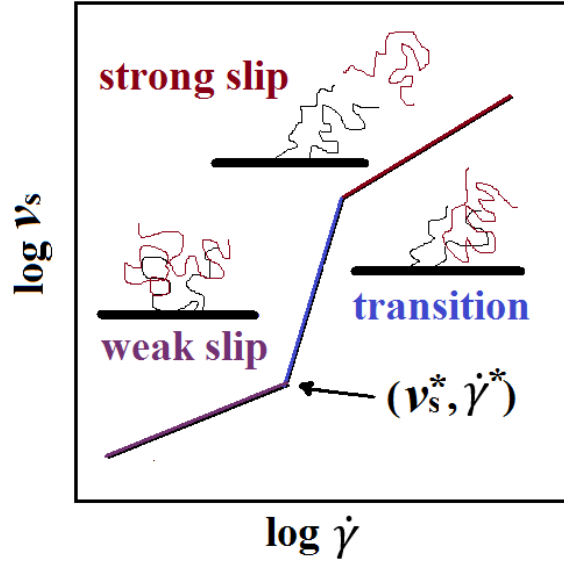


Figure 2.2. A schematic of the three slip regimes in a log-log plot of slip velocity versus shear rate (adapted from ref [21]).

In the weak slip regime, slip is drastically suppressed due to the presence of entanglements between adsorbed and bulk chains. The weak slip regime slip length  $b_0$  is very small, on the order of a few hundred nanometers, and independent of the slip velocity. At higher shear rates above a critical value,  $\dot{\gamma}^*$ , the slip velocity shows a stronger dependence on shear rate. The slip length in this regime is a function of the slip velocity and may show a power law dependence [46]. At higher shear rates, above a second critical shear rate value, strong slip occurs and slip length becomes independent of the shear rate once again. According to the disentanglement slip mechanism, mobile chains in the strong slip regime completely disentangle from those adsorbed to the wall and the slip length becomes close to  $b_\infty$  [29].

Durliat *et al.* reported that the three slip regimes are always present for semi-ideal surfaces although  $v_s^*$  is highly sensitive to the molecular weight of both bulk and adsorbed chains [46]. They showed that  $v_s^*$  follows the power laws  $v_s^* \propto Z^{-1.02 \pm 0.06} P^{-3.3 \pm 0.3}$  where  $P$  and  $Z$  are the degree of polymerization of bulk and adsorbed chains, respectively.

### 2.5.1.3. Non-ideal Surfaces

Non-ideal surfaces refer to substrates with a highly-dense layer of adsorbed chains. Examples include a) a bare high-energy surface, b) surfaces with a thin crystallized or glassy layer of polymer in the immediate vicinity of the interface, and c) specifically prepared surfaces with a highly-dense layer of grafted chains [26]. Polymers flowing over non-ideal surfaces exhibit drastically suppressed wall slip. Migler *et al.* studied wall slip of PDMS on bare silica and a low density OTS monolayer [21]. The strong slip regime previously observed for PDMS on the fully dense OTS monolayer was not observed within the experimental window. A dense layer of immobilized chains with a pseudobrush structure formed on the surface was thought to prevent the strong slip [21]. The onset of the strong slip in this case is shifted to higher shear stresses and slip length is very small [19].

### 2.5.1.4. Adsorbed Chains versus End-grafted Chains

As discussed, the adsorbed density of polymer chains onto the solid surface is the most important factor in driving the subsequent slip mechanism in the flow of polymer melts over solid substrates. Producing a solid surface with an accurate density of *adsorbed* chains is not an easy task if not impossible. For this reason, many slip studies use solid substrates having polymer chains *grafted* rather than adsorbed. Leger and co-workers studied polymer wall slip on semi-ideal surfaces using both adsorbed and end-grafted monodisperse chains at low and moderate grafting densities [19]. Experiments showed qualitatively very similar results; the three slip regimes of low-density adsorbed surfaces were present for end-grafted surfaces too. Some features were however different; most importantly in the transition regime, the slip length linearly varied with the slip velocity  $b \sim v_s^\alpha$  with  $\alpha = 1$  as opposed to  $\alpha < 1$  for the adsorbed chains. The slip behavior on the surface with a low density of end-grafted chains was in full quantitative agreement with predictions from the Brochard and de Gennes theory.

The authors explained that the difference between the two experiments comes from what they referred to as the ‘polydispersity effect’ in adsorbed chains as compared to the

monodisperse nature of end-grafted chains being grafted to the surface only by their end-groups. Polymer chains may adsorb onto the substrate at any of their monomers along their length offering two tails dangling from the substrate with a length distribution as opposed to constant-length end-grafted chains. The length polydispersity affects the number of entanglements between bulk and adsorbed chains and causes deviation from theoretical models established for monodisperse polymers only. The results in many practical cases would therefore be affected by the polydispersity effect of the adsorbed chains.

#### 2.5.1.5. Surface Roughness

The general understanding of slip literature on the effect of surface roughness on wall slip is that slip velocities are lower on rough surfaces. Slip studies using particle image velocimetry of PBD on glass substrates by Mhetar and Archer showed that cleaned roughened silica surface shows no evidence of stick-slip unlike smooth silica surfaces [24]. Furthermore, experiments using uncleaned silica surfaces at stresses above the critical stress showed significant void and/or shear fracture formation near the interface which were attributed to non-uniform slip velocities due to surface heterogeneity. Using gap-dependent rheometry experiments, Sanchez-Reyes and Archer showed that the surface roughness causes a decrease in the polymer slip length and that surface roughness root-mean-square values on the order of the polymer molecular dimensions (radius of gyration), could be enough to suppress slip completely [17]. Capillary experiments by Wang and Drda showed that roughening the die surface increases the critical stress for the onset of stick-slip instabilities [6]. Mhetar and Archer showed that the critical shear stress for the onset of macroscopic slip is doubled when smooth silica surfaces are replaced by roughened similar surfaces [24]. Molecular dynamics simulations of Niavarani and Nikolai revealed that slip decreases with increase of the wavelength of periodically corrugated surfaces for wetting fluids and that the surface roughness may induce a small curvature to the linear velocity profile of the simple shear flow near both interfaces [47].

The effect of surface roughness on polymer slip was well explained by several researchers through the differences in molecular relaxation dynamics over smooth and

rough surfaces [6,24]. The surface morphology in rough surfaces provides a larger area of adsorption sites – ‘hills and valleys’ - where polymer chains may become trapped compared to smooth surfaces. Bulk chains are now dominantly interacting with a ‘penetrable’ adsorbed polymer layer rather than an ‘impenetrable’ layer of solid molecules over the smooth surface. This in turn favors more adsorption of bulk chains towards the interface. The higher polymer adsorbed density over the rough surface consequently decreases the interfacial slip since the slip length is proportional to the inverse of the adsorbed polymer density per unit area,  $\nu$ , as shown by Brochard-Wyart and de Gennes in their theory:  $b \sim \nu^{-1}$ . The critical stress is however proportional to the polymer adsorbed density. Therefore,  $\sigma^*$  increases with  $\nu$  for the case of rough surface.

#### 2.5.1.6. Substrate Composition: Low- versus High-energy Surfaces

A large extent of slip studies in the past was devoted to understanding the effect of die material on wall slip [2]. The die surface composition is a key factor in driving the chain-wall interactions. The chemistry of die material mostly affects the binding energy of polymer chains to the substrate. Since the most commonly used die materials in polymer processing are chemically inactive to polymer chains, the relative surface energy of the die with respect to that of the polymer becomes the crucial factor in wall slip. Industrially, steel and aluminum are predominantly used as core die materials - both bearing high surface energies. In contrast, silanized and fluorinated surfaces extensively used as coatings are well-known for their low surface energies [48].

At equilibrium, most polymers are nonwetting on low surface energy surfaces such as polytetrafluoroethylene, PTFE; hence, they exhibit extensive slip under flow conditions. Piau *et al.* reported that the extrusion of PBD through slit dies coated with PTFE shows flow rates about 30%-500% higher than that through a bare steel die at the same driving pressure [8]. They also showed that the onset of instabilities in PTFE-coated dies is delayed up to 24 times by the critical flow rate through a bare steel die. Further investigation revealed that the velocity profile changes from fully-developed Poiseuille flow to almost plug flow when the die material is changed from steel to PTFE where the energy dissipation

mechanism is viscous dissipation on steel interfacial friction on PTFE. In addition, the introduction of slip by surface treatment or use of additives reduces chain deformations in the flow and relaxes the material. This further reduces the stresses resulting in smooth extrudate surfaces.

Mhetar and Archer showed that, for PBD, the magnitude and functionality of slip velocity dramatically changes from bare silica to fluorocarbon-coated silica in a planar Couette geometry [24]. The authors reported that, on fluorinated silica, PBD exhibits very large slip velocities close to the slip characteristics of non-adsorbing surfaces. Slip lengths were however still an order of magnitude smaller than those of ideal substrates.

Wang and Drda studied the effect of wall chemistry on stick-slip instabilities of the flow of highly entangled linear PE in capillary dies [6,9]. They showed that surface treatment of the die material (steel in this case) with fluoropolymer coating removes the stick-slip transition completely and causes massive slip. The authors concluded that this is likely due to the change of slip mechanism from the disentanglement mechanism on steel to the desorption mechanism on the fluorocarbon coated die.

By lowering the die surface energy, the density of adsorbed chains is reduced significantly. The lower number of adsorptions per unit area reduces the contribution of entanglements between bulk and adsorbed chains and increases that of the less-significant chain-wall friction forces on the shear stress. The result is occurrence of larger slip velocities at lower shear stresses [6].

### **2.5.2. Effect of Polymer Characteristics on Wall Slip**

Among several characteristics of polymers influencing their wall slip, polymer chemistry and surface energy affect the chain-wall interactions by governing the bonding energy of adsorbed chains to the wall. On the other hand, polymer molecular weight, molecular weight distribution, and chain architecture influence chain-chain interactions by governing the relaxation dynamics among the mobile and adsorbed chains. Previous studies have addressed contributions of molecular weight and chain architecture which we

briefly review in the following sections. The effect of molecular weight distribution on the polymer slip has rarely been previously explored and is the subject of the present study.

#### 2.5.2.1. Low Molecular Weight Polymers, Branched Polymers, and Polymer Solutions

The reason that polymers exhibit significant slip is their large molecular size. In fact, the presence of highly-entangled chains is an essential requirement for polymers to exhibit measurable amounts of slip. Macroscopic slip and flow instabilities are mostly observed for linear highly entangled polymers including high density polyethylene (HDPE), LLDPE [7], PBD [13,23], polyisoprene (PI) [13], PS [41] and PDMS [23]. In general, low molecular weight linear polymers [13,16,23], highly long-chain branched polymers [2,7,8], and low-concentration polymer solutions [3,17,41] are unlikely to undergo strong slip since they have much fewer entanglements compared to high molecular weight linear polymers [2,5,7,13].

#### 2.5.2.2. Critical Stress Likely to be Independent of Molecular Weight

The critical shear stress for the onset of flow instabilities or macroscopic slip,  $\sigma^*$ , appears for highly entangled polymers only. It is believed to be a material property proportional to the plateau modulus  $G_e$  and independent of the polymer molecular weight as suggested by Vinogradov *et al.* [13] and Mhetar and Archer [16] who summarized results from several studies. Mhetar and Archer concluded that  $\sigma^*$  may therefore be obtained from bulk rheology measurements. This argument is consistent with molecular theories based on the disentanglement slip mechanism suggesting  $\sigma^* \sim G_e$  [14,16,17,49].

#### 2.5.2.3. Slip Length Increases with Molecular Weight

As the polymer molecular weight increases, the number of physical entanglements in the bulk increases. Slip length is related to the number of entanglements in the bulk and thus increases with the molecular weight. Wang and Drda carried out a series of flow

experiments using four linear HDPE resins in a capillary steel die and showed that the critical slip length,  $b_c$ , at the onset of stick-slip scales with molecular weight as  $b_c \sim M_w^{3.4}$  [10]. The certainty of the value of the exponent is however low due to sparse data. Mhetar and Archer [16] using particle image velocimetry studied the slip of PBD on a clean silica surface and showed that the low-velocity slip length and infinite slip length increase with the polymer molecular weight as  $b_0 \sim M_w^{1.94}$  and  $b_\infty \sim M_w^{1.3}$ , respectively. Similar relationships were obtained by Sanchez-Reyes and Archer using rheology gap measurements on a PS/diethyl phthalate (DEP) solution [17].

#### 2.5.2.4. Polymer Molecular Weight Distribution

Commercially produced polymers are most often polydisperse with a broad molecular weight distribution. To properly characterize a polydisperse polymer, we require the exact molecular weight distribution but often well-defined average values are used. The most common molecular weight averages include number average, weight average, and z-average denoted by  $M_n$ ,  $M_w$ , and  $M_z$ , respectively. The averages are the first, second, and third moment of the molecular weight distribution as follows:

$$M_n = \frac{\sum N_i M_i}{\sum N_i} \quad (2.3a)$$

$$M_w = \frac{\sum N_i M_i^2}{\sum N_i M_i} \quad (2.3b)$$

$$M_z = \frac{\sum N_i M_i^3}{\sum N_i M_i^2} \quad (2.3c)$$

where  $N_i$  is the number of chains of molecular weight  $M_i$ . The averages are related by  $M_n \leq M_w \leq M_z$  where equality holds for monodisperse samples. Polymer molecular weight is usually represented by one of  $M_n$  or  $M_w$  while the ratio  $M_w/M_n$  called the polydispersity index,  $PI$ , is used to represent the breadth of the distribution.

In general, physical properties of polymers are very sensitive to molecular weight distribution. In linear polymers, surface tension  $\gamma$  as an example, is inversely correlated to the number average molecular weight as  $\gamma \propto M_n^{-\alpha}$  where  $\alpha$  is between 2/3 and 1 [50,51]. Polymer density, coefficient of thermal expansion, and glass transition temperature also change with  $M_n^{-1}$  [51,52]. Rheological properties such as the zero shear viscosity  $\eta_0$  and relaxation time  $\tau_0$  vary with the weight average molecular weight ( $\eta_0$  or  $\tau_0 \propto M_w^{3.4}$ ). In small amplitude oscillatory shear, the frequency dependence of the complex viscosity,  $\eta^*$ , is very sensitive to the molecular weight distribution [53]. Samples with broad molecular weight distributions are well-known to leave the plateau region at smaller frequencies compared to narrowly distributed samples.

Polydispersity is of significant importance in polymer processing where elastic behavior is a crucial factor. A number of parameters including first normal stress difference, extrudate swell, extrudate surface distortions, and capillary end effects are found to be sensitive to the polymer molecular weight distribution [53].

Most studies of the effect of polydispersity on polymer processing behavior is focused on the capillary flow of polyethylene. Myerholtz showed that stick–slip instabilities may decrease or disappear at very large  $PI$  values ( $PI > 30$ ) [54]. Ansari *et al.* reported similar observations: the ranges of the stick–slip transition decrease as molecular weight distribution broadens until it completely disappears for  $PI > 19$  [55]. In a similar study, Blyler and Hart showed that the flow curve discontinuity may significantly reduce if a low molecular weight polyethylene wax is added to a high molecular weight linear PE [56].

The general understanding is that increasing polydispersity improves processability of the polymer in several ways [55,57]: i) the severity of shark-skin is reduced, ii) the weak to strong slip transition becomes less abrupt and spurt and flow curve hysteresis may disappear entirely [53], and iii) the range of shear rate over which stick-slip occurs shrinks and the instability may disappear at very large  $PI$  values ( $PI > 30$ ) [54].

The effect of short chains on polymer properties has been the subject of interest in many previous studies. There is much experimental evidence that short chains or low molecular weight species play a critical role in physics and flow dynamics of molten

polymers. Several researchers showed that incorporation of short chains into the network of long chains accelerates relaxation of long chains and reduces the mixture plateau modulus,  $G_N(\varphi)$  [58-61]. In capillary extrusion, Schreiber showed that the shape of molecular weight distribution influences the flow curve discontinuity and blends containing “components with widely different molecular weights are far more effective than broader but more normally shaped distributions” at reducing the magnitude of the discontinuity [62]. Recently, Inn studied capillary flow of three bimodal PE resins of similar viscosity [63]. The author observed that the sample with i) higher content of the low molecular weight population and ii) highest molecular weight of the high molecular weight population showed the largest slip as determined indirectly. These observations imply that short chains play a significant role in flow dynamics of highly entangled polymers.

Although it is generally agreed that polydispersity improves processability of polymers (polyethylene in specific) [64,65], there has not yet been a general agreement on how polydispersity affects polymer slip [64,66,67]. Part of the issue is due to not having direct and systematic studies of the problem. Hatzikiriakos in a recent review of the subject reminded us of the necessity of further work to investigate the effect of polydispersity on wall slip of polymers [57]. Also, available molecular theories on polymer wall slip are only applicable to monodisperse systems and have not yet been extended to polydisperse systems typical of industrial polymers.

## **2.6. Wall Slip and Surface Enrichment of Short Chains in Polydisperse Polymers**

Wall slip of polydisperse polymers has long been related to the surface enrichment of short chains at the polymer-wall interface. Surface or interfacial segregation in linear polydisperse polymers [50,68-71] is the enrichment of short chains at the surface/interface region and has extensive implications in polymer processing and end-product surface characteristics. In polymer processing, several phenomena such as wall slip [63], die drool [72-74] and extrudate surface instabilities [2] have been related to the surface segregation

and enrichment of low molecular weight species at the interface. Surface properties on the other hand are of great importance specifically in lubrication and polymer thin film industries. These issues make surface segregation an important subject of study in polydisperse systems typical of industrial polymers.

In polydisperse linear polymers, the chains are chemically identical and differ only in molecular weight. The segregation is thus mainly induced from factors motivated by the chain length disparities. These factors can be entropically driven by the reduced conformational entropy at the surface or enthalpically driven by the surface attraction of chain ends. The latter reflects the surface energy difference between the backbone and end groups of the chain [50]. Under certain flow conditions such as capillary extrusion, surface segregation is believed to be mechanically driven by the shear stress gradient across the flow channel - this is called shear induced fractionation [63,73,75].

The conformational entropy of a polymer chain is reduced at the surface. In a polydisperse polymer, the shorter chains suffer less from this entropy loss than longer chains and hence are thermodynamically driven to the surface to maximize the entropy of the system [70,76]. Van der Gucht *et al.* [69] used the self-consistent field model of Scheutjens and Flerer and investigated the surface segregation of polydisperse linear polymers solely driven by entropy loss. The authors showed that the integrated surface excess of a component of chain length  $N$  can be obtained from:  $A(1 - N/N_w)\phi_{s0}$  where  $A \approx 0.195$  is a universal prefactor,  $N_w$  is the weight average chain length and  $\phi_{s0}$  is the concentration of  $N$  chains in the bulk of the sample. The proposed relationship suggests that the ratio of the integrated surface excess of linear short chains to their bulk composition, solely driven by the entropy loss at the surface, cannot exceed 19.5%.

In the presence of energetic attractions, surface segregation becomes strongly enhanced. This occurs when end segments are chemically different from backbones and results in a larger magnitude of the prefactor  $A$  in the van der Gucht *et al.* equation. In a linear system since all chains possess two ends, the number of backbone units defines the migrating chains meaning that the shorter chains are those that are enriched or depleted at the surface. The surface segregation of chain end groups has been reported for

monodisperse PS and their mixtures [77]. One way to understand the surface energy difference between the backbone units and end groups is to measure the surface tension of monodisperse samples as a function of chain length. Any dependency between the surface tension and molecular weight means that chain ends are chemically different with backbone units [50-51].

Several studies in the past suggested that surface enrichment can be due to shear induced molecular weight fractionation across the flow channel [63,73,75]. Near the wall, long chains gain more free energy by elastic deformations than shorter chains which may yield a thermodynamic driving force to concentrate the longer chains near the centerline. With depletion of long chains in the vicinity of the wall, there can thus be an enrichment of short chains. This mechanism has not been widely accepted considering the short time span during which chain migration is supposedly taking place in the highly viscous polymer media. There have been experimental studies proving and disproving the hypothesis as well; a brief list of these works can be found in refs [37,63].

Despite great interest in the subject, it has been difficult to quantitatively understand to what extent the surface segregation occurs. We note that characterizing the surface composition of a mixture of chemically identical components has been one of the most challenging problems in surface segregation studies [78,79]. On the one hand, use of direct molecular weight distribution characterization techniques has been drastically hindered by experimental difficulties in collecting samples: for instance, the depth of the enrichment layer is so narrow - within molecular size - that it is physically almost impossible to be separated from the bulk for gel permeation chromatography measurements. Indirect characterization techniques, on the other hand, always suffer from the lack of a proper test probe to monitor the enrichment without labeling - labeling of chains induces additional energetic terms. For example deuterium labeling of a chain lowers its surface energy and hence induces an energetic driving force [79,80].

Tanaka and colleagues [79] were the first, to our knowledge, that measured the surface enrichment of short chains in thin PS films without chain labeling. They measured the glass transition temperature  $T_g$  of the air-polymer surface of binary and ternary mixtures of short

and long chains and compared that to the surface  $T_g$  of pure constituents. They applied the bulk  $T_g$  mixing rule to the surface  $T_g$ s and extracted the surface composition. The results of their work was indeed interesting illustrating significant relative excess of short chains ( up to  $\sim 90\%$  as seen in Figure 6 from ref [79]) much higher than the value predicted from the van der Gucht *et al.* relation which only took into account the enrichment due to the surface entropy loss. As the authors reported in their previous work [77], preferential attraction of chain ends to the surface was a contributing factor as well.

## 2.7. Slip in Dewetting of Thin Polymer Films

One easy and powerful tool to characterize polymer slip on nonwetting substrates is the dewetting experiment. Dewetting is a fascinating aspect of the physics of polymers in which a thin film of liquid polymer placed on a nonwetting solid substrate breaks up at different sites and retracts (Figure 2.3). The phenomenon takes place as a result of the presence of a pressure gradient along the surface caused by the surface energy difference between polymer and substrate and follows a Poiseuille flow velocity profile [48,81].

The retraction velocity, known as the dewetting velocity, has been well characterized based on the bulk and interfacial properties of the polymer and substrate. Interfacial slip may highly influence the dewetting dynamics depending on the thickness of the polymer film; thin films with thicknesses on order of the polymer slip length may completely slide on the substrate leading to significantly higher dewetting velocities compared to thick films. Slip can hence be characterized using carefully-performed dewetting experiments.

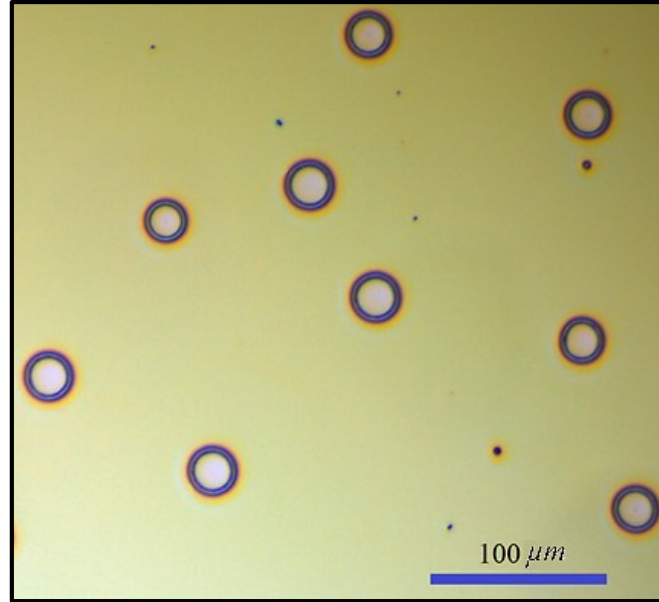


Figure 2.3. Optical image of several dewetting holes of a thin film (200 nm) of PS on a fluorinated (AF 2400) silicon substrate at 150 °C after 30 minutes.

### 2.7.1. Dewetting Mechanisms

Below a critical thickness  $h_c = 2k^{-1} \sin(\theta_e/2)$ , on the order of 1 nm, a film of polymer melt dewets its substrate if the spreading parameter  $S = \gamma_S - (\gamma_L + \gamma_{SL})$  is negative, where  $k^{-1} = \sqrt{\gamma/\rho g}$  is the capillary length,  $\gamma$  the surface tension,  $\rho$  the density,  $g$  the gravitational constant,  $\theta_e$  the equilibrium contact angle and subscripts  $S$  and  $L$  refer to solid and liquid, respectively [26,82]. Dewetting mechanisms are similar to those in phase transitions; the film can be unstable – ultra-thin films less than 10 nm thick – and dewet spontaneously through the spinodal mechanism or it can be metastable – thicker than 100 nm– and dewet by nucleation and growth. In the latter case, the dewetting initiates at a nucleus and grows by developing a circular hole progressively accumulating material in its rim. The adjacent film to the rim is usually undisturbed. Dewetting by nucleation and growth is more common since spinodal dewetting is limited to very thin films and requires ultra-pure conditions where nucleation can be avoided [81,83].

### 2.7.2. Dewetting Dynamics

Dewetting dynamics are governed by the balance between capillary forces and dissipation mechanisms; primarily viscous and friction dissipations. Redon *et al.* were the first to quantitatively examine dewetting of liquid polymer films and alkanes on nonwetting substrates [81]. They showed that dewetting dynamics of liquid films with thicknesses,  $h$ , about a few tens of microns ( $h > 10 \mu\text{m}$ ) on solid substrates is independent of the film thickness and inversely related to the liquid viscosity. They showed that the dewetting velocity,  $V_d$ , of such films within limits of weak slip ( $b \ll h$ ) is time-independent following:

$$V_d = \kappa \frac{\gamma}{\eta} \theta_e^3 \quad (b \ll h) \quad (2.4)$$

where  $\kappa$  a pre-factor depending on the nature and molecular weight of the liquid. Later on, to explain the dependence of  $\kappa$  on the polymer molecular weight, Redon *et al.* used the lubrication approximation and showed that  $\kappa$  is slightly dependent on  $b$  through a logarithmic term  $\kappa = 1/(12\sqrt{2} \ln(\theta_e w/b))$  where  $w$  is the rim width [84].

Thinner films with thicknesses about a few hundred nanometers, in contrast, are significantly more affected by slip and exhibit a time-dependent dewetting velocity ( $V_d \propto t^{-1/3}$ ). In general, aside from the melt viscosity and polymer/wall interfacial properties, the dewetting dynamics depend on the geometry: films thinner than the polymer slip length ( $h < b$  typically  $h < 1 \mu\text{m}$ ) undergo strong slip and time-dependent velocity whereas thicker films are most likely to show non/weak slip resulting in a dewetting velocity that remains constant over time [25,26,84-86]. The difference is due to a change in energy dissipation mechanism; in the no-slip regime, energy is mostly dissipated via viscous dissipation within the liquid with a Poiseuille velocity profile whereas under strong slip dissipation is mostly due to the friction at the polymer/wall interface. In the latter case, the velocity profile is close to plug flow since the slip length is larger than the thickness of the film [25,84,87]. Redon *et al.* also developed a simple scaling relation for the dewetting velocity of thin polymer films at strong slip ( $b \gg h$ ) as [84]:

$$V_d = \frac{b\gamma}{2\eta w} \theta_e^2 \quad (b \gg h) \quad (2.5)$$

Equation 2.5 shows that the dewetting velocity of thin films undergoing strong slip is directly related to the slip length at the polymer-solid interface. Figure 2.4 shows an example of the evolution of a dewetting hole in a  $\sim 200$  nm film of PS on Teflon-coated (AF2400) silicon substrate at  $150^\circ\text{C}$ . Slip properties can therefore be simply extracted using carefully designed dewetting experiments.

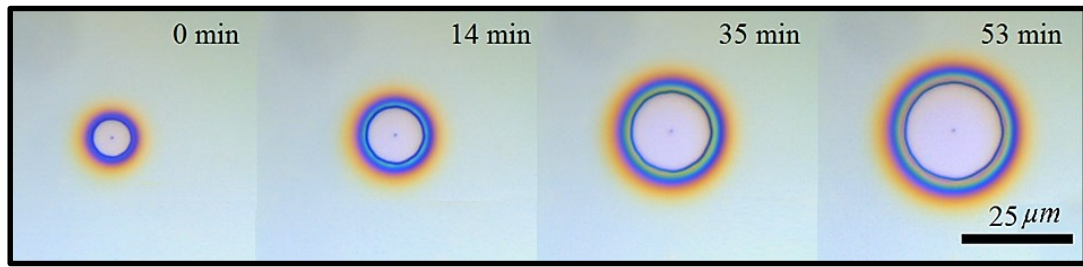


Figure 2.4. Evolution of a dewetting hole of a thin film (200 nm) of PS on a fluorinated (AF 2400) silicon substrate at  $150^\circ\text{C}$ .

Jacobs and coworkers extensively studied dewetting of thin polymer films on nonwetting substrates [25,45,88]. In their study of liquid films with partial slip, Jacobs *et al.* proposed that the dewetting dynamics can be obtained by the superposition of dissipation mechanisms of the two extreme cases, i.e., viscous dissipation in the no-slip and friction dissipation in the slip boundary condition [88]. The dewetting velocity in the case of thin films with partial slip can hence be obtained from:

$$V_d = \frac{|S|b}{3\eta w(t)} + C_v(\theta_r) \frac{|S|}{\eta} \quad (b \sim h) \quad (2.6)$$

where  $w(t)$  is the rim width which grows with time and  $C_v(\theta_r)$  is a prefactor characterizing the flow field near the contact line (being a function of the receding contact angle  $\theta_r$  only) [45]. The first term in right-hand side of Equation 2.6 represents the dewetting dynamics at short times (small  $w$ ) where the friction dissipation by slip mechanism is dominant. The second term in right-hand side of Equation 2.6 is the long time behavior where a

significantly large rim is built up and the viscous dissipation thus becomes the dominant dissipation mechanism. The slope of the line in graph of  $V_d$  versus  $w(t)$  thus gives the slip length at the liquid-solid interface.

### 2.7.3. Rim Morphology of Dewetting Hole/Front

Dewetting experiments can be used as a simple tool to investigate slip properties in thin film polymers [48,89-91]. Recent theoretical and experimental studies on the morphology of the dewetting hole/front on nanoscale thin films have revealed very interesting results. Jacobs and coworkers used atomic force microscopy, AFM, to characterize the height profiles of dewetting fronts and showed that the boundary condition at the polymer-wall interface directly governs the rim morphology [92,93]. They found that the strong slip boundary condition at the polymer-wall interface results in a monotonically decaying rim on the wet-side with a large decay length. The no-slip or weak slip boundary condition, on the other hand, gives an oscillatory rim profile with a very small decay length.

Figure 2.5 shows an AFM micrograph of a portion of a dewetting hole of PS ( $M_w = 490$  kg/mol) on a fluoropolymer (AF 2400) coated silicon wafer. A radial cut extending beyond the decay length of the wet-side of the rim is then used for profile analysis. Figure 2.6 shows a comparison of rim profiles of  $\sim 24$   $\mu\text{m}$  holes of two monodisperse PSs (PS(28k) with  $M_w = 28$  kg/mol and PS(490k) with  $M_w = 490$  kg/mol) placed on AF 2400. The vertical axis is the rim height  $h$  normalized by the film thickness  $h_0$  and the horizontal axis is distance to contact line  $\xi$  normalized by hole radius  $R$ . The oscillatory profile of PS(28k) represents weak slip whereas the monotonically decaying profile of PS(490k) represents strong slip at the buried interface.

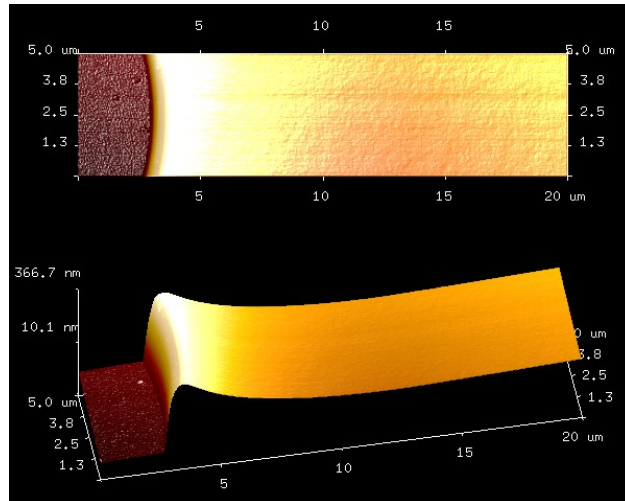


Figure 2.5. AFM micrograph of a portion of a dewetting hole of PS:  $M_w = 490$  kg/mol on AF 2400 coated silicon wafer; vertical view (top) and isotropic view (bottom).

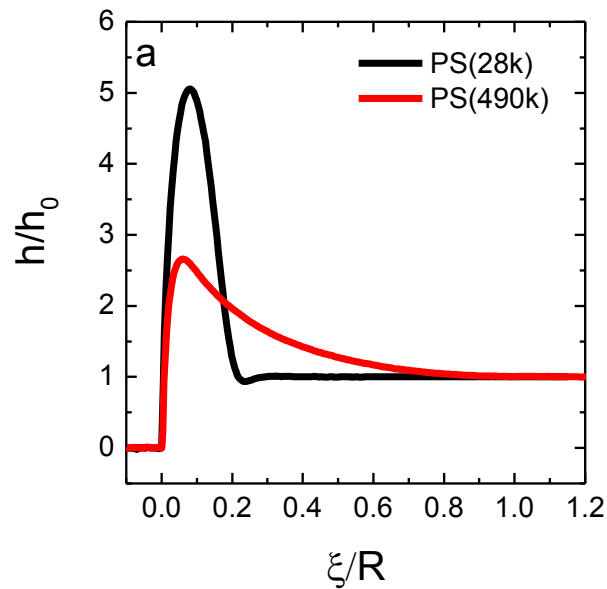


Figure 2.6. Rim height profiles of dewetting holes ( $\sim 24 \mu\text{m}$ ) between two monodisperse PSs: PS(28k) with  $M_w = 28$  kg/mol and PS(490k) with  $M_w = 490$  kg/mol placed on AF 2400. The profiles were characterized by AFM.

Fetzer *et al.* used hydrodynamic equations along with appropriate boundary conditions at the free surface and liquid-solid interface to model the rim height profile of the dewetting front [92,93]. The model in turn can be used to extract the slip length from the experimental data by a fitting procedure. Authors developed three models: the strong-slip lubrication

model, full Stokes model, and a third-order Taylor approximation of the full Stokes model. Among these models, the latter gives the least cumbersome characteristic equation with the widest range of validity and most accurate slip parameters. The characteristic equation of the third-order Taylor approximation model is as follows [93]:

$$\left(1 + \frac{h}{3b}\right)(h\Gamma)^3 + 4Ca \left(1 + \frac{h}{2b}\right)(h\Gamma)^2 - Ca \frac{h}{b} = 0 \quad (2.7)$$

where  $Ca$  is the capillary number defined as  $Ca = V_{d,f}\eta/\gamma$  in which  $V_{d,f}$  is the final dewetting velocity of the rim before the film is cooled to room temperature for height profile capture. The above characteristic equation gives one positive real root and either two negative or two complex conjugate roots from which only roots with negative real parts are physically relevant. By using the two roots  $\Gamma_1$  and  $\Gamma_2$  which are called the inverse decay lengths (they can be obtained from fitting a superposition of two exponential functions to monotonic rims or an exponentially damped oscillation to oscillatory rims), Equation 2.7 can be solved for  $b$  and  $Ca$  to obtain:

$$b = \frac{1}{4h} \frac{\Gamma_1^2 + \Gamma_1\Gamma_2 + \Gamma_2^2}{\Gamma_1^2\Gamma_2^2} - \frac{h}{2} \quad (2.8a)$$

$$Ca = \frac{h^3}{6} \frac{\Gamma_1^2\Gamma_2^2}{\Gamma_1 + \Gamma_2} - \frac{h}{4} \frac{\Gamma_1^2 + \Gamma_1\Gamma_2 + \Gamma_2^2}{\Gamma_1 + \Gamma_2} \quad (2.8b)$$

The technique for rim profile analysis of dewetting holes can be used to study polymer-solid boundary conditions of different kinds. Jacobs and coworkers studied slip of PS on silanized and fluorinated surfaces [25,45,90-93]. They reported that slip of polymers on silanized surfaces is highly sensitive to minute details of the grafted chains. They found that the slip properties of PS dewetting from a self-assembled monolayer (SAM)-coated silicon wafer changes significantly when the number of carbon atoms of the grafted monolayer changes slightly. In this regards, an unentangled PS on decyltrichlorosilane (DTS)-coated silicon wafer exhibits a higher slip length (an order of magnitude) than on octadecyltrichlorosilane (OTS)-coated silicon wafer. The two SAMs differ chemically only in the number of carbon atoms: DTS has 12 carbon atoms while OTS has 18 carbon atoms.

Using dewetting experiments of PS on a fluoropolymer (AF 1600) coated silicon wafer, the authors could furthermore reproduce the scaling law:  $b \propto M^3$  (for  $M > M_c$ ) of the Brochard and de Gennes theory of polymers on ideal surfaces ( $M_c$  is the critical molecular weight of the polymer) [25,45]. Dewetting as a result is a convenient tool to study slip of polymers on nonwetting surfaces.

## **2.8. Theoretical Disentanglement Models Predicting Slip**

As explained earlier in this chapter, the disentanglement mechanism is generally believed to be responsible for polymer wall slip on adsorbing surfaces [16,39]. The theoretical basis of the disentanglement mechanism was first introduced by Brochard and de Gennes in 1992 [29]. Their scaling model was later modified or extended. The theory is nevertheless applicable to monodisperse samples only and theories of the slip of polydisperse polymer melts flowing over grafted or adsorbed surfaces are not yet developed.

### **2.8.1. Brochard and de Gennes Scaling Model**

Brochard and de Gennes developed a scaling model for the shear flow of a highly entangled polymer melt on a solid substrate on which a few polymer chains were grafted [29]. At low shear rates where  $\sigma < \sigma^*$ , viscous dissipation by friction due to entanglements is dominant. Near  $\sigma^*$ , grafted chains undergo a coil stretch transition in which grafted chains constantly undergo deformation and relaxation. At  $\sigma > \sigma^*$ , grafted chains disentangle from the bulk and friction is dominant by Rouse behavior due to monomeric interactions. Significant slip may occur at this stage.

#### **i) Slip of Monodisperse Mobile Chains on Semi-Ideal Surfaces**

With polymer brushes, substrates are categorized based on the grafted density of polymer chains  $\nu$  defined as the reciprocal of the area between one chain and the adjacent grafted chain:  $\nu = d^{-2}$  where  $d$  is the distance between grafting points. On a semi-ideal substrate, grafted chains are independent and do not overlap hence more or less act like

single chains pinned at one end to the substrate. This is called the mushroom regime at which  $v \leq 1/R_0^2$  where  $R_0 = aN^{1/2}$  is called the coil size of the grafted chain ( $a$  is a monomer size and  $N$  is the number of monomers per grafted chain). Progressively increasing the grafting density results in the transition from the mushroom regime to a polymer brush where grafted chains overlap and become tightly packed.

Brochard and de Gennes first started with modeling the slip behavior of a single tethered chain ( $Z$ -mers in length) immersed in a moving polymer melt with chains  $P$ -mers in length. The problem was then generalized to the case of a surface with a few chains grafted to it (the mushroom regime). Scaling laws were established based on the sliding motion of the entangled melt on grafted chains. The extent of slip therefore depends on the amount of friction that bulk chains exert on grafted chains.

A few assumptions were made: i) mobile chains are longer than those grafted  $N > Z$ , ii) the melt viscosity  $\eta$  is the same at all scales, iii) the shear stress is the same at all distances from the interface, i.e., simple shear flow near the surface, and iv) there is a finite velocity at the interface  $V|_{z=0} = v_s = \dot{\gamma}b$ .

At small velocities at the weak slip regime, the relaxation time of grafted chains is smaller than the time scale of shear deformation hence chains remain un-deformed. Slip is drastically suppressed and slip length becomes a small constant value independent of the shear rate:

$$b_0 \cong (vR_0)^{-1} \quad (2.9)$$

where  $R_0 = Z^{1/2}a$  is the grafted chain coil size and  $a$  is the monomer size. This relationship gives small  $b_0$  values on the order of a few nanometers. In the transition regime, the slip velocity is between two critical values  $v_s^* < v_s < v_{s1}$  and grafted chains undergo a coil stretch transition in which they repeatedly entangle and disentangle from the bulk. The critical slip velocity  $v_s^*$  is defined by the balance between the friction force acting on a grafted chain and the ‘entropic elastic restoring force’ due to its deformation:

$$v_s^* \cong \frac{kT}{\eta R_0^2} = \frac{kT}{\eta Z a^2} \quad (2.10)$$

where  $kT$  is the energy unit in molecular scales. The corresponding shear stress and slip length are obtained from:

$$\sigma^* \cong \frac{\nu kT}{aN_e^{1/2}} \quad (2.11)$$

$$b^* \cong \frac{N_e^{1/2}}{\nu Z a} \quad (2.12)$$

The shear stress remains almost constant throughout the transition region. In this regime, the slip length increases linearly with the slip velocity:

$$b(v_s) = \frac{\eta v_s}{\sigma^*} = \frac{aN_e^{1/2}\eta v_s}{\nu kT} \quad (2.13)$$

At a second characteristic velocity termed as  $v_{s1}$  larger than  $v_s^*$ , disentanglements starts to occur and the friction force reduces to Rouse friction which is much weaker than the entangled friction in bulk dissipation. The friction force in this stage becomes a sum of independent contributions from each monomer. The  $v_{s1}$  is defined as:

$$v_{s1} = v_s^* \frac{\eta}{\eta_m N_e^{1/2}} \quad (2.14)$$

where  $\eta_m$  and  $N_e$  are the monomer viscosity and number of monomers between entanglements, respectively. At even higher velocities above  $v_{s1}$ , bulk chains completely disentangle from grafted chains and slip length becomes independent of the slip velocity again. This is called the disentangled regime. Since the substrate was originally in the mushroom state, the slip length finally saturates to its value for an ideal substrate  $b_\infty$ :

$$b \sim b_\infty \cong a \frac{N^3}{N_e^2} \quad (2.15)$$

Brochard and de Gennes explained that the upper limit of the linear relationship  $b(v_s)$  is not  $v_s = v_{s1}$  but a smaller velocity they called  $v_{s2}$ . When  $v_s = v_{s2}$ , the slip length becomes equal to  $b_\infty$ . At this stage, the dissipation due to grafted chains become negligible. The shear stress after disentanglements becomes linear in  $v_s$  ( $\sigma \sim k_m v_s$ : this term describes the weak friction due to monomer wall interactions). The ratio of slip lengths between the two extreme cases of weak to strong slip  $b_\infty/b_0$  is very large:

$$\frac{b_\infty}{b_0} \sim \frac{\eta}{\eta_m} Z^{-1/2} \quad (2.16)$$

Schematics of the behavior of slip velocity versus surface shear stress and slip length versus the slip velocity for a melt flowing on a grafted surface are shown in Figure 2.7. In this figure, E, M and D stand for entangled, marginal, and disentangled regimes, respectively.

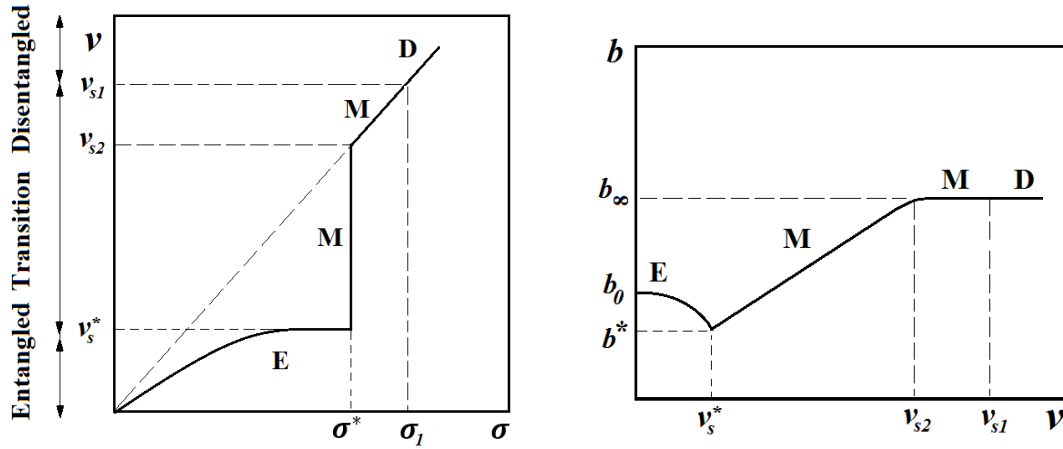


Figure 2.7. (a) A schematic of slip velocity versus surface shear stress for a melt flowing on a grafted surface and (b) slip length versus slip velocity (Adapted from ref [29]). E, M and D stand for entangled, marginal, and disentangled regimes, respectively.

## ii) Effect of Polydispersity

Brochard and de Gennes briefly discussed the effect of polydispersity of grafted chains on the slip velocity [29]. The polydispersity was considered as the number distribution of grafted chains with different chain length through  $\nu(Z)$ , the number of grafted chains with

$Z$  units per unit area. It was explained that in the transition regime the sharp transition in the velocity-stress plot blurs by introducing the polydispersity effect.

### 2.8.2. Later Disentanglement Slip Models

Ajdari *et al.* added relaxation mechanisms such as arm retraction and constraint release of grafted chains into their scaling laws [32]. In their work, the problem of a single chain pulled from one end through an entangled melt was modeled. They took into account the effect of non-homogenous deformation of the grafted chain due to different relaxation mechanisms acting on different parts of the chains. Different cases of short, intermediate and long mobile chains flowing on a surface grafted with moderately long chains in the mushroom regime were solved. They constructed similar shear stress-slip velocity curves as shown in Figure 2.7a). They found that the details of  $v(\sigma)$  before  $\sigma^*$  slightly changes although the general picture of Figure 2.7a) remains valid.

Brochard *et al.* extended their slip model and included the effect of different grafting densities while the surface is still in the mushroom regime [30]. They argued that for low grafting densities below a critical value  $\nu < \nu_c$ , one mobile chain is entangled with one mushroom and the effect of grafted chains is additive. Above the threshold however, one mobile chain is entangled with more than one mushroom and therefore the sliding motion of one mobile chain releases many entanglements. This cooperative effect reduces the effective dissipation per chain. The grafted and mobile chains at the interface thus deform less at a fixed velocity and the characteristic velocity for the onset of chain deformation and transitional regime increases.

Starting with the slip model of Ajdari *et al.*, Mhetar and Archer developed a new scaling model for slip of a highly entangled  $P$ -mer melt flowing on a surface with a few  $Z$ -mer grafted chains in the mushroom regime [16,41]. The relaxation dynamics and configuration of grafted chains including arm retraction and constraint release were taken into account. They found that the friction force between mobile and grafted chains strongly depends on the slip velocity. A more detailed slip velocity – shear stress curve including 5 different slip regimes (for the case of  $P = Z$ ) was constructed. The first 3 regimes included

the chain-chain entangled behavior; transition to the disentanglement regime started at regime 4; regime 5 included the disentangled slip behavior which models flow of a melt on a layer of monomers with a very large slip length as discussed before.

Gay reviewed the progress of slip models after the 1992 model of Brochard and de Gennes in addition to some experimental results [34]. The author modified the sliding motion of mobile chains in the slip model by incorporating the tube renewal mechanism to more realistically describe the interfacial friction of the entangled melt. This did not result in a better prediction although a deeper understanding of the chain behavior in a more realistic manner was achieved.

The behavior of entangled melt on a grafted brush was also investigated. It was proposed that there is a critical grafting density above which the number of mobile chains trapped with those grafted becomes fixed. In other words, the effect of grafting density becomes saturated. As a result, in the saturated regime, the low velocity slip length is a constant value independent of the grafting density, as:

$$b_0 \cong aP^{\frac{1}{2}} = R_p \quad (2.17)$$

This was shown to be consistent with experimental results from Durliat *et al.* [46] although an order of magnitude difference in prefactors exists. The critical slip velocity  $v_s^*$  for the onset of the transition regime was found to be proportional to the grafting density. Durliat *et al.* however showed that  $v_s^*$  starts to decrease when grafting density increases above a certain value at very high grafting densities. Gay suggested that there exists a new topological behavior at high grafting densities and the exact behavior of grafted chains at this point is not yet understood.

Joshi *et al.* proposed a unified transient network model which can predict both disentanglement and desorption slip mechanisms depending on a chain-wall interaction parameter [35,37]. They modeled the capillary flow of a fluid on a very high energy surface. The entanglements form the transient network and the entanglement – disentanglement process is written as a kinetic reaction.

In transient network models, the entanglement points are called junctions and segments are Gaussian springs connecting two neighboring junctions. The stress is assumed to be localized at these junctions and sum of individual contributions from each segment makes the total stress. To solve the problem of slip, it was assumed that the entanglement – disentanglement dynamics of the chains adsorbed to the wall is different from those in the bulk. The capillary was divided into two domains, the wall and the bulk. The wall domain was considered to be of thicknesses on order of radius of gyration of the chains.

The kinetics of entanglement – disentanglement process is determined by the rate of creation and loss of these segments. For simplicity, they assumed that creation and loss rates are functions of the effective strain. To model the disentanglement slip mechanism, the creation and loss rates of entanglements increase up to a threshold after which they remain constant. The main resulting equation is [37]:

$$\tau_{rx} \equiv G_0 \gamma_e \frac{f}{g} = -\frac{r}{2} \frac{\partial P}{\partial x} \quad (2.18)$$

in which  $\tau_{rx}$  is the shear stress at the wall along the flow direction,  $G_0$  is the constant modulus,  $\gamma_e$  is the effective strain,  $f$  and  $g$  are rates of creation and loss of entanglements, respectively,  $r$  is the radial coordinate, and  $\frac{\partial P}{\partial x}$  is the pressure gradient along the flow direction  $x$ . In this equation,  $f$  and  $g$  are explicit functions of  $\gamma_e$ . The equation describes the stress-strain relation on a fluid element in capillary flow although it can be defined for other simple shear flows.

The predictions of the transient network model of Joshi *et al.* could predict polymer wall slip in qualitative agreement with those of the Brochard and de Gennes model. Three distinct slip regimes were predicted. It was also found that the critical shear stress for the onset of transition depends directly on the density of adsorbed chains.

Joshi *et al.* also developed a molecular constitutive equation according to the contour variable tube model to predict polymer wall slip by the disentanglement mechanism [38]. They dealt with the dynamics of tethered chains grafted on a high energy surface in the

mushroom regime above which an entangled melt flows. The key was to incorporate certain important differences between the dynamics of mobile and grafted chains in their contour variable tube model.

In the basic tube model, a probe chain is supposed to be trapped in a tube constrained by its neighboring chains. The motion of the tube is limited laterally normal to the tube wall and can only move forward or backward along its contour. The chain as a result can only have snake-like motion - called reptation - along its contour.

Under flow conditions, chain dynamics is governed by several mechanisms including convection, constraint release, and thermal fluctuations [39]. Convection is the deformation of the primitive path of a chain by convective flow of the surrounding bulk chains. In case of a tethered chain, convection forces the chain to be aligned with the flow direction and ultimately presses it against the wall. Tethered chains under flow are hence stretched due to convection. The chain responds to such stretch by retracting inside its own tube which is called convective constraint release. Retraction works in parallel with convection. Since the tube of a chain is made by confinements – entanglements – of the neighboring chains, the motion of each neighbor may release a constraint on the tube. The tube thus experiences a local relaxation within a distance about the size of the tube diameter. The constraint release by the reptation of neighboring chains thus randomizes the configuration of tethered chains and prevents them from being aligned by convection. Finally, chain thermal fluctuations inside the tube change the length of its primitive path. This causes further relaxation of the chain along its length (contour length fluctuations) and near its free end: in the case of tethered chains this is similar to the arm retraction relaxation in branched polymers.

In the contour variable tube model, the chain can relax and renew its configuration via all relaxation mechanisms provided by its own motion or that of neighboring chains. In their model, Joshi *et al.* included all known forms of tethered chain relaxations: arm retraction, contour length fluctuation, thermal constraint release (reptation), and convective constraint release [94,95]). Their scaling model gives predictions in agreement with previous slip theories. As they wrote, the importance of their work with respect to previous

slip theories was that the grafted chains experience a *suppressed* convective contour relaxation so that they become oriented along the flow above the critical shear stress. They believed that this is a “main molecular mechanism that drives strong slip by sudden disentanglement and has not been recognized in any of the previous scaling models for slip”. The authors made a comparison with experimental data from Leger and coworkers and presented a good agreement with their model predictions. Predictions of slip length versus slip velocity seemed to be deviating from experimental data at the strong slip regime [38].

Tchesnokov *et al.* proposed a new molecular model of polymer wall slip in accord with the disentanglement mechanism [39]. Their model accounts for a wide range of grafting densities beyond the typical mushroom regime investigated in many other slip studies. They assumed that there exists a near-the-wall boundary layer of adsorbed chains - called the interfacial layer – the dynamics of which coupled with that of bulk chains governs the polymer wall slip behavior. Furthermore, for simplicity, adsorbed chains were treated as end-tethered chains and their length distribution was considered uniform (these simplifications are typical of all slip models). Similar to Joshi *et al.* [38], the authors included all known relaxation mechanisms of tethered chains. It was found that flow dynamics of near-the-wall boundary layer of chains is governed by a nonlinear equation of motion. Predictions of their model were in good agreement of experimental works of Leger and coworkers within the weak and transition regimes. The onset of critical slip was related to the disentanglement of the bulk from the adsorbed chains. The decrease of the critical shear rate with the increase of the surface density of grafted chains was related to the disentanglement and suppressed constraint release. Their final constitutive equations have a simple structure not requiring expensive numerical calculations [39]. They, however, did not provide any knowledge of the slip behavior of the strong slip regime.

### **2.8.3. Limitations of Slip Models**

All polymer slip theories are applicable to monodisperse samples flowing on surfaces with well controlled density of end-grafted chains. In a real system however, chains adsorb

onto the solid surface instead of being end-tethered, thus: i) there may be several adsorption sites per chain giving rise to many loops and tails and ii) the density of chain adsorption is unknown. Even for a monodisperse melt, as a result, there exists a polydispersity effect peculiar to chain adsorption [19]. The average molecular weight, entanglement density, and radius of gyration of the adsorbed chains may also be consequently lower than that of the bulk. Shorter chains are more resistant to flow orientation, they have lower elasticity and deform less, they diffuse faster, and they have shorter relaxation times than longer chains. Chain relaxation mechanisms have to be extensively modified; constraint release and constraint convective release becomes faster due to shorter chains [38]. Slip dynamics as a consequence are expected to be highly influenced by the polydispersity effect.

In flow of polydisperse melts, the effect of the polydispersity of the adsorbed chains can be significantly stronger or different compared to monodisperse melts: the length distribution of adsorbed chains can be wider or even skewed depending on chain segregation mechanisms. The mobile chains are also polydisperse and their relaxation mechanisms need to be modified. Relaxation dynamics of adsorbed chains are further affected by the presence of polydisperse mobile chains in the immediate vicinity of the adsorbed layer. Overall, slip dynamics can be significantly different in polydisperse polymers.

Most slip models are limited to low densities of grafted chains where there exist no overlap between the two neighboring chains. In a real system, the density of adsorbed chains can be quite high specifically on high surface energy substrates and therefore interactions between neighboring adsorbed molecules as well as subsequent implications on their orientation and structure need to be taken into account. Specific cases including polymer brushes and SAMs coated substrates in which the degree of interdiffusivity of bulk chains into the interfacial layer significantly differs from commonly used substrates need particular attention. Recent dewetting studies of thin polymer films on silanized substrates show that chain ordering and roughness of atomic scale are of significant importance on polymer wall slip [92,93].

### 3. CHAPTER 3

#### Wall Slip of Bidisperse Linear Polymer Melts<sup>1,2</sup>

S. Mostafa Sabzevari †, Itai Cohen ‡, and Paula M. Wood-Adams \*†

† *Department of Mechanical and Industrial Engineering, Concordia University, Montreal, QC, Canada*

‡ *Department of Physics, Cornell University, Ithaca, New York 14853, United States*

#### Abstract

We have characterized the effect of molecular weight distribution on slip of linear 1,4-polybutadiene samples sandwiched between cover glass and silicon wafer. Monodisperse polybutadiene samples with molecular weights in the range of 4 to 195 kg/mol and their binary mixtures were examined at steady-state in planar Couette flow using tracer particle velocimetry. Slip velocity was measured at shear rates over the range of  $\sim 0.1 - 15 \text{ s}^{-1}$ . Our results revealed that weakly entangled short chains play a crucial role in wall slip and flow dynamics of linear polymer melts. It was found that the critical shear stress for the onset of the transition to the strong slip regime is significantly reduced when a small amount of weakly entangled chains is added to a sample of highly entangled polymer. Within the same range of shear stresses, binary mixtures of long and short chains exhibit significantly enhanced slip compared to the moderate slip of the individual long chains. This is attributed to the reduced friction coefficient at the polymer-solid interface which is likely a complicated function of the nature of entanglement, chain adsorption and relaxation dynamics of chains at the interface.

---

<sup>1</sup> This chapter is published as: S. Mostafa Sabzevari, Itai Cohen, and Paula M. Wood-Adams, “Wall Slip of Bidisperse Linear Polymer Melts”, *Macromolecules*, **2014**, 47, 3154–3160.

<sup>2</sup> Additional information is given in Appendix A.

### 3.1. Introduction

Historically, the no-slip liquid-solid boundary condition was presumed to be true for every type of problem in the field of fluid dynamics until implications of slip such as shear stress reduction, gap dependence shear stress, and flow rate discontinuity (spurt) showed up in the study of non-Newtonian fluids specifically polymers [1]. Today, it is well established that highly entangled linear polymer melts and concentrated solutions exhibit perceptible slip during flow on solid substrates [49]. Nevertheless, the extent to which polymers slip and its relationship to polymer structure still remains ambiguous due to the vast number of influential factors and the complexity of the phenomenon [2,57].

Slip plays an important role in the flow dynamics of polymers in various practical applications such as extrusion, mixing, coating, and lubrication. Depending on the application, slip can be beneficial or detrimental. In polymer processing, slip is beneficial where i) it reduces the required force/pressure for a certain drag/flow rate of fluid by lowering the wall shear stress and ii) it (potentially) expands the margins within which defect-free and smooth-surface products can be produced (slip has been long related to surface distortions in extrusion-based polymer processing techniques although a clear cause-effect understanding has not yet been obtained) [2,4,6-13,18,23,63].

Slip is detrimental i) in polymer mixing where high shear is desired and ii) in rheometry where accurate measurement of material properties requires ideal flow conditions. Therefore the thorough characterization of slip is necessary not only to collect accurate rheological measurements but also to precisely design and produce polymers for particular applications such as lubricants, anti-slip polymers, and products with desirable surface finishes. Another important advantage of having this knowledge is that it allows for the development of accurate slip theories that can be used in flow simulations and other design analyses.

The factors influencing slip of polymers include the chemical and physical properties of both substrate and polymer: slip is most importantly affected by substrate surface energy, substrate roughness, polymer chemistry, molecular weight, molecular weight distribution, and chain architecture [3,5,14-16,19-21,24,41,46]. Although a great deal of

knowledge has been well established on this subject – several comprehensive reviews can be found in Refs. [2,19,57] – the effects of parameters such as molecular weight distribution and low molecular weight chains have rarely been thoroughly explored in previous studies [57,67].

Polydispersity in molecular weight is a rather complicating factor in the field of polymer physics and it has not yet been fully incorporated in polymer molecular theories even those for bulk rheology [58]. In the case of slip of polymers, the available molecular theories [26,30-34] are applicable to monodisperse systems only and were never extended to polydisperse systems typical of industrial polymers. In the most recent review of the subject in 2012 by Hatzikiriakos [57], the author reminds us of the necessity of further work to investigate the effect of polydispersity on wall slip of polymers.

There is much experimental evidence that short chains or low molecular weight species play a critical role in physics and flow dynamics of molten polymers. Samples with broad molecular weight distributions are well known to begin shear thinning at smaller shear rates compared to narrowly distributed samples. Several researchers [58-61] showed that incorporation of short chains into the network of long chains accelerates relaxation of long chains and reduces the mixture plateau modulus,  $G_N(\varphi)$ . In capillary extrusion, Blyler and Hart [56] observed a considerable reduction in the magnitude of the flow curve discontinuity when different fractions of a low molecular weight polyethylene (PE) wax were added to a sample of high molecular weight linear PE. Similar results were found by Schreiber [62] who also showed that the shape of molecular weight distribution influences the flow curve discontinuity and blends containing “components with widely different molecular weights are far more effective than broader but more normally shaped distributions” at reducing the magnitude of the discontinuity. Recently, Inn [63] studied capillary flow of three bimodal PE resins of similar viscosity. They observed that the sample with i) higher content of the low molecular weight population and ii) highest molecular weight of the high molecular weight population showed the largest slip as determined indirectly. These observations imply that short chains play a significant role in flow dynamics of highly entangled polymers. Here, we investigate slip of monodisperse and binary mixtures of polybutadiene (PBD) samples comprising long and short chains and

varying “Struglinski-Graessley parameter”  $G_r$  [60] where  $G_r = M_2 M_e^2 / M_1^3$ ,  $M_1$  and  $M_2$  are molecular weights of short and long chains, respectively, and  $M_e$  is the molecular weight between entanglements (for PBD  $M_e = 1650$  g/mol). The long chains in binary mixtures with  $G_r > 1$  are known to exhibit constraint release in a dilated tube [59-61,96]. This indicates that the disentanglement believed to cause the onset of strong slip may be very different when  $G_r > 1$ . It would be interesting to examine the influence of short chains on slip of highly entangled polymers using a series of binary mixtures with  $G_r > 1$ .

In the present work, using tracer particle velocimetry in steady-state planar Couette flow, we report for the first time that a monodisperse sample of long chains exhibiting moderate slip undergoes substantial slip when mixed with a small fraction of weakly entangled short chains. These results can conveniently be exploited towards improving the existing slip theories. We also note that the use of planar Couette flow rules out the long-debated hypothesis of shear-induced fractionation which leads to the formation of a low-viscosity layer by migration of short chains towards the interface [63].

## 3.2. Materials and Experiments

We use narrow-distributed linear 1,4-polybutadiene (PBD) (cis 68%, trans 27% and 1,2 addition 5%) with four different weight average molecular weights:  $M_w = 4, 73, 88$  and  $195$  kg/mol and polydispersity indices  $PI \leq 1.08$  (Table 3.1) provided by Polymer Source Inc. Molecular weight distributions were measured using a Waters gel permeation chromatograph with tetrahydrofuran as diluent. The molecular weights are reported relative to polystyrene standards as determined from elution time and a refractive index detector.

All slip measurements were performed at room temperature. Experiments were carried out on monodisperse samples and their binary mixtures as shown in Table 3.2 ( $\varphi_L$  is the weight fraction of long chains and  $\eta_0$  is the zero shear viscosity). The Struglinski-Graessley parameters for the 4k/88k, 88k/195k, and 4k/195k binary mixtures are 3.023, 0.001, and 6.694 respectively.

To prepare binary samples, 5 wt% solutions of monodisperse PBDs in dichloromethane were mixed together in the appropriate proportions by weight to obtain the desired composition. A small amount (less than 0.5 wt%) of surface-treated (hexyltrimethoxysilane) fluorophore nanoparticles (nominal size of 75 nm) suspended in ethanol (2mg/ml) was then added to each sample to be used as tracer particles for velocimetry measurements. Samples were dried at room temperature and under vacuum for 3 days to minimize residual traces of solvent molecules.

The dynamic linear viscoelastic properties were characterized by small-amplitude-oscillatory-shear (SAOS) measurements using a stress-controlled Paar Physica rotational rheometer (MCR 500). Measurements were done using 8-mm diameter stainless steel parallel plates with a gap of 1 mm under a nitrogen atmosphere. The plateau modulus  $G_N(\varphi)$  was calculated from  $G_N = 3.56G''_{max}$  which is an appropriate estimation for bidisperse samples of long and short chains as shown by Wang *et al.* [58] and Liu *et al.* [97]. The disentanglement relaxation time  $\tau_d$  was calculated from  $\tau_d = 1/\omega_c$  where  $\omega_c$  is the angular frequency at which  $G'(\omega_c) = G''(\omega_c)$  [58].

Slip measurements were done by tracer particle velocimetry [49] utilizing a microfluidic shear cell and confocal microscopy. A detailed description of the experimental procedure can be found elsewhere [49]. The top plate was a silicon wafer whereas the bottom plate was a thin cover glass to transmit fluorescent light to, and, from nanoparticles. The gap was set to 85 - 90  $\mu\text{m}$  and the drag flow was provided by moving the bottom plate. During shearing, the polymer sample was illuminated by fluorescent light and the reflection at the center of the sample and distance  $z$  from the top plate was captured by a high speed digital camera at 50 fps and with a 63x objective. Samples were sheared well into steady-state as confirmed by the velocity-time data (see e.g. Figure 3.1) for all results here.

Table 3.1. Molecular characteristics of monodisperse PBDs

Sym.	$M_w$ [kg/mol]	$M_w/M_n$ <sup>i</sup>	$M_w/M_e$
4k	4.3	1.06	3
73k	73.1	1.03	44
88k	88.2	1.05	53
195k	195.3	1.08	118

<sup>i</sup>  $M_n$  is the number average molecular weight.

The velocity data including slip velocity and the corresponding shear rate in the steady-state region were obtained through image processing using a modified version of MATPIV [49,98]. Confocal microscopy let us observe the velocity profile across the gap.

The main quantity examined in this work is the slip velocity of PBD over the silicon wafer  $v_s^t$  (which we refer to as  $v_s$  hereafter). In order to locate the PBD-silicon wafer interface ( $z = 0$ ), the focal point of the objective was moved up towards the silicon wafer (stationary plate) until no tracer particles could be observed. The focal point was then slowly moved down (with increments of  $0.1 \mu\text{m}$ ) into the polymer sample until the very first tracer particles were observed. This point was regarded as  $z = 0$ . This interface identification process was repeated three times to ensure the same location is inferred as the interface for each shear flow experiment. Considering the spatial resolution of the confocal microscope and the method we used to locate the interface, uncertainty in the location of polymer-solid interface as well as the slip length is  $\sim \pm 0.1 \mu\text{m}$ .

Table 3.2. Molecular characteristics of binary PBD mixtures

Sample	Sym.	$\varphi_L$ [wt%]	$\eta_0$ [kPa.s]	$G_N$ [kPa]	$\tau_d$ [s]	$\sigma^*$ [kPa]
4k/88k	B1	0.76	NA <sup>i</sup>	NA <sup>i</sup>	NA <sup>i</sup>	NA <sup>ii</sup>
88k/195k	B2	0.51	21.5	NA <sup>i</sup>	0.03	NA <sup>ii</sup>
4k/195k	L0	0	0.002 <sup>iii</sup>	NA <sup>i</sup>	NA <sup>i</sup>	NA <sup>ii</sup>
4k/195k	L30	0.30	0.9	73	0.03	2
4k/195k	L50	0.50	7.9	252	0.04	6
4k/195k	L74	0.74	27.0	502	0.07	20
4k/195k	L90	0.90	53.2	862	0.08	59
4k/195k	L100	1.00	71.7	1040	0.09	66

<sup>i</sup> LVE properties of this melt not measured due to instrument limitations

<sup>ii</sup> Does not exhibit strong slip

<sup>iii</sup> Obtained from Ref. [52]

The slip velocity at PBD-silicon wafer interface was measured over a wide range of nominal shear rates:  $\dot{\gamma}_n \sim 0.1 - 15 \text{ s}^{-1}$ . It is important to note that the maximum shear rate imposed on each sample is limited either geometrically or by the melt rupture of PBD at high shear stresses. We performed additional measurements to examine the velocity profile across the gap at several rates. The profiles were found to be linear or slightly curved as

shown for example in Figure 3.2. Since obtaining the velocity profile requires a large amount of image processing, the velocity profile was measured only at 5 different rates  $\sim 0.6, 1.2, 2.4, 4.8,$  and  $7 \text{ s}^{-1}$  covering the entire range of weak to strong slip behavior.

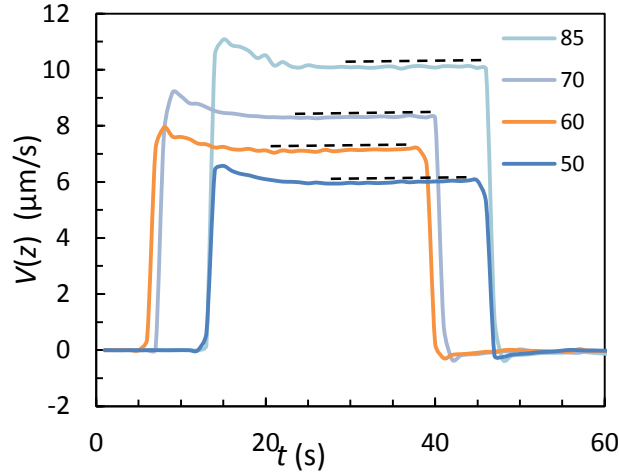


Figure 3.1. Velocity of nanoparticles  $V(z)$  of binary sample L74 at different values of  $z$  as labeled (units are in  $\mu\text{m}$ ) as a function of time  $t$ . Steady-state velocity was ensured at long times. Dashed lines indicate steady-state values.

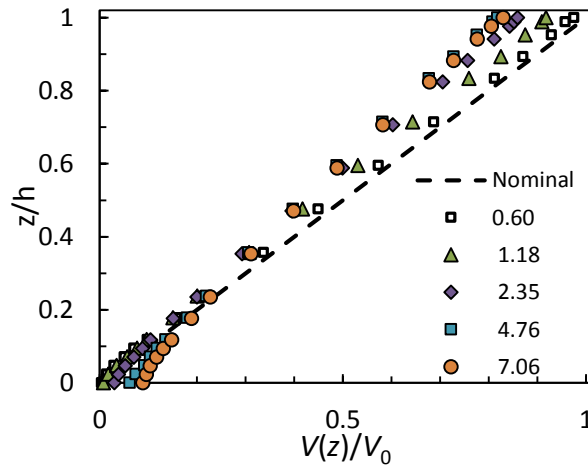


Figure 3.2. Normalized velocity profiles of binary sample L74 at nominal shear rates  $\dot{\gamma}_n$  as labeled (units are in  $\text{s}^{-1}$ ). The vertical axis is the distance  $z$  from the stationary plate (silicon wafer) normalized by the gap  $h$  and the horizontal axis is the velocity of nanoparticles  $V(z)$  normalized by the moving plate (cover glass,  $z = 1$ ) velocity  $V_0$ .

Finally, we would like to consider the slip length  $b$ . The slip length is defined as the distance from the interface at which the velocity profile extrapolates to zero. In the planar Couette flow  $b$  is defined as  $b = v_s/\dot{\gamma}_T$  where  $\dot{\gamma}_T$  is the true shear rate experienced by the sample:  $\dot{\gamma}_T = \dot{\gamma}_n - (v_s^t + v_s^b)/h$ . Here,  $v_s^t$  and  $v_s^b$  are slip velocities at the top (silicon wafer) and bottom (cover glass) plates, respectively, and  $h$  is the gap between the two plates. We note that values of  $v_s^t$  and  $v_s^b$  are not the same. To calculate  $\dot{\gamma}_T$  and hence  $b$ , we use the same  $v_s^t$  based on direct measurement of slip velocity on silicon wafer. Since we measured the  $v_s^b$  only at a few nominal shear rates (the same shear rates we did the velocity profile measurements), we estimate the rest of  $v_s^b$  data through interpolation/extrapolation from those measured ( $v_s^b$  versus  $V_0$ , see e.g. Figure 3.3).

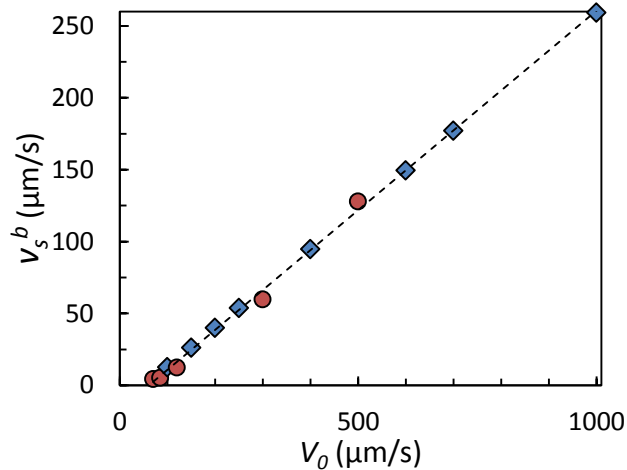


Figure 3.3. Slip velocity of L90 on cover glass  $v_s^b$  versus moving plate velocity  $V_0$ . Solid circles are experimental data whereas solid diamonds are estimated data-points by interpolation/extrapolation through linear regression (dashed line).

### 3.3. Results and Discussion

Understanding the wall slip of polymers requires knowledge of bulk rheological properties importantly viscosity in addition to near-wall properties. Figure 3.4 displays the rheological properties of binary 195k/4k PBD mixtures. As we will discuss in the upcoming sections, the systematic shift of the complex viscosity curve to lower values is a result of the simple dilution effect of short chains. This is important since it rules out the

role of viscosity in any *abrupt* change in slip characteristics of binary samples as compared to the monodisperse constituents.

In the past, it was shown both experimentally [19,21,46] and theoretically [29,30] that slip of *highly entangled polymers* over solid substrates can be characterized by three distinct slip regimes; the weak slip regime, the transition regime, and the strong slip regime (known as macroscopic slip in capillary experiments).

The slip velocity as a function of shear stress  $\sigma$  for the flow of monodisperse PBDs on silicon wafer is shown in Figure 3.5. The shear stress was calculated from  $\sigma \cong \dot{\gamma}_T |\eta^*(\omega = \dot{\gamma}_T)|$  which is a realistic estimation since we use  $\dot{\gamma}_T$  and we are close to the Newtonian plateau in all cases such that the Cox-Merz relation is very likely to be appropriate. For all samples (except the 4k chains)  $\eta^*(\omega)$  was measured by SAOS using rotational rheometer. For the 4k chains, the Newtonian viscosity was taken from literature [52].

Several features can be understood from the data in Figure 3.5. Except for the high-shear stress portion of 195k, all monodisperse PBDs exhibit a power-law relationship between the slip velocity and shear stress:  $v_s \propto \sigma^\alpha$  (here  $\alpha$  varies from 0.74 to 1). Several previous researchers established similar relationships for the slip of linear polymers [41,46,49]. The 195k PBD sample exhibits different behavior: at high shear stresses, the slip transitions to a higher slip velocity regime (strong slip). For PBD, the strong slip regime has been observed for molecular weights above  $\sim 100$  kg/mol only [13,16,99]. Similarly, Figure 3.5 confirms that PBD 195k is the only sample exhibiting a slight transition to the strong slip regime.

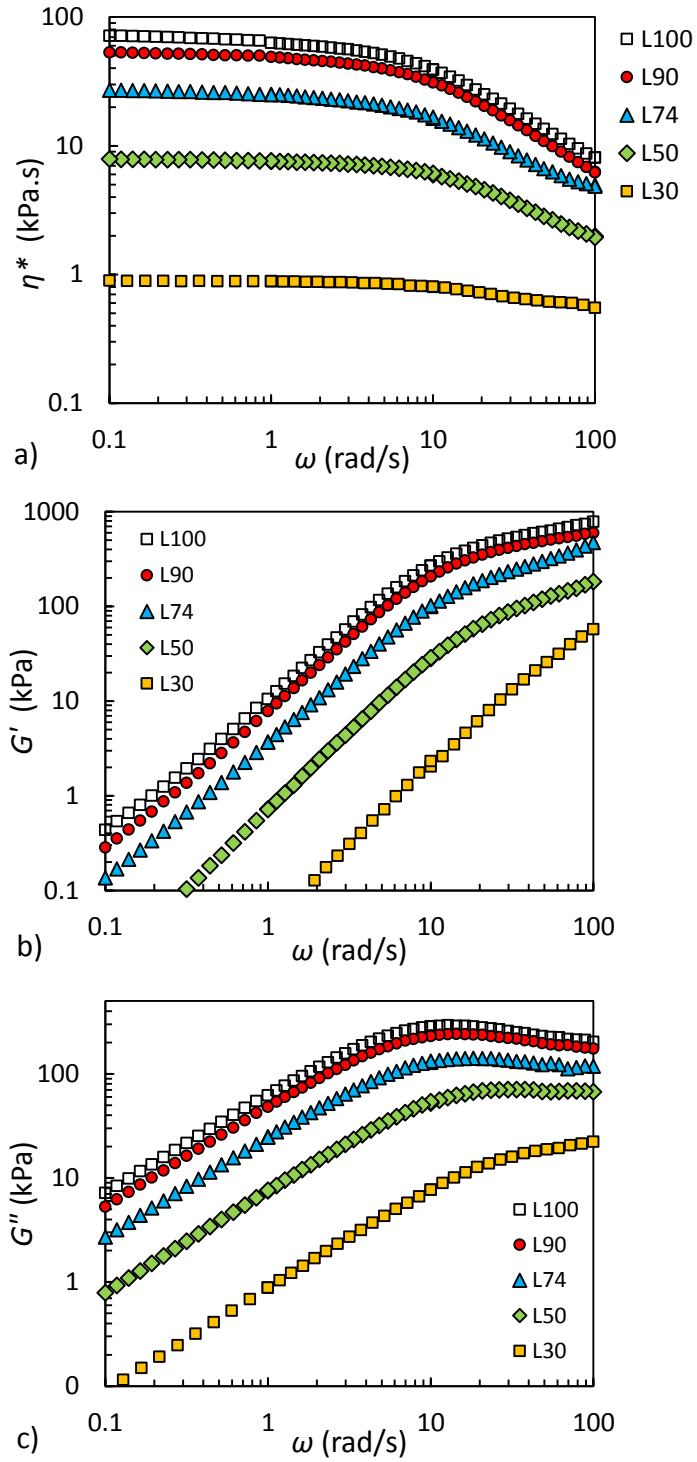


Figure 3.4. a) Complex viscosity  $\eta^*(\omega)$ , b) storage modulus  $G'(\omega)$ , and c) loss modulus  $G''(\omega)$  as a function of angular frequency  $\omega$  of binary 4k/195k PBD mixtures.

The data in Figure 3.5 as well illustrates another important feature; monodisperse PBDs with higher molecular weights require higher shear stresses to slip. For instance, 195k sample compared to 4k requires shear stresses orders of magnitude larger to exhibit the same slip velocity. This is an indication of a difference in the corresponding friction coefficient.

Brochard and de Gennes in their 1992 slip theory [31] introduced an alternative relationship for the shear stress under slip conditions:  $\sigma = k_f v_s$  where  $k_f$  is the friction coefficient indicating the interactions between i) the adsorbed and mobile chains (chain-chain interactions) and ii) the mobile chains and wall (chain-wall interactions). Using the data in Figure 3.5, we calculate  $k_f$  and plot it versus shear stress in Figure 3.6.

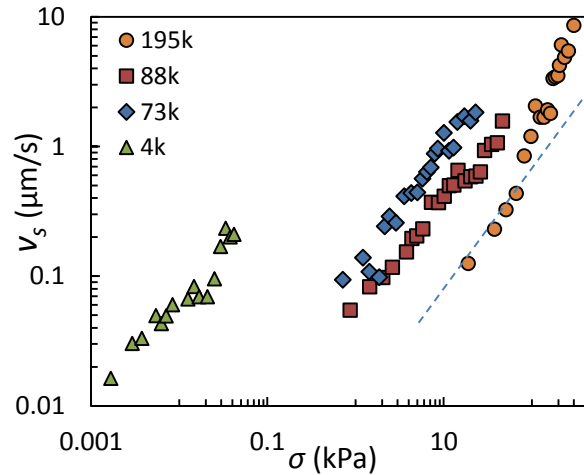


Figure 3.5. Slip velocity vs. shear stress of monodisperse PBDs on silicon wafer. The dashed line is an extrapolation of the weak slip regime of the 195k sample to guide the reader’s eye.

Figure 3.6 shows the friction coefficient as a function of shear stress for monodisperse PBDs and selected binary samples on silicon wafer. For monodisperse PBDs, the friction coefficient at the weak slip regime  $k_{f0}$  scales with the weight average molecular weight as  $k_{f0} \propto M_w^{2.1}$ . This is in good agreement with the power of 1.5 that can be extracted using  $k_{f0} = \eta_0/b_0$  from the work of Archer and coworkers [41] on monodisperse PBDs where

they reported  $b_0 \propto M_w^{1.94 \pm 0.07}$  and  $\eta_0 \propto M_w^{3.4 \pm 0.02}$  ( $b_0$  is the slip length at the weak slip regime).

To begin to understand the effect of polydispersity on slip, the first step is to investigate the slip of bidisperse mixtures. As seen in Figure 3.6, binary samples may exhibit significantly different behavior compared to monodisperse samples. Among three binary combinations of monodisperse 4k, 88k, and 195k PBDs, two of them 195k/88k and 88k/4k follow a close behavior to that of the long-chain constituent. The binary mixture of the longest and shortest chains (195k/4k:  $G_r = 6.694$ ) however exhibits a different behavior with the other two; a very sharp transition towards much smaller values of friction coefficient.

Our first naïve impression from the results is that given sufficiently entangled long chains ( $M_w/M_e > 118$ ) to exhibit strong slip, the onset of the transition to the strong slip occurs much sooner once long chains are mixed with a sample of short-enough chains ( $G_r > 1$ ). Note that the binary sample 4k/88k with  $G_r = 3.023 > 1$  did not exhibit transition to strong slip simply because 88k chains are not entangled enough. We therefore examine the effect of long chain content of 195k/4k mixtures on their wall slip in the following.

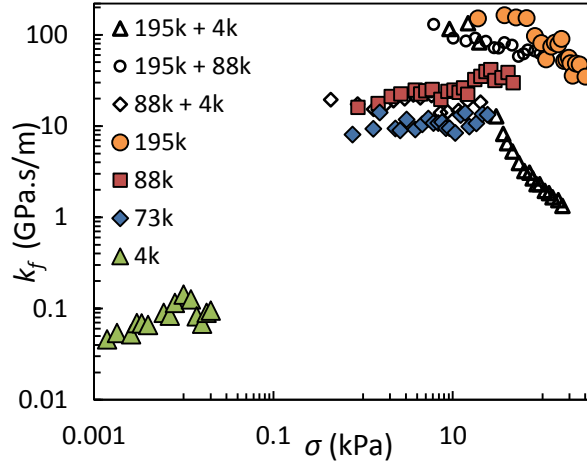


Figure 3.6. Friction coefficient vs. stress of monodisperse PBDs (solid symbols) and their binary mixtures (open symbols) on silicon wafer.

The slip velocity as a function of the shear stress of 195k/4k binary mixtures on silicon wafer is shown in Figure 3.7 where slip curves of 195k and 4k, denoted by L100 and L0, respectively, were added to this graph for comparison. The results were striking; all binary samples exhibit a smooth transition from the weak slip regime to the strong slip regime where their slip velocity seem to follow the same trend as that of the short-chain component, i.e., 4k chains (once extrapolated). Compared to 195k chains, the binary mixtures exhibit strong slip at smaller shear stresses and they reach much higher slip velocities as well.

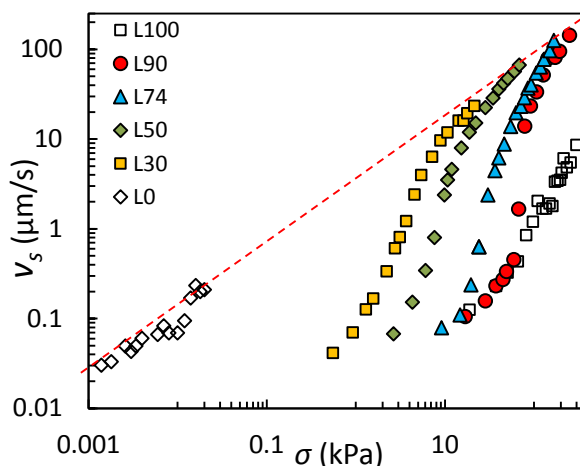


Figure 3.7. Slip velocity of binary 195k/4k PBDs (solid symbols) and their monodisperse constituents (open symbols) versus shear stress. The dashed line is an extrapolation of the slip of the 4k sample to guide the reader's eye.

As seen in Figure 3.7, both the onset and slope of the transition regime change when a small amount of weakly entangled chains is added to a high molecular weight linear polymer. The slip curves of binary mixtures systematically vary with composition: the whole curve shifts to higher shear stresses and the transition to the strong slip regime becomes more *abrupt* as the content of long chains increases. In comparison, slip is suppressed in the case of the pure long chain sample. Moreover, the slip velocity of binary samples exhibits a smooth monotonic increase with stress in contrast to the increasing but rather erratic behavior of the monodisperse samples.

We start our analysis with investigating the effect of bidispersity on the value of the shear stress at the onset of the transition regime known as the critical shear stress  $\sigma^*$ . Several previous slip studies on heavily entangled polymer melts and solutions suggested that  $\sigma^*$  which can be described as the critical shear stress required to disentangle adsorbed chains from the bulk is likely to scale with  $G_N$  (a summary of these results can be found in Refs. [1,16,41]). No unique coefficient of proportionality can be established due to the large variation in different studies.

The data in Figure 3.7 shows that in our case  $\sigma^*$  varies with the content of the long chains in a systematic manner (we chose  $\sigma^*$  of each binary mixture as the point right after which the slip curve branches off and the transition to higher slip velocities begin). Values of  $\sigma^*$ ,  $G_N$ , and,  $\eta_0$  for binary and monodisperse constituents are listed in Table 3.2. Interestingly,  $\sigma^*$  scales linearly with  $\eta_0$  indicating a clear dependence of  $\sigma^*$  on the weight average molecular weight of binary samples. We note that this is likely because we are observing strong slip very close to the Newtonian plateau. Furthermore, we obtain  $\sigma^* \propto G_N^{1.4}$  rather than the power of 1 found in the other studies. This relationship has not previously been characterized since we study binary mixtures instead of monodisperse samples [16].

As mentioned previously, for PBD, the strong slip regime has been observed for molecular weights above  $\sim 100$  kg/mol only. For binary mixtures comprised of heavily- and weakly-entangled chains with  $G_r > 1$ , the minimum degree of entanglement for strong slip reduces to about half of that of monodisperse samples: monodisperse PBD samples exhibit strong slip at  $M > 100$  kg/mol while a binary sample with  $M_w$  as low as 62 kg/mol (L30) showed strong slip in this work. We note that Inn's [63] proposal that high content of small chains induces significant wall slip needs to be refined based on our results which clearly show that slip depends strongly on the chain length of both constituents.

Based on the Brochard-de Gennes' theory [26,30], slip of highly entangled linear polymers can be explained by an entanglement-disentanglement mechanism between the moving and surface-adsorbed chains. The surface-adsorbed chains undergo a coil-stretch transition depending on the flow of the surrounding chains. According to this mechanism,

in the weak slip regime at low slip velocities, the chains adsorbed on the wall are still entangled with the flowing chains and hence forced to comply with regulations of the bulk rheology. In the transition regime at intermediate velocities, the flowing chains start to undergo a repeating disentanglement - re-entanglement process with the adsorbed chains. In the strong slip regime at higher slip velocities, the moving chains become fully disentangled from the surface-adsorbed chains which consequently results in a friction coefficient similar to that of a flow of monomers.

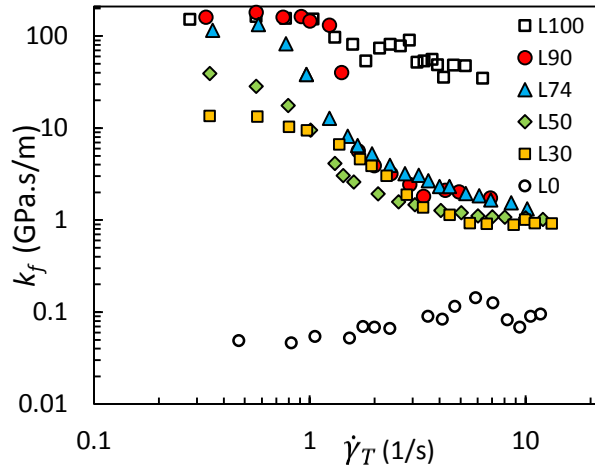


Figure 3.8. Friction coefficient versus true shear rate of binary 195k/4k PBDs (solid symbols) and their monodisperse constituents (open symbols).

Figure 3.8 displays the friction coefficient as a function of true shear rate for binary mixtures and their monodisperse constituents on silicon wafer. The use of shear rate instead of the shear stress on the horizontal axis allows us to study chain friction coefficient as a function of the rate of deformation. As can be seen in this Figure, there is a fundamental difference between the behavior of friction coefficient in the weak and strong slip regimes denoted by  $k_{f0}$  and  $k_{f\infty}$ , respectively.

At low shear rates, we can see the characteristic large entanglement-dominated friction factor which decreases by orders of magnitude as the average number of entanglements per chain is decreased with increasing low molecular weight chain content. Similarly to monodisperse PBDs, the  $k_{f0}$  of binary mixtures scales with the weight average molecular

weight as  $k_{f0} \propto M_w^{2.2}$  indicating that flow dynamics and interfacial properties of linear polymers at low deformation rates is mainly governed by their bulk rheology.

From the data in Figure 3.8, it is evident that the critical shear rate at the onset of the transition regime is almost the same as that of 195k:  $\dot{\gamma}_T^* \sim 1 \text{ s}^{-1}$ . This indicates that in binary mixtures, it is the relaxation dynamics of the long-chain constituent that primarily governs the onset of the slip transition regime.

A very crucial outcome of this work is however the behavior of  $k_{f\infty}$  of binary samples. As shown in Figure 3.8, the friction coefficient of all binary mixtures seems to be leveling off towards a plateau region. Under strong slip conditions, the mobile chains are disentangled from the chains adsorbed to the wall and the friction factor represents both unentangled chain-chain interactions and mobile chain-wall interactions. The fact that the pure L100 exhibits a higher  $k_f$  than the binary mixtures indicates that one or both of these types of interactions is affected by the presence of the short chains. We recall that given the planar Couette flow conditions we do not expect any significant amount of shear-induced segregation of low molecular weight chains to the interface. Therefore, their presence at a concentration equal to that in the bulk is sufficient to cause a large increase in slip. It is important to note that we do not have enough data points to completely describe  $k_{f\infty}$  of pure L100 since its  $k_f$  seems to decrease further once we increase the deformation rate to higher values (not accessible with our current setup).

Slip length can also be described as  $b = \eta/k_f$  where  $\eta$  is the melt viscosity. This relationship states that slip length depends on both the friction coefficient and viscosity of the polymer and therefore cannot be an independent measure of the amount of slip. However, slip length can be a proper measure of the amount of viscous dissipation that a polymer sample undergoes during flow. In fact, it is the  $b/h$  ratio ( $h$  is the shear cell gap or tube diameter) that indicates how important the slip effects are at a macroscopic scale:  $b/h \ll 1$  indicates negligible slip while  $b/h > 1$  signifies considerable slip resulting in a velocity profile close to plug flow.

The slip length of binary 195k/4k PBD mixtures as a function of shear stress are shown in Figure 3.9. Similar to the behavior of monodisperse PBDs in the weak slip regime,  $b_0$

of binary mixtures increases weakly with  $M_w$  as a result of the increase in bulk viscosity. The slip length at the strong slip regime  $b_\infty$  behaves differently since the  $k_{f_\infty}$  is drastically affected by the presence of short chains. The behavior of  $b_0$  and  $b_\infty$  as a function of  $\varphi$  are shown in Figure 3.10.

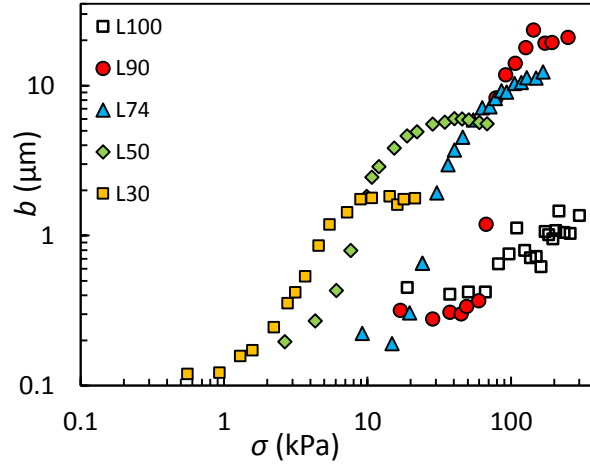


Figure 3.9. Slip length of binary 195k/4k PBDs versus shear stress.

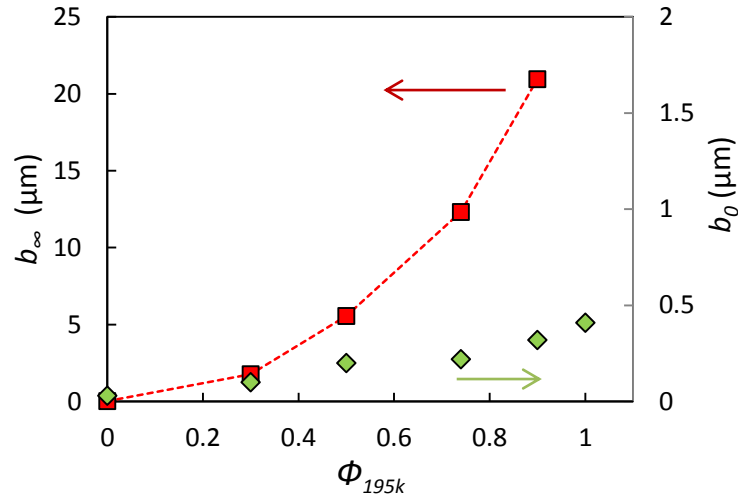


Figure 3.10. Slip length of binary 195k/4k PBDs versus weight fraction of 195k chains.

As shown, for binary mixtures of long and short chains (195k/4k),  $b_\infty$  shows a stronger dependence on  $\varphi$  than  $b_0$ :  $b_\infty \propto \varphi^{2.2}$  versus  $b_0 \propto \varphi^{1.1}$ . The difference between the power law dependence of  $b_0$  and  $b_\infty$  on  $\varphi$  indicates that the presence of short chains in a binary

mixture is more pronounced at higher stresses where mobile chains begin to disentangle from those adsorbed to the surface. The power law dependence of  $b_\infty$  of binary mixtures on  $\varphi$  is similar to that established between  $G_N$  and  $\varphi$  as  $G_N \propto \varphi^{2.2}$  [58,60,61]. The similarity between these parameters would be a promising starting point for further study of slip in polydisperse samples. It is important to note that  $b_\infty$  of 195k may have not been reached within the range of shear stresses examined in this study and hence it is not included in Figure 3.10. Sample L90 containing the highest content of long chains exhibited the most extreme slip with  $b_\infty$  on order of 20  $\mu\text{m}$ . The increase in  $b_\infty$  of binary samples is most certainly due to a decrease in their corresponding friction coefficient as it was shown in Figure 3.8 signifying the important role of short chains in wall slip and flow dynamics of linear polymers.

### 3.4. Conclusion

The results highlight the important role of weakly entangled chains in the course of polymer flow. Slip of binary mixtures of long and short chains with  $G_r > 1$  in the strong slip regime is significantly affected by the presence of short chains. We showed that the addition of a small amount of short chains with  $M \sim M_c \sim 3M_e$  to a monodisperse sample of sufficiently entangled long chains  $M \sim 118M_e$  significantly reduces the strong slip friction coefficient resulting in a significant increase in wall slip compared to moderate slip of long chains at the same shear stress.

Surprisingly, for binary mixtures the strong-regime slip length,  $b_\infty$ , scales with the content of long chains,  $\varphi$ , as  $b_\infty \propto \varphi^{2.2}$ , a relationship similar to that established between binary mixtures plateau modulus  $G_N$  and  $\varphi$  as  $G_N \propto \varphi^{2.2}$ . While the weak slip friction coefficient seems to scale well with bulk rheology and entanglement density of chains, the strong slip friction coefficient requires detailed knowledge of disentangled chain-chain and chain-wall interactions at the interface in addition to rheological properties. The lower stress decrease in  $k_f$  of binary mixtures compared to monodisperse long chains indicates that the disentangled chain-chain and/or the chain-wall interactions at the interface are strongly affected by the presence of short chains.

We found that the critical shear stress  $\sigma^*$  for the onset of transition to strong slip in binary PBD samples scales with  $\eta_0$ . We also showed that a binary sample with  $M_w$  as low as 62 kg/mol could exhibit significant strong slip; although there exists specific requirements on the chain length of both of the individual constituents. In contrast, monodisperse samples with  $M$  up to 195 kg/mol exhibited moderate slip only. These results provide the foundation for the development of new theoretical underpinnings for the mechanism by which short chains influence interfacial slip.

## 4. CHAPTER 4

### Wall Slip of Tridisperse Polymer Melts and the Effect of Un-Entangled versus Weakly-Entangled Chains<sup>1,2</sup>

S. Mostafa Sabzevari †, Itai Cohen ‡, and Paula M. Wood-Adams \*†

† *Department of Mechanical and Industrial Engineering, Concordia University, Montreal, QC, Canada H3G 2J2*

‡ *Department of Physics, Cornell University, Ithaca, New York 14853, United States*

#### Abstract

We characterized wall slip of tridisperse linear 1,4polybutadiene on a silicon wafer in a parallel plate shear cell and tracer particle velocimetry. Tridisperse mixtures of fixed weight average molecular weight  $M_w$  and varying number average molecular weight  $M_n$  were prepared from nearly-monodisperse polybutadienes. Their steady state slip behavior was examined at shear rates over the range of  $\sim 0.1 - 15 \text{ s}^{-1}$ . The results show that the slip behavior in the transition regime depends on  $M_n$  at constant  $M_w$ . This study also revealed that weakly-entangled and un-entangled chains in the mixtures influence wall slip differently: mixtures containing moderate amounts of weakly-entangled chains exhibited enhanced slip while those containing un-entangled chains did not. We explain this observation using the tube dilation theory through the slip disentanglement mechanism proposed by Brochard and de Gennes in 1992 and conclude that the slip behavior is changed because of the force balance between the mobile and adsorbed chains and the reduced entanglement density and coil stiffness related to the incorporation of short chains of different lengths.

---

<sup>1</sup> This chapter is published as: S. Mostafa Sabzevari, Itai Cohen, and Paula M. Wood-Adams, “Wall Slip of Tridisperse Polymer Melts and the Effect of Un-Entangled versus Weakly-Entangled Chains”, *Macromolecules*, **2014**, 47, 8033–8040.

<sup>2</sup> Additional information is given in Appendix A.

## 4.1. Introduction

In general, the no-slip boundary condition holds for simple fluids with small molecules. Violations may be observed in extreme cases such as flow on very smooth surfaces, when the surface is highly nonwetting, or where the flow channel has dimensions on the order of molecular sizes [1,2]. For complex fluids such as polymers, the boundary condition is highly influenced by physical and chemical characteristics of the polymer in addition to the substrate properties. Almost all polymer melts and concentrated solutions slip on solid surfaces to some extent [2,29].

Polymer wall slip is important in applications including coating, lubrication, mixing, and particularly in extrusion-based polymer processing techniques. In the past, there has been a long debate over the relationships between polymer slip and extrudate surface distortions (also known as flow instabilities). The link between slip and extrusion instabilities comes from the fact that highly entangled molten polymers exhibit both macroscopic slip and extrusion instabilities at high shear stresses. The slip literature generally encompasses two areas of discussion: i) the correlation between polymer slip and flow instabilities [2,4-14,18,20,22,23,36,100,101] and ii) slip characterization and parameters influencing polymer slip [3,15-17,19,21,24,25,41,46,49,57,86]. Our objective in the present work is to characterize wall slip of polydisperse polymer melts and to elaborate on slip mechanisms.

Although there is a great deal of experimental data on wall slip of monodisperse samples, polydisperse samples have rarely been explored previously [57]. The majority of molecular theories in this field are based on ideal monodisperse systems and have not yet been generalized to highly polydisperse systems typical of industrial polymers [1,26,29-34,48,82]. In our previous work, we described wall slip of mixtures of long and short chains, i.e. binary polybutadienes, in an effort to take the first step toward a full understanding of slip of polydisperse samples [102]. In the present work, we take a step further and study ternary mixtures comprising long, medium-size, and short chains in a systematic manner and with specific molecular weight characteristics. The results illustrate

the need for further experiments and new computer simulations as well as development in slip theory.

To better understand the role of different factors influencing polymer wall slip, it is vital to review slip mechanisms. Interfacial slip requires adhesive failure right at the interface (also known as true slip). This necessitates either an ideal condition of having a smooth and non-adsorbing surface or a detachment (desorption) mechanism. The alternative is polymer cohesive failure by the entanglement/disentanglement mechanism in which polymer chains in the bulk disentangle from those adsorbed to the solid surface [29]. Slip by cohesive failure is called *apparent slip* since failure occurs at a distance about one molecular size away from the interface and does not contradict the original no-slip boundary condition [24]. Both mechanisms have been subjects of interest in literature [2].

The disentanglement mechanism however has drawn more attention specifically in slip characterization studies [19,24,46]. A remarkable slip theory was developed by Brochard and de Gennes in 1992 based on the disentanglement mechanism [29]. Many experimental results from previous slip studies were consistent with this slip theory and various modifications to the theory were proposed over the years although none deal with polydispersity [1,19,32].

The lubrication mechanism similar to two-phase flow is a third slip mechanism particularly proposed for polymers that contain fluoropolymer additives [14,16]. This mechanism proposes that a stress-induced low-viscosity layer forms in the vicinity of the interface due to the migration of additives or low molecular weight species. The stress-induced migration is due to the shear stress gradient across the gap in pressure driven flows. A similar mechanism has been proposed for the slip of polymers with glass transition temperatures above the room temperature, particularly for polyethylene (PE) in which an interfacial low-viscosity structured mesophase is formed at the interface [6,9,10].

The critical factors influencing polymer wall slip can now be classified based on their contribution to slip mechanisms: i) those contributing to the density of adsorbed chains and their surface-bonding strength (chain-wall interactions) and ii) those influencing physical interactions between bulk and adsorbed chains (chain-chain interactions). As a result,

substrate surface roughness, polymer and substrate chemistry, and the relative surface energy of polymer and substrate determine the chain-wall interactions. In contrast, monomer chemistry, molecular weight, molecular weight distribution, and polymer architecture govern the entanglement density which successively determines the onset of transitions to different slip regimes. Among these, polydispersity has remained a weakly-explored area.

There have been a great number of indirect slip studies of the effects of polydispersity using capillary extrusion of polyethylene resins. Myerholtz [54] showed that stick-slip instabilities may decrease or disappear at very large polydispersity index,  $PI$ , values ( $PI > 30$ ) in capillary flow of polyethylene. Ansari *et al.* [67] reported similar observations: the ranges of the stick-slip transition decreases as molecular weight distribution broadens until it completely disappears for  $PI > 19$ . In a similar study, Blyler and Hart [56] showed that the flow curve discontinuity may significantly reduce if a low molecular weight polyethylene wax is added to a high molecular weight linear  $PE$ . Recently, Inn [63] studied capillary flow of three bimodal polyethylene resins of similar viscosity. They observed that the sample with i) the higher content of the low molecular weight portion of the population and ii) the highest molecular weight of the high molecular weight population showed the largest slip.

Although it is generally agreed that processability of polyethylene improves when polydispersity increases [64,65] there has not yet been a general agreement on how polydispersity affects polymer slip [64,66,67] part of the issue is due to not having direct and systematic studies of the problem. Hatzikiriakos [57] in the most recent review of the subject reminded us of the necessity of further work to investigate the effect of polydispersity on wall slip of polymers.

Since the breadth of a molecular weight distribution strongly depends on the content and size of short chains, it is essential to design experiments in a systematic approach. To this end, ternary samples with fixed weight average molecular weight  $M_w$  and varying number average molecular weight  $M_n$  were prepared from monodisperse polybutadiene samples. Two sets of samples (W and U) each containing different sized short chains were

designed; the first set is comprised of weakly-entangled, moderately entangled, and highly entangled chains while the second set contains un-entangled chains in the place of weakly-entangled chains.

## 4.2. Materials and Experiments

We use linear 1,4-polybutadiene (PBD: cis 68%, trans 27% and 1,2 addition 5%) as a model polymer since it is possible to purchase samples with very narrow molecular weight distributions as well as the ease of performing experiments at room temperature. Four PBDs with  $M_w$  in the range of 1 to 195 kg/mol and  $PI < 1.08$  were purchased from Polymer Source Inc. Canada (Table 4.1). In this table,  $M_e$  is the molecular weight between entanglements, for PBD:  $M_e \cong 1.65$  kg/mol.

We studied wall slip of tridisperse samples: two sets of ternary samples with fixed  $M_w \cong 143.5$  kg/mol  $\pm 0.6\%$ , and varying  $M_n$  were examined. Both sets have 88k and 195k chains in common but the short-chain component is different: set W contains 4k (weakly-entangled chains) and set U contained 1k (un-entangled chains) as the third component. This study was designed to investigate how short chains with different degrees of constraints contribute to wall slip of polydisperse polymers. Table 4.2 lists the composition and molecular weights of our ternary samples. The average molecular weights in this table were calculated from  $M_w = \sum w_i M_{wi}$  and  $M_n = (\sum w_i / M_{ni})^{-1}$  where  $w_i$ ,  $M_{wi}$ , and  $M_{ni}$  are the weight fraction, weight average molecular weight, and number average molecular weight of the  $i^{\text{th}}$  constituents, respectively. For the purpose of comparison with the behavior of binary samples in our previous work (Ref. 43), we added the data of one binary mixture containing 4k and 195k chains which is denoted by sample W\_Mn\_14 in Table 4.2 (sample L74 in Ref. 102).

To confirm the molecular weight distribution of our polymers, we performed gel permeation chromatography (GPC) relative to linear polystyrene (Waters 1525; THF at 35°C with a flow rate of 1 mL/min; Phenomenex column; refractive index detector) on all pure PBD samples as well as certain ternary samples. Figure 4.1 shows the molecular weight distribution of samples W\_Mn\_17 and U\_Mn\_5 which have the highest content of

short chains within each set of mixtures. These data confirm the presence of the three distinct modes in each sample and clearly shows that the molecular weight distribution of the two samples differ only by the molecular weight of the short chain constituent. We note that the small peak in the high M region originates from the 195k sample.

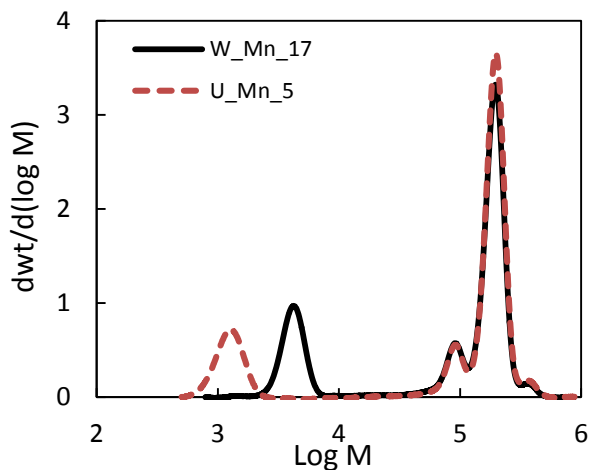


Figure 4.1. GPC chromatograms of two ternary PBD samples: W\_Mn\_17 containing 4k, 88k, and 195k (solid line) and U\_Mn\_5 containing 1k, 88k, and 195k (dashed line).

Ternary mixtures were prepared in solution by combining 5 wt% solutions of monodisperse PBDs in dichloromethane in the appropriate proportions by weight. A small amount (less than 0.5 wt%) of surface-treated (hexyltrimethoxysilane) fluorophore nanoparticles (nominal size of 75 nm) suspended in ethanol (2mg/ml) was then added to each sample to be used as tracer particles for velocimetry measurements. Samples were dried at room temperature and under vacuum for 3 days to minimize residual traces of solvent molecules.

Tracer particle velocimetry measurements were carried out using a shear cell and confocal microscopy. For each measurement, a few milligrams of polymer was placed between the two parallel plates of the shear cell separated by a small gap ( $h \cong 90 \mu\text{m}$ ). Drag flow was produced by moving the bottom plate while the top plate was fixed to a firm stationary structure. The top plate was a silicon wafer whereas the bottom plate was a cover glass to enable imaging of the tracer particles.

In each experiment, the sample was sheared at a constant nominal shear rate well into steady state as confirmed by the velocity vs. time responses. The motion of tracer particles for different heights at the center of the shear zone was captured at 50 fps with a 63x objective. The slip velocity and corresponding shear rate in the steady state region were then obtained through image processing using a modified version of MATPIV. A detailed description of the experimental set up can be found in Refs [49,102].

Table 4.1. Basic characteristics of monodisperse PBDs.

Sym.	$M_w$ [kg/mol]	$M_w/M_n$	$M_w/M_e$
1k	1.3	1.07	0.8
4k	4.3	1.06	3
88k	88.2	1.05	53
195k	195.3	1.08	118

The dynamic linear viscoelastic properties were characterized by small-amplitude-oscillatory-shear (SAOS) using a stress-controlled PaarPhysica rotational rheometer (MCR 500). Measurements were done using 8-mm diameter stainless steel parallel plates with a gap of 1 mm under a nitrogen atmosphere. The complex viscosity data  $\eta^*(\omega)$  is used as an estimation of the steady state viscosity  $\eta(\dot{\gamma})$  based on the Cox-Merz rule.

Table 4.2. Molecular weight and composition of PBD mixtures

Sym.	$M_n$ [kg/mol]	$M_w$ [kg/mol]	1k [wt%]	4k [wt%]	88k [wt%]	195k [wt%]	$\sigma^*$ [kPa]
W_Mn_14	14	145	0	26	0	74	20
W_Mn_17	17	145	0	22	8	70	51
W_Mn_21	21	144	0	17	17	66	54
W_Mn_27	27	144	0	12	27	61	78
W_Mn_43	43	143	0	6	38	56	NA <sup>i</sup>
W_Mn_61	61	143	0	3	43	54	NA <sup>i</sup>
U_Mn_5	5	145	22	0	8	70	NA <sup>i</sup>
U_Mn_11	11	144	10	0	30	60	NA <sup>i</sup>
U_Mn_17	17	143	6	0	38	56	NA <sup>i</sup>
U_Mn_23	23	143	4	0	41	54	NA <sup>i</sup>
U_Mn_40	40	142	2	0	46	52	NA <sup>i</sup>

<sup>i</sup> Did not exhibit strong slip in the experimental window in this work which covered up to 200 kPa.

### 4.3. Results and Discussion

The effect of  $M_w$  on wall slip has previously been extensively explored [1,2]. In the present work, we study the effect of  $M_n$  on wall slip;  $M_n$  is highly affected by the presence of short chains within the molecular weight distribution of the polymer.

SAOS measurements were performed in order to confirm that the approximately constant  $M_w$  of our mixtures resulted in similar complex viscosity curves. Figure 4.2 compares the complex viscosity versus angular frequency of W\_Mn\_17 and W\_Mn\_61 from set W with U\_Mn\_5 and U\_Mn\_40 from set U. Results shows that although there is a small difference in the zero shear viscosity (lowest value is 23% below highest) of these mixtures, the general frequency dependence is similar.

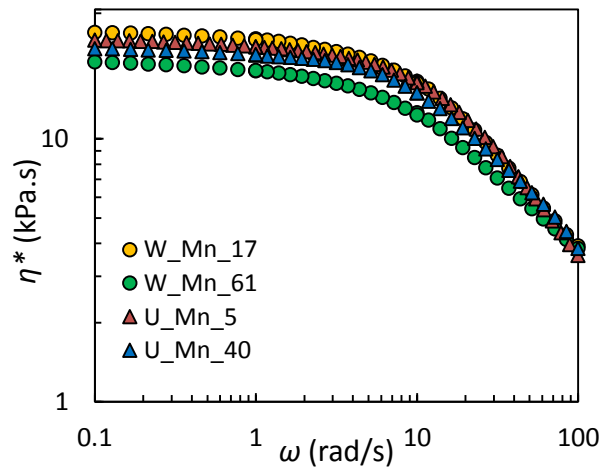


Figure 4.2. Complex viscosity versus angular frequency of W\_Mn\_17 and W\_Mn\_61 compared to U\_Mn\_5 and U\_Mn\_40.

Figure 4.3 compares the dynamic storage ( $G'$ ) and loss ( $G''$ ) moduli of the mixtures as a function of the angular frequency  $\omega$ . The main quantity examined in this work is the slip velocity  $v_s$  of ternary PBD samples on silicon wafer in planar Couette flow over a range of shear rates between  $0.1 - 15 \text{ s}^{-1}$ . Figure 4.4 shows slip velocity versus shear stress of samples in set W, comprised of 4k, 88k, 195k chains with fixed  $M_w = 143 \text{ kg/mol}$  and varying  $M_n$ . Here  $\sigma$  is calculated from  $\sigma \cong \dot{\gamma}_T |\eta^*(\omega = \dot{\gamma}_T)|$  which is a realistic estimation

since we use the true shear rate  $\dot{\gamma}_T$  and we are close to the Newtonian plateau in all our experiments such that the Cox-Merz relation is very likely to be appropriate.

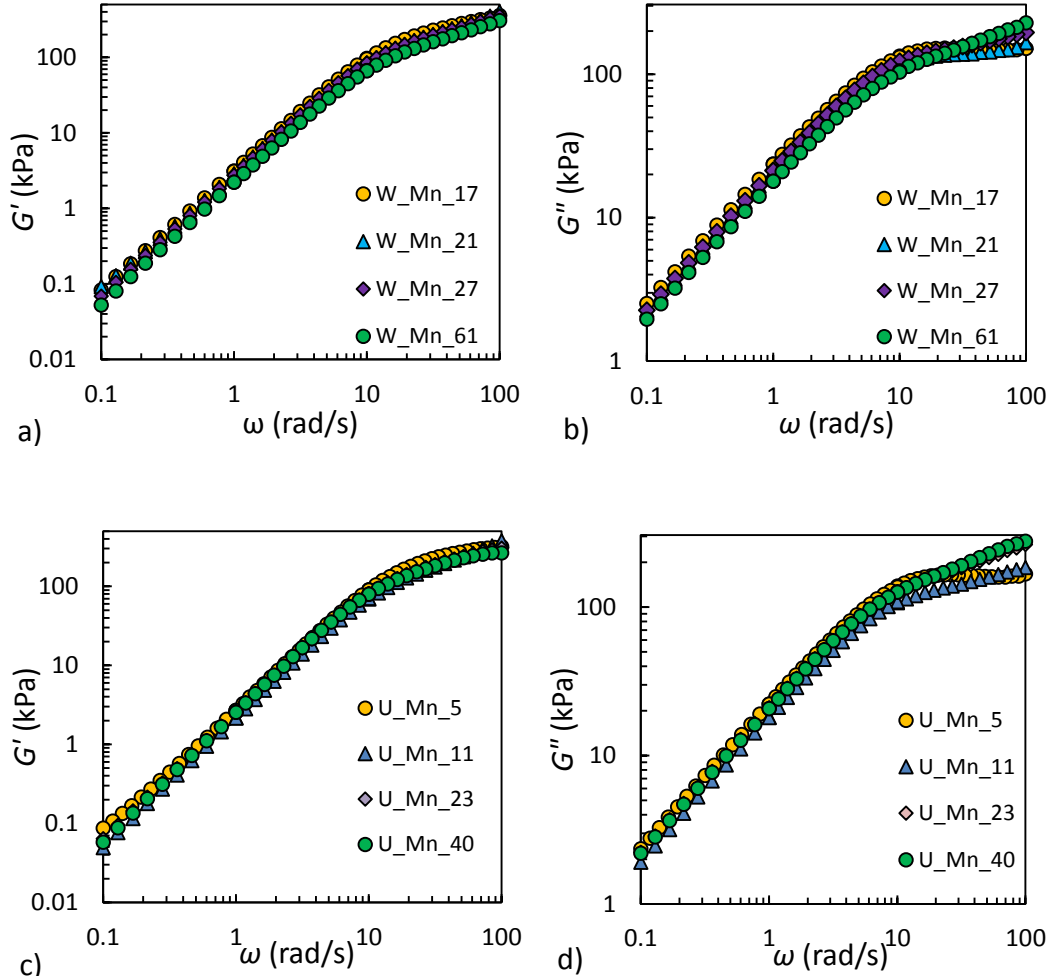


Figure 4.3. Linear viscoelastic properties, storage  $G'$  and loss  $G''$  moduli, as a function of the angular frequency  $\omega$  of samples with different  $M_n$  as labeled (kg/mol): (a-b) set W containing 4k chains, and (c-d) set U containing 1k chains.

The true shear rate is calculated from  $\dot{\gamma}_T = \dot{\gamma}_n - (v_s^t + v_s^b)/h$  where  $\dot{\gamma}_n = v/h$  is the nominal shear rate imposed to the sample,  $v$  is the bottom plate drag velocity, and  $v_s^t$  and  $v_s^b$  are the slip velocities on the top (silicon wafer) and bottom plates (cover glass), respectively. The results in Figure 4.4 are very interesting and indicate that wall slip of linear polymer melts depends significantly on  $M_n$  at constant  $M_w$ . As seen in this graph, samples with smaller  $M_n$  branch off to higher slip velocities at the high shear stress region.

This transition to large slip velocities is an indication of chain disentanglement that was both theoretically [29] and experimentally [19] introduced previously. Another interesting feature in this graph is the distinct behavior of the binary sample W\_Mn\_14 which exhibits the largest slip.

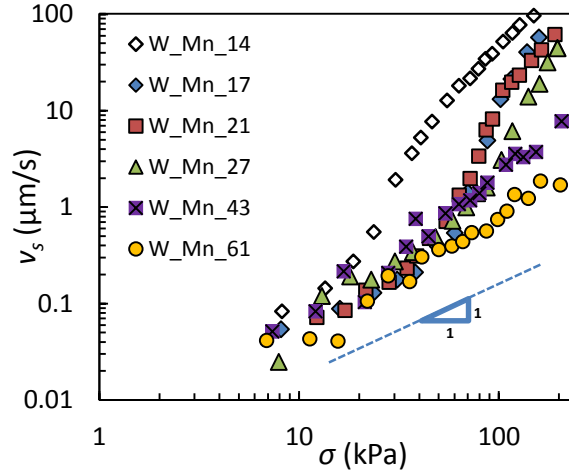


Figure 4.4. Slip velocity as a function of shear stress of ternary PBDs containing weakly-entangled chains on silicon wafer (set W). The data for the binary sample W\_Mn\_14, containing 4k and 195k chains only, from Ref. 43 are included for the sake of comparison.

In the flow of an entangled polymer over a solid substrate on which a few polymer chains are adsorbed, three distinct slip regimes are commonly observed namely: the weak slip regime (low-velocity slip), transitional regime, and strong slip regime (high-velocity slip). At low velocities, the adsorbed chains are un-perturbed by the shear. Hence, the moving chains remain entangled with the adsorbed chains. Within this region, the slip velocity is proportional to the shear stress:  $v_s \propto \sigma$ . As velocity is increased, the adsorbed chains become stretched and an elastic force which balances the viscous dissipation is introduced. Above a critical slip velocity, the moving chains can no longer hold entanglements with those adsorbed and thus disentangle. Once disentangled, the adsorbed chains relax to their original un-perturbed state with large diameters and immediately become entangled with moving chains once again. This is the transitional region within which the adsorbed chains are constantly deforming and relaxing due to undergoing the entanglement-disentanglement process and the slip velocity and shear stress are no longer

proportional. At higher velocities, the moving chains become completely disentangled from those adsorbed and the viscous force is so high that adsorbed chains remain highly stretched. In this regime, slip velocity becomes proportional to the shear stress once again similar to the weak slip regime but with much higher magnitudes. It is important to note that, in the strong slip regime, the friction coefficient  $k_f$  correlating slip velocity and shear stress through  $k_f = \sigma/v_s$  is close to that of a flow of monomers.

Referring to Figure 4.4, we can see that ternary samples containing a moderate amount of weakly-entangled chains undergo a transition to the strong slip regime (the dashed guide line with the slope of unity indicates the linear dependence of  $v_s$  and  $\sigma$  in the weak slip regime in good accord with the Brochard and de Gennes theory). In contrast, high  $M_n$  samples seem to follow their weak slip regime proportionality with stress. In slip the friction coefficient corresponds to the chain-chain and chain-wall interactions at the plane of slip. In Figure 4.4, the difference between the slip of samples with different short-chain contents corresponds to different friction coefficients.

To further understand the slip mechanism, it is interesting to investigate the change in friction coefficient of ternary samples as the shear stress (or slip velocity) increases. Figures 4.5a) and 4.5b) show the friction coefficient of ternary PBD samples in set W as a function of the shear stress and slip velocity, respectively. The friction coefficient was calculated from the data in Figure 4.4 using  $k_f = \sigma/v_s$ .

As can be seen, PBD samples with different compositions but the same  $M_w$  may exhibit different  $k_f$  while experiencing the same shear stress. Figure 4.5a) shows that the  $k_f$  of sample W\_Mn\_61 (containing the lowest content of short chains) has the weakest dependency on shear stress. In comparison, the  $k_f$  of samples with  $M_n < 43$  kg/mol decreases at high shear stresses to values orders of magnitude lower than those of the high  $M_n$  samples. Comparing the compositions of set W ternary samples in Table 4.2 with their  $k_f$  behavior in Figure 4.5a), it can be seen that  $k_f$  exhibits an abrupt drop the magnitude of which increases as the content of the middle-sized component (88k) decreases. In fact, the most distinct slip behavior belongs to the binary sample W\_Mn\_14 which contains the long and short chains only. In other words, slip is favored in binary samples of weakly- and

heavily-entangled chains in contrast to ternary samples containing a third middle-sized constituent. A similar conclusion was made by Schreiber [62] in a work when he studied the flow instability of linear polyethylene in capillary experiments. Schreiber showed that the shape of the molecular weight distribution influences the flow curve discontinuity and “blends utilizing components with widely different molecular weights are far more effective than the blends with broader but more normally shaped distribution functions” in reducing the breadth of the discontinuity. Referring to the results of binary mixtures in our previous study [102], it can be said that it is the short chain content of a highly-entangled polydisperse polymer that mainly governs the slip characteristics over a high-surface energy substrate such as silicon wafer. Binary mixtures of sufficiently long and short chains are favored in this regard.

Figure 4.5b) shows  $k_f$  as a function of  $v_s$ . Plotted in this way, the abrupt changes in the friction coefficient essentially vanish and a more general behavior appears instead helping to correctly distinguish different slip regimes. The friction coefficient in the weak slip regime  $k_{f0}$  is governed by bulk rheology and relaxation dynamics of the long chains due to the low slip velocities. As shown in Figures 4.5a) and 4.5b),  $k_{f0}$  is essentially independent of the molecular weight distribution at constant  $M_w$  and not affected by the presence of short chains since at low velocities the dynamics of the long chains are dominant. In the transitional regime, the dynamics of slip are highly influenced by the degree of entanglement between the mobile and surface-adsorbed chains as seen in Figure 5b). In the strong slip regime where the adsorbed chains are disentangled from the bulk, however, the friction coefficient  $k_{f\infty}$  is close to that of the flow of monomers. Based on Figure 4.5a) we may assume that samples with different  $M_n$  show different  $k_{f\infty}$ . However, Figure 4.5b) shows that we have not reached  $k_{f\infty}$  within the range of shear stresses (or slip velocities) studied here. Therefore, what we are seeing in Figures 4.5a) and 4.5b) is in fact the weak slip and transitional slip regimes only in which the degree of entanglements between chains still play a crucial role. In order to reach  $k_{f\infty}$  which supposedly is independent of the chain length based on the disentanglement slip model, the slip velocity for all samples has to be extended beyond the limit of their transitional regime.

Accordingly, the difference in the  $k_f$  behavior of low- and high- $M_n$  samples with the same  $M_w$  observed in Figure 4.5a) is because they are at different points in the slip regimes: the slip velocity of the high- $M_n$  samples is within their weak slip regime only whereas the low- $M_n$  samples are in the process of transitioning to the strong slip regime. The key differences then is in the critical shear stress  $\sigma^*$  at the onset of the transitional regime and the slope of the transition which is strongly dependent on the chain length distribution of samples. As a result, polymer samples with the same  $M_w$  but different  $M_n$  may exhibit different slip behavior at the *onset* and *within* the transitional regime.

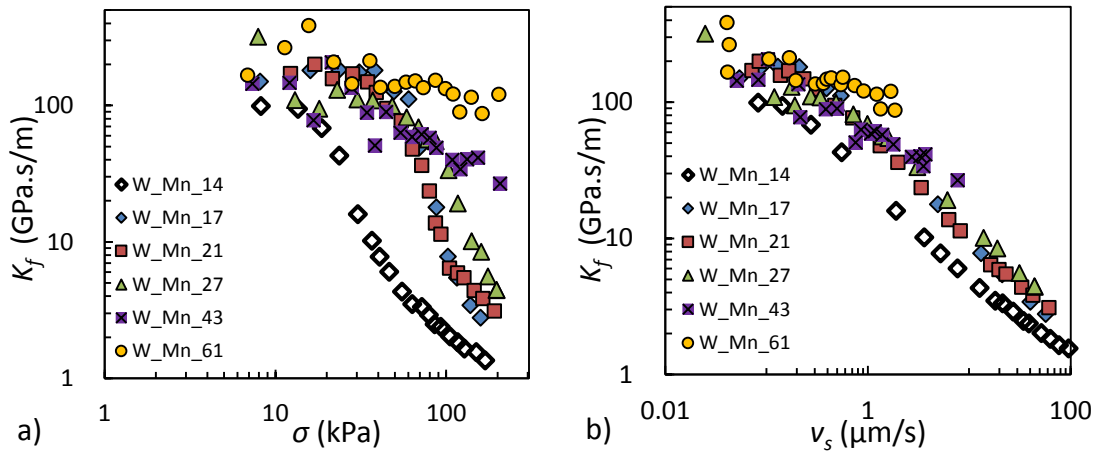


Figure 4.5. Friction coefficient versus shear stress (a) and slip velocity (b) of ternary PBDs containing weakly-entangled chains over silicon wafer (set W) calculated from the data in Figure 4.4 using  $k_f = \sigma/v_s$ . The data for the binary sample W\_Mn\_14, containing 4k and 195k chains only, are reproduced from Ref. [102] and included for the sake of comparison between ternary and binary samples.

As listed in Table 4.2, for those samples which did exhibit the transition to the strong slip regime, the critical shear stress at the onset of the transition decreases with increasing short chain content in the mixture (this is consistent with the data in Ref. 102). This behavior is likely due to a decrease in the number of long chains that are adsorbed on the interface. When the shear stress is high enough to deform the adsorbed chains, the amount of force transferred to the bulk becomes a sum of the friction force at the slip plane and the elastic force in the adsorbed chains. The total elastic force is additive over all adsorption sites per unit area. As the content of short chains in the mixture increases, the number of

adsorbed chains that are entangled with the bulk and thus the elastic force decreases. The critical shear stress required for the disentanglement/desorption of the adsorbed chains thus decreases. As a conclusion, the incorporation of short chains into a system of highly entangled chains facilitates the transition to the strong slip regime.

We now investigate the effect of short chain length on the wall slip of ternary PBD samples by examining the second set of samples in which weakly-entangled chains (4k in set W) are replaced by un-entangled chains (1k in set U). We note that the use of 1k chains results in values of  $M_n$  significantly lower than those of samples using 4k chains when the same composition is used while the  $M_w$  is constant (Table 4.2).

Figure 4.6 shows the slip velocity of set U as a function of shear stress. In contrast to Figure 4.4, the data in this graph shows no indication of the transition to the strong slip. As can be seen, the slip velocity remains in the weak slip regime over the same range of shear stresses of Figure 4.4. This distinct difference between the wall slip of the two sample sets indicates that there is a fundamental difference in the slip dynamics of entangled ternary PBD samples containing un-entangled and those containing weakly-entangled chains.

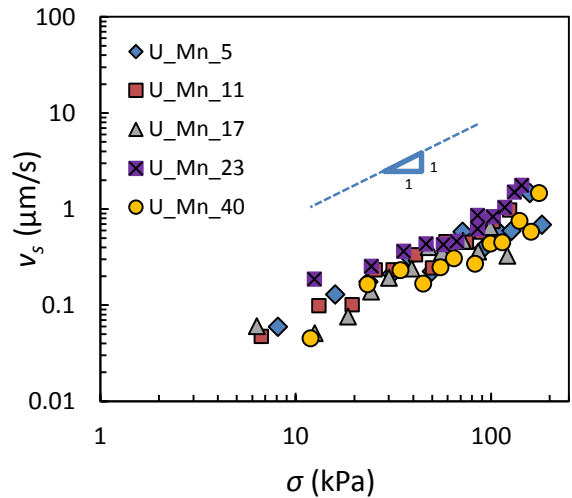


Figure 4.6. Slip velocity as a function of shear stress of ternary PBDs containing un-entangled chains on silicon wafer (set U).

Figures 4.7a) and 4.7b) shows the friction coefficient of ternary samples in set U as function of shear stress and slip velocity, respectively. Ternary PBDs containing un-

entangled chains behave in a similar way to the high- $M_n$  samples in set W and show no evidence of the transition to the high slip velocity slip regime.

Figure 4.8 compares the slip velocity versus shear stress of 2 samples from each sample-set. As can be seen, there is a distinct difference between the effect of un-entangled and weakly-entangled chains on wall slip of PBD over a high-energy surface such as silicon wafer. Evidently, as the content of weakly-entangled chains increases in the mixture, the critical shear stress at the onset of the transition regime decreases to lower values. Furthermore, the weakly entangled chains contribute to slip more than the un-entangled chains do.

In previous studies, surface segregation of short chains is named as one possible cause of the discrepancies in surface properties of very polydisperse polymer melts compared to monodisperse systems [69]. It is commonly said that the surface excess of short chains induces a thin low-viscosity layer over which the bulk polymer can easily slip. Surface segregation may be driven by entropic or enthalpic factors, for instance by the reduced conformational entropy at the surface (entropic) [70] or the surface energy difference between the chain ends and the backbone (enthalpic) [71] or it may as well be mechanically driven by shear-induced fractionation under certain flow conditions [63].

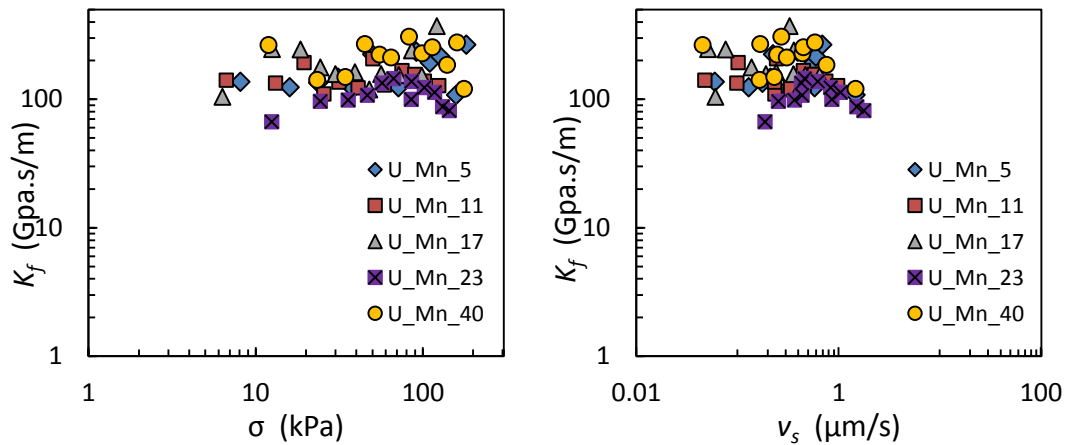


Figure 4.7. Friction coefficient versus shear stress (a) and slip velocity (b) of ternary PBDs containing un-entangled chains on silicon wafer (set U).

In our work, there is no shear-induced segregation since we use planar Couette flow in which the shear stress is constant across the flow channel. Only enthalpic and entropic factors can be responsible for any surface enrichment of short chains in our case. Therefore we expect that the degree of surface enrichment of short chains would be similar in our two sample-sets and certainly cannot explain the observed difference between the slip of mixtures containing un-entangled and weakly-entangled chains.

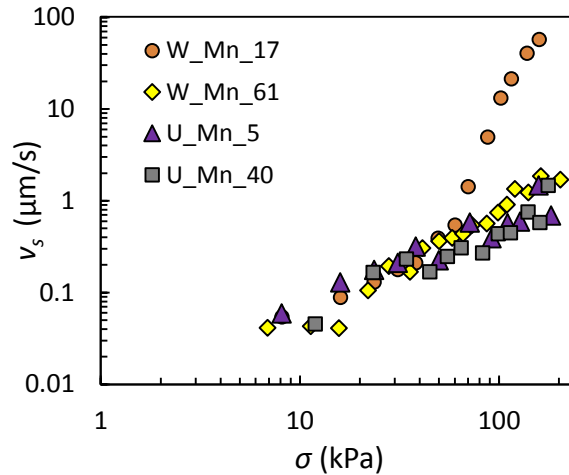


Figure 4.8. Slip velocity versus shear stress of W\_Mn\_17 and W\_Mn\_61 compared to U\_Mn\_5 and U\_Mn\_40.

The difference between the effect of un-entangled and weakly-entangled chains on wall slip of PBD over a high-energy surface such as silicon wafer likely relies on the force balance and load transfer mechanism between the mobile and adsorbed chains. Here, to explain the observed behavior, we use the same fundamental assumptions in the Brochard - de Gennes disentanglement slip model [29]. In this model, i) the entangled adsorbed chains are treated as coils grafted from one end to the solid surface while the other end is floating in a flow of surrounding chains moving with velocity  $v$  equivalent to  $v_s$ ; and ii) there is a force balance between the viscous and elastic forces at the critical slip velocity. The slip behavior is then characterized based on the magnitude of the slip velocity. In the weak slip regime, coils are un-perturbed and the load is transferred by chain-chain or chain-wall interactions. As the slip velocity increases, coils start undergoing deformations and hence holding some internal stresses due to elastic forces. From this velocity forward, coils

begin to reduce their size in diameter while being elongated. At a critical slip velocity  $v_s^*$ , the coil size diameter  $D$  is reduced to a limiting point corresponding to  $D = D^* = aN_e^{1/2}$  below which they can no longer hold entanglements with the mobile chains -  $a$  is the monomer size and  $N_e$  is the number of monomers per entanglement [29].

At the critical slip velocity, there is a balance of the viscous and elastic forces between the mobile and adsorbed chains. The viscous force is due to the friction between chains and is proportional to the slip velocity. The total viscous force exerted on a coil is determined by the average number of entanglements between the mobile chains and each coil [34]. The elastic force is due to the coil stiffness and is proportional to the coil elongation. The total elastic force is additive over all adsorption sites per unit area. To see the effect of short chains on slip, we have to investigate how the force balance is affected by the incorporation of short chains.

The presence of short chains in the neighborhood of long chains changes the details of entanglements which consequently changes: i) the amount of viscous force transferred to the adsorbed chains and ii) the coil stiffness of the adsorbed chains. The key difference between unentangled chains and weakly entangled chains is in how they affect these two phenomena at the interface: the magnitude of the viscous force is more strongly dependent on the length of the short chain than is the coil stiffness. Therefore we have a balancing of the two effects which results in the combination of a higher viscous force transferred in the case of a system containing weakly entangled chains and a coil stiffness which is approximately the same in both systems containing weakly entangled and unentangled chains.

A greater degree of entanglement allows for the transfer of higher loads to adsorbed coils as compared to less entangled systems. This means that a system containing long chains and weakly-entangled chains transfers higher loads to the adsorbed coils than an equivalent system containing un-entangled short chains.

The stiffness  $K$  of the adsorbed coils also changes due to the presence of short chains. Short chains (weakly- or un-entangled) in a mixture with long chains increase the coil size of the adsorbed long chain  $R_0$  and therefore reduces  $K$ . The coil size is defined as  $R_0^2 =$

$Za^2$  where  $Z$  is the number of monomers per adsorbed chain [29]. The coil stiffness<sup>3</sup> scales with the coil size as  $K \propto R_0^{-2}$ . Similar to tube dilation [58], the adsorbed long chain coil inflates once short chains are included in the system. As  $R_0$  increases, the coil stiffness decreases and coils reach their critical diameter  $D^*$  for disentanglement at lower stresses.

The difference in the slip behavior hence relies on the amount of the viscous force transferred to each adsorbed coil and the coil stiffness which determines the critical stress for the onset of the transition slip regime. The critical conditions for the onset of the transition regime thus is extremely sensitive to the *content* and *size* of short chains.

The results in this study along with those from our previous work on the slip of bidisperse PBD samples signify the crucial role played by short chains in the slip of molten polymers. Moreover, there is a clear difference between the slip of a polydisperse polymer and a polymer mixture containing two or more components having distinctly separated molecular weights. Since the theoretical models on the slip of polydisperse polymer melts have not yet been established and even the experimental database on this subject is poor we hope these interesting findings can be used as some preliminary steps towards understanding the complex slip behavior of polydisperse polymers.

#### 4.4. Conclusion

The experimental results presented here highlight the important role of short chains in wall slip of molten polymers: the wall slip of highly-entangled tridisperse polybutadienes with fixed weight average molecular weight  $M_w$  and varying number average molecular weight  $M_n$  over a silicon wafer substrate is very sensitive to the *content* and *size* of short chains. The experiments revealed that weakly-entangled and un-entangled chains influence wall slip of polydisperse polymers differently. Ternary samples containing moderate amounts of weakly-entangled chains  $M \sim 3M_e$  exhibited enhanced slip over silicon wafers compared to equivalent systems with un-entangled chains.

In ternary PBD samples containing weakly-entangled chains, the wall slip at fixed  $M_w = 143$  kg/mol strongly depends on the value of  $M_n$ . Over our experimental window of

shear stress, the high- $M_n$  samples were within their weak slip regime while the low- $M_n$  samples were in the process of transitioning to the strong slip regime. The key differences amongst these samples are their critical shear stresses  $\sigma^*$  at the onset of the transitional regime and the slopes in the transition. Since the differences become more pronounced at lower values of  $M_n$ , it is evident that slip is favored in binary mixtures with two distinct molar modes in contrast to ternary samples containing a third middle-size constituent. As a result, polydisperse polymers with low  $M_n$  may not necessarily show the same enhanced slip behavior as the ternary samples did.

We explain the difference in the slip behavior of the samples containing the weakly- and un-entangled chains using the tube dilation theory through the Brochard and de Gennes disentanglement slip mechanism. The slip behavior depends on the amount of viscous force transferred to surface adsorbed coils and the coil stiffness in the two cases which determines the critical coil diameter for the onset of the transition regime. The slip behavior is different in these two cases since the force balance between the mobile and adsorbed chains changes through the reduced entanglement density and coil stiffness due to the incorporation of short chains.

## 5. CHAPTER 5

### **Disentanglement Induced Surface Enrichment of Short Polymer Chains in Simple Shear Flow with Slip<sup>1,2</sup>**

S. Mostafa Sabzevari, Paula M. Wood-Adams\*

*Department of Mechanical and Industrial Engineering, Concordia University, Montreal, QC, Canada*

#### **Abstract**

We present the first experimental results of disentanglement induced surface enrichment of short chains under simple shear flow with slip validating the disentanglement slip theory of Brochard and de Gennes. The surface enrichment of short chain species occurs to extents higher than predicted by thermodynamic segregation theories. Previously, flow induced fractionation has been reported only in Poiseuille flow with fractionation being attributed to the presence of a shear stress gradient across the channel. The phenomenon that we describe is likely present to a significant extent in strong flows in which the polymer contains two distinct separate molar modes of highly and weakly entangled chains. We emphasize the distinction between samples of broad, unimodal molecular weight distribution as compared to bimodal distributions – explaining contradictory results in the literature. We also propose a simple disentanglement induced enrichment model that fits our experimental data very well. These findings will significantly impact our understanding of many polymer flow related phenomena including wall slip, die drool, and extrudate surface instabilities.

---

<sup>1</sup> This chapter is submitted for journal publication as: “Disentanglement Induced Surface Enrichment of Short Polymer Chains in Simple Shear Flow with Slip”, S. Mostafa Sabzevari, Paula M. Wood-Adams.

<sup>2</sup> Additional information is given in Appendix B.

## 5.1. Introduction

Surface enrichment of short chains in polydisperse polymers [50,63,69-71] has extensive implications in polymer processing and end-product surface characteristics. In polymer processing, wall slip [63,102,103], die drool [72,73] and extrudate surface instabilities [2] have been related to surface enrichment of low molecular weight species at the interface. Also affected are surface properties that are important specifically in lubrication and polymer thin film applications. These issues make the surface enrichment of short chains an important but poorly understood aspect of the behavior of polydisperse systems typical of industrial polymers.

In linear polydisperse polymers, chains are chemically identical differing only in molecular weight. Surface segregation is thus mainly induced from factors motivated by chain length disparities. These factors in both flow and static conditions can be entropically driven by the reduced conformational entropy at the surface or enthalpically driven by the surface attraction of chain ends. The latter reflects the surface energy difference between the backbone and end groups of the chain [50,69]. Under certain flow conditions such as capillary extrusion, surface segregation is also believed to be mechanically driven by the shear stress gradient across the flow channel - this is called the shear induced fractionation hypothesis [63,73,75].

Shorter chains suffer less from entropy reduction at a surface than longer chains and hence are thermodynamically driven to the surface to maximize the entropy of the system [70,76]. Van der Gucht *et al.* [69] used the self-consistent field model of Scheutjens and Fler to show that the entropically driven integrated surface excess of a component of chain length  $N$  from a mixture of linear chains is:  $A(1 - N/N_w)\phi_{N,b}$  where  $A \approx 0.195$  is a universal prefactor,  $N_w$  is the weight average chain length, and  $\phi_{N,b}$  is the bulk volume fraction. This relationship suggests that the relative surface excess of linear short chains due to the entropy loss at the surface cannot exceed 19.5%.

Energetic factors strongly enhance surface segregation when end segments are preferentially attracted to the surface as compared to backbone units resulting in a change in the prefactor  $A$  in the van der Gucht *et al.* relation. In a linear system since all chains

possess two ends, the number of backbone units determines which chains are more affected by the energetic force. This means that the shorter chains are enriched or depleted at the surface [50,69] depending on the relative surface attraction of the chain ends and the backbones. [77]

We previously studied the slip of binary and ternary mixtures of short and long chains of polybutadiene PBD on silicon wafer in a planar Couette flow [102,103]. We showed that apparent slip – due to cohesive failure – is most favored in mixtures with two distinctly separate molar masses in contrast to polydisperse systems. We found the maximum slip of long chains occurs when mixed with 10 wt% weakly entangled chains: both content and size of short chains affect apparent slip. In accord with previous studies yet in the absence of the shear induced fractionation, the observed behavior may be related to short chain surface enrichment, the topic of the current work.

A key factor missing from the current understanding of the surface enrichment phenomenon under strong flow and related macroscopic behavior (die drool, wall slip, extrudate surface instabilities) is an enrichment mechanism that is consistent with all empirical knowledge. The mechanism must be appropriate to the time span of experiments – the diffusion time for the migration of chains due to a shear gradient or thermodynamic factors has always been a subject of concern. The mechanism should not require a shear gradient in order that observations from simple shear are explained as well as those from Poiseuille flow. Finally, the mechanism should be able to explain apparently contradictory results that exist in the Poiseuille flow literature.

The objective of the present study is to provide the first experimental data on the extent of the surface enrichment of short chains after strong slip in planar Couette flow and to propose a new enrichment mechanism that is consistent with all available experimental observations.

The measurement of surface enrichment and its relationship to slip is extremely difficult. Characterizing the surface composition of a mixture of chemically identical chains has been one of the most challenging aspect [78,79]. The use of MWD analyses has been hindered by experimental difficulties in collecting samples: the depth of the

enrichment layer is so narrow that it is practically impossible to separate it from the bulk for gel permeation chromatography (GPC) measurements. Spectroscopic characterization techniques, on the other hand, suffer from the lack of a proper test probe to monitor the enrichment without inducing additional energetic effects, e.g. deuterating a chain lowers its surface energy and induces an energetic driving force [79,80].

Tanaka *et al.* [79] were the first to measure the surface enrichment of short chains in thin polystyrene PS films without chemical labeling. They measured the glass transition temperature  $T_g$  of the air-polymer surface of binary and ternary mixtures of short and long chains and compared those to the surface  $T_g$  of the pure constituents. By using a typical  $T_g$  mixing rule, they inferred the surface composition. Their work is indeed interesting, illustrating relative excess of short chains to more significant extents than the maximum value predicted by the van der Gucht *et al.* relation which only takes into account entropic effects. As the authors reported [77], preferential attraction of chain ends to the surface was clearly a contributing factor.

To explore the surface enrichment of short chains under flow conditions, we examine the surface composition of binary and ternary mixtures of linear monodisperse polybutadiene PBD samples after strong slip. In sliding plate rheometry with steel plates at small gaps ( $\sim 0.7$  mm), a hazy debris remains on the substrate after the sample undergoes strong slip. Since the polymer slip plane on adsorbing substrates occurs at one or a few molecular chains above the interface [1,37], the debris represents the outermost surface of the polymer sample in contact with the substrate.

We collect this debris and measure its MWD using GPC without need for chain labeling. This work is the first presentation of the MWD of the interfacial layer at the polymer-solid interface after strong slip in Couette flow. The results indicate significant surface enrichment of short chains at the polymer-solid interface. We interpret the observed behavior in the frame of the disentanglement slip theory and extend it to account for surface enrichment of short chains. We propose that disentanglement-induced surface enrichment of short chains is significant in every flow involving slip given that the polymer possesses an appropriate molecular weight distribution, close to bimodal rather than unimodally

polydisperse. This mechanism may be the key to solving many polymer processing limitations including die drool. Schmalzer and Giacomini [74] recently showed that the rate of die drool production can be described by a simple fluid dynamics approach incorporating slip. We believe that our proposed mechanism can explain die drool production.

## 5.2. Materials and Experiments

For the experimental studies we use three narrowly distributed linear 1,4-polybutadiene (PBD: cis 68%, trans 27% and 1,2 addition 5%) with  $M_w = 6, 165, \text{ and } 329$  kg/mol and polydispersity index,  $PI \leq 1.17$  provided by Polymer Source Inc. The polymers were synthesized by living anionic polymerization using *sec*-butyllithium initiator in toluene or cyclohexane. This process results in chains with a *sec*-butyl group at one end and a proton at the other. Binary and ternary mixtures were prepared in solution ( $\sim 10$  wt% polymer) with dichloromethane (DCM) by mixing for 3 days. Solvent was evaporated at room temperature followed by further drying under  $\sim 70$  cmHg vacuum for 3 days.

All SPR [5] experiments were done at room temperature. To prepare specimens,  $\sim 2.5$  g of polymer was placed inside a compression mold and pressed for 30 minutes to allow for relaxation. The specimen was placed at the center of the SPR stationary plate and the plates were fixed at the gap of 0.7 mm. The sample was allowed to relax for  $\sim 30$  minutes after which it was sheared at a nominal shear rate in the range of  $3 - 5 \text{ s}^{-1}$  which based on direct slip measurements [102,103] is known to be within the strong slip regime.

All samples containing the high molecular weight PBD (329k) left a hazy debris behind on both plates (Figure 5.1) confirming strong slip [5]. The length of debris is the same on both plates indicating equal slip. We carefully collected the central portion of the debris from the bottom plate using tetrahydrofuran (THF) and a pipette. A sample of bulk material was taken from the middle of the sheared specimen for comparison. The MWD were then characterized using GPC relative to linear polystyrene (Waters 1525; THF at  $35^\circ\text{C}$  with a flow rate of 1 mL/min; Phenomenex column; refractive index detector).

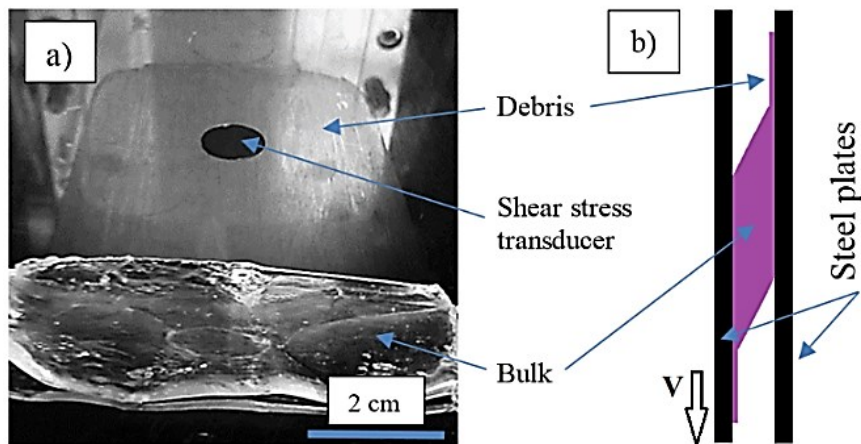


Figure 5.1. (a) Bulk and debris material after strong slip of PBD and (b) schematic of polymer slip in the SPR shear cell [104]. Both plates have mirror polished finishing.

### 5.3. Results and Discussions

The GPC chromatograms of the bulk and debris samples of binary and ternary PBD mixtures are shown in Figure 5.2. These chromatograms are the first presentation of the MWD of the interfacial layer at the polymer-solid interface during strong slip under Couette flow. The remarkable feature observed in all chromatograms is the increase in the short chain content of the debris as compared to the bulk. The second important feature is the narrowness of the high molecular weight peak of the debris compared to that of the bulk. Interestingly, the debris seems to contain predominantly the longest chains within the high molecular weight mode.

It is surprising that such a high degree of surface enrichment of short chains is observed in planar Couette flow where there is no shear stress gradient. Musil and Zatloukal [73] previously showed that the MWD of die drool of polydisperse HDPE after extrusion through a capillary has a lower molecular weight than the original polymer. The authors attributed this to shear induced fractionation. In our experiments however, there is no shear gradient and we propose that the disentanglement process occurring during strong slip determines composition of the debris layer. This will be considered later.

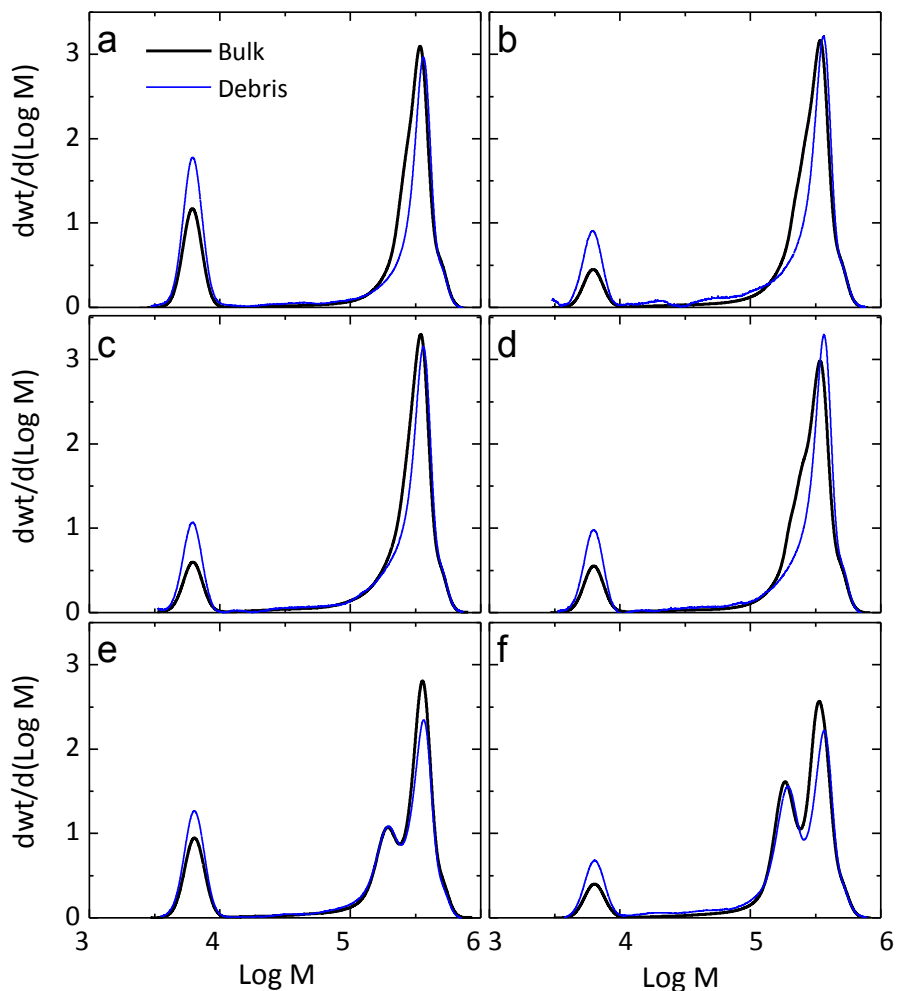


Figure 5.2. GPC chromatograms of bulk and debris samples of binary (a-d) and ternary (e and f) PBD mixtures.

Table 5.1 lists the weight average molecular weights,  $M_w$ , and compositions of the bulk and debris. The weight fraction values were obtained from the area under each modal peak of the data in Figure 5.2. For ternary mixtures, the peaks at the high molecular weight end were resolved using the MWDs of the original constituents. We also define the relative excess of a component of chain length  $N$  in the debris  $\theta_N$  as  $\theta_N = (\phi_{N,d} - \phi_{N,b})/\phi_{N,b}$  where  $\phi_{N,d}$  and  $\phi_{N,b}$  are the weight fractions of chain length  $N$  in the debris and bulk, respectively. All debris are enriched in the lower molecular weight modes 6K and 165K. Evidently, there is a depletion of the highest molecular weight mode 329K in all debris resulting in lower values of  $M_w$ .

Table 5.1. Molecular weight and composition of PBD mixtures: bulk versus debris\*

Sym	$M_{w,b}$ [kg/mol]	$\phi_{6K,b}$ [wt%]	$\phi_{165K,b}$ [wt%]	$M_{w,d}$ [kg/mol]	$\phi_{6K,d}$ [wt%]	$\phi_{165K,d}$ [wt%]	$\theta_{6K}$ [%]	$\theta_{165K}$ [%]
<b>a</b>	285	8.3	0	264	17.2	0	+107	NA
<b>b</b>	278	10.5	0	269	17.8	0	+70	NA
<b>c</b>	280	11.3	0	262	19.5	0	+73	NA
<b>d</b>	254	21.2	0	228	33.1	0	+56	NA
<b>e</b>	268	7.7	29.5	247	13.0	32.4	+69	+10
<b>f</b>	257	18.2	13.6	229	24.4	18.6	+34	+37

\* The balance of all systems consists of 329K long chains.

The fractionation of our mixtures is in accord with the van der Gucht *et al.* relation [69] in that the components with molecular weights below the overall mixture molecular weight are enriched in the debris. The surface excesses that we observe, however, are far above the maximum predicted value. Additionally, the van der Gucht *et al.* relation predicts a relative surface excess dependency  $N/N_w$  that saturates at its maximum for all of our experimental compositions while the data do not (Table 5.1). This clearly indicates that mechanisms other than surface entropy loss induced segregation are in play in the enrichment of shorter chains at the interface under strong slip.

Next we consider surface segregation driven by preferential attraction of chain ends to the surface. Archer *et al.* [50] used the linear response theory to investigate the effect of polydispersity on surface segregation. They produced a similar surface excess relationship to that of van der Gucht *et al.* with the parameter  $A$  replaced by  $U_e$  containing contributions both energetic and entropic effects. The expression of the relative surface excess remains the same though a different maximum is obtained depending on  $U_e$  taking into account the attraction or repulsion of end groups to the interface. The model still fails to capture the strong dependence of  $\theta_{6K}$  on  $\phi_{6K,b}$  that we observe. Therefore we conclude that the thermodynamic models for surface segregation are insufficient for describing the behavior under strong slip in simple shear.

We note that the fractionation we observe in our MWD graphs has the potential to be related to our sample collection method. This is due to the fact that longer chains in contact with solid substrates have more adsorption sites and therefore they may require longer

dissolution time. Since we have been very careful with our debris collection technique and dissolved the polymer three times on the same area, we assume that no polymer chains remain on the steel substrate after dissolution.

The picture we are describing next is a flow induced fractionation mechanism driven by the disentanglement process of strong slip instead of the shear stress gradient typical of channel flows. The idea is established on the basis of the slip disentanglement mechanism [77,29,30] and we focus on the molecular weight distribution of a polydisperse polymer near the polymer-wall interface after strong slip occurs.

In the Brochard and de Gennes slip theory of monodisperse chains of size  $P$  flowing over a layer of grafted chains of size  $N$  where  $P > N$ , it is assumed that some mobile chains are entangled with grafted chains and “are confined in a certain “skin” of thickness  $R_p = aP^{1/2}$  near the solid surface” [30]. At high slip velocities above a critical slip velocity ( $V^{**}$ ), mobile chains in the skin region become disentangled from grafted chains [30]. Brochard and de Gennes state that “we have no deep knowledge of what happens at  $V > V^{**}$ , but we suspect that the  $P$  chains are torn out from the grafted chains and that a completely novel regime follows”. We attempt to address that regime.

In the case of surface adsorption instead of end-grafting, the average length of free ends of the adsorbed chains would always be smaller than that of the bulk due to adsorption sites along each chain. Therefore, a similar condition as  $P > N$  stands in general. If the chains are polydisperse, some mobile chains may be trapped in the adsorbed layer under strong slip. In fact the likelihood of them being pulled out depends on the proportion of their entanglements with the bulk as compared to adsorbed chains.

Our understanding is that: with a polydisperse melt in the strong slip regime, some mobile chains near to the slip plane are pulled out of the interfacial layer by the bulk flow while others remain trapped among the adsorbed chains. This picture describes the interfacial layer after strong slip as a system containing both adsorbed and trapped (non-adsorbed) chains. The slip plane is therefore located between this layer and the bulk. Such an assumption is consistent with the slip model of Joshi *et al.* [77] and perhaps with that of Tchesnokov *et al.* [39].

Next, we make the following assumptions: (a) the slip plane is located at one radius of gyration of the longest chains  $R_{g,l}$  above the wall, i.e., the interfacial debris layer has a thickness of  $\sim R_{g,l}$  and (b) a portion,  $r$ , of chains located within half their radius of gyration from the slip plane are pulled out and carried away by the bulk flow (Figure 5.3).

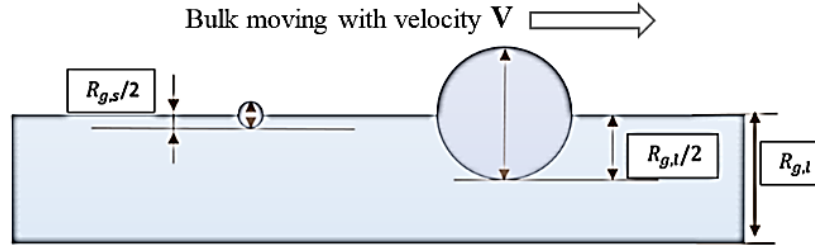


Figure 5.3. Schematic of the simple disentanglement induced enrichment model.

We consider a tridisperse system containing short, intermediate, and long chains with  $R_{g,s}$ ,  $R_{g,m}$ , and  $R_{g,l}$  as their radius of gyration, respectively. The density of all species is assumed to be the same. The content of each species in the interfacial layer after strong slip is calculated as their original content (the same as that of the bulk) minus those chains pulled out of the system. Therefore, the concentration of short chains in the debris layer after strong slip,  $\phi_{s,d}$ , is:

$$\phi_{s,d} = \frac{(R_{g,l} - r R_{g,s})\phi_{s,b}}{(R_{g,l} - r R_{g,l})\phi_{l,b} + (R_{g,l} - r R_{g,m})\phi_{m,b} + (R_{g,l} - r R_{g,s})\phi_{s,b}} \quad \text{Eq. (5.1)}$$

where  $\phi_{s,b}$ ,  $\phi_{m,b}$ , and  $\phi_{l,b}$  are concentration of short, intermediate, and long chains in the bulk. Figure 5.4a) compares the experimental data from binary mixtures of PBD 329 and 6 kg/mol with our model assuming  $r = 50\%$  and  $\phi_{m,b} = 0$ . The predictions of the van der Gucht *et al.* model and bulk composition are also added for comparison. In Figure 5.4b), the experimental behavior of ternary mixtures is compared to the model predictions for ternary mixtures with fixed contents of intermediate chains  $\phi_{m,b} = 0.295$  and  $0.136$  (similar to samples ‘e’ and ‘f’). The proposed model very closely follows our experimental data. It is also interesting that the choice of  $r = 50\%$  (i.e. half of the chains within  $R_g/2$

from the slip plane are pulled out by the bulk flow due to strong slip) gives a good agreement with our experimental data.

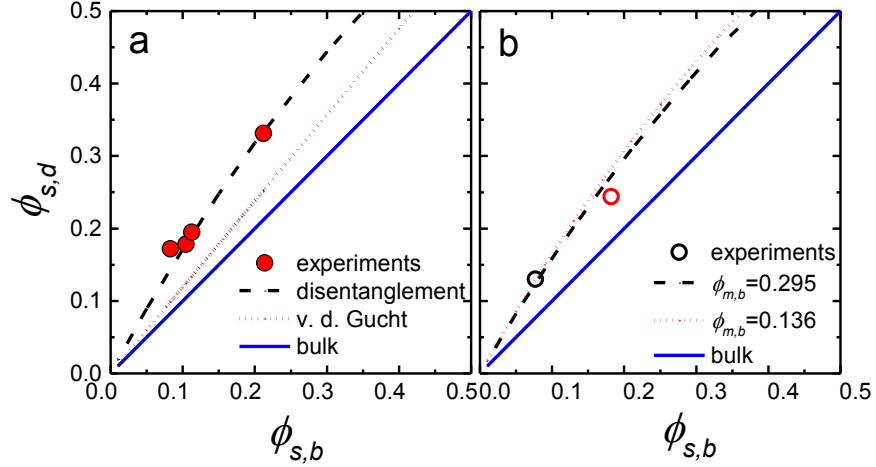


Figure 5.4. Concentration of short chains in the debris layer plotted versus that of the bulk. Experimental data are compared to model predictions: (a) binary mixtures and (b) ternary mixtures. The solid line represents bulk composition.

The proposed model describes the MWD of the interfacial layer of polydisperse polymer melts after strong slip requiring only the length and content of molecular species within the sample. Equation (1) shows that the enrichment depends on the size and content of short chains. Maximum enrichment occurs when both  $R_{g,l}/R_{g,s}$  and  $\phi_{s,b}$  have large values. This means that the short chain surface enrichment is higher in bimodal mixtures compared to polydisperse samples of unimodal MWD. We have previously shown that strong slip of polydisperse polymers in planar Couette flow occurs at a lower stress in binary mixtures of two separate molecular modes as compared to ternary samples of the same  $M_w$  [102,103] provided that all species are entangled. Therefore we are now able to infer that the surface enrichment of short chains is intimately linked to the nature and magnitude of slip

## 5.4. Conclusion

Our model explains that surface segregation in Poiseuille flow may be insignificant if strong slip is not present or the MWD of the sample is far from bimodality. Additionally, the timescale of the enrichment in our viewpoint would be on the order of the disentanglement time and therefore rather short. With this new understanding, the proposed model can be used to facilitate the development of molecular theories to deal with slip dynamics of polydisperse polymer melts flowing over adsorbing surfaces.

## 6. CHAPTER 6

### **Sacrificial Mica Substrates Influence the Slip Boundary Condition of Dewetting Polymer Films<sup>1,2</sup>**

S. Mostafa Sabzevari †, Joshua D. McGraw ‡, Karin Jacobs ‡, Paula Wood-Adams †

† *Department of Mechanical and Industrial Engineering, Concordia University, Montreal, Canada*

‡ *Department of Experimental Physics, Saarland University, Saarbrücken, Germany*

#### **Abstract**

In the experimental study of thin polymer films, a two-stage sample preparation scheme is commonly used: the polymer film is cast first onto mica, and then the film is transferred to another substrate via a water bath. We present evidence of polymer chain conformational or compositional changes arising from the annealing history of the film on mica. Flow dynamics and rim morphology of dewetting holes in monodisperse polystyrene films on hydrophobized silicon wafers are examined using optical and atomic force microscopy. A significant difference in flow dynamics and rim morphology of holes is observed. The difference depends on whether the interface of the film that was previously in contact with mica remains the interface that touches the hydrophobized substrate from which the film dewets. In this case the difference is consistent with a reduced slip boundary condition, and the reduction depends on pre-annealing to be observed. Furthermore, the slip length disparity is sensitive to the molecular weight distribution of the dewetting films. The disparity of boundary conditions is attributed to long-lasting compositional or conformational arrangements arising from surface segregation and/or surface ordering of chains or their segments.

---

<sup>1</sup> This chapter is accepted for publication in *Polymer* as: “Sacrificial Mica Substrates Influence the Slip Boundary Condition of Dewetting Polymer Films”, S. Mostafa Sabzevari, Joshua D. McGraw, Karin Jacobs, Paula Wood-Adams.

<sup>2</sup> Additional information is given in Appendix C.

## 6.1. Introduction

Thin polymer films are extensively studied due to their ubiquitous industrial applications, from microelectronic fabrication to coatings and adhesives. The interest comes as well from the fact that polymer physics may be significantly affected by chain confinement at an interface in which case surface properties are different from those of the bulk [89,105]. As the ratio of the surface to bulk increases, confinement may induce apparent variations in bulk properties such as the glass transition temperature [90,106,107] or the viscosity [108]. Other important physical aspects of polymer chains that can change with confinement include free volume [109], chain conformation [110,111], chain stiffness, and entanglement density [89,112,113]. The causes of these changes may include chain end surface localization [114-116], chain ordering [117], and entropic– or enthalpic–driven surface segregation [50,69,71,76,79,118,119]. Hydrodynamic transport properties can thus in principle be greatly affected by the properties of a polymer melt inherited from its confining interface [120,121]. As we show here, pre-annealed polymer films show differing slip boundary conditions after transfer to hydrophobic substrates, depending on whether the pre-transfer solid/liquid or liquid/vapour interface is probed.

While many of the thin polymer film properties discussed above appear in equilibrium, experimental observations are often conflated with effects arising from the film preparation [122]. One example is the presence of residual stresses due to spin coating [89,123] which may affect the entanglement network [124-126]. In this regard, the effect of annealing and more importantly annealing time is still an open question. The extent of change in surface and thin film properties listed above is therefore a complicated function of all changes owing to confinement effects and preparation history. Having a thorough understanding of all these effects when examining surface properties is, though a considerable challenge, thus essential.

Surface effects induced by the use of sacrificial substrates in the preparation of thin polymer films have not yet to our knowledge been explored. As in this study, the investigation of thin polymer films often includes a two-step film casting procedure using

such a sacrificial mica sheet: the polymer film is first spin coated onto a freshly cleaved sheet of mica, which offers a complete wetting condition [48] for polystyrene. The film is then transferred to the desired substrate by floating onto a clean water bath [90,127-130]. Films may as well be pre-annealed on mica. This two-step procedure is typically used when: i) the polymer solution is ejected from the hydrophobized substrate [127,128], precluding the formation of a film; ii) direct deposition of the solution dissolves an underlying coating [129,130]; or, iii) the study of free-standing films is undertaken [90,112,131]. It is of crucial importance to understand whether these preliminary steps influence final properties in any way [89].

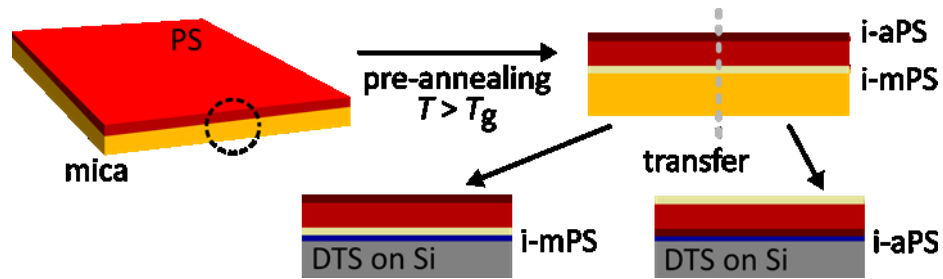


Figure 6.1. Schematic of the sample preparation undertaken in this study. A polystyrene (PS) film is spin coated onto a mica substrate. Annealing above the polymer glass transition,  $T_g$ , results in differences between the air/PS interface (i-aPS) and the mica/PS interface (i-mPS). After placing these interfaces in contact with a hydrophobic substrate (DTS schematically indicated, native  $\text{SiO}_2$  layer not shown), it is possible to detect differences between i-aPS and i-mPS through dewetting of the polymer film on a hydrophobic substrate.

One way to investigate this possibility is to use the dewetting experiment that has long been used to study flow dynamics and surface behavior of polymer melts [132]. In dewetting experiments, the rim morphology of the dewetting front (or dewetting hole) reflects physical characteristics of the polymer/solid interface represented by the slip length [93]. The linear Navier slip length is defined as the ratio of bulk viscosity to the friction coefficient at the slip plane [26]. Any compositional or structural change of the molecular layer in the immediate vicinity of the slip plane thus has the potential to be reflected in slip properties and consequently the rim morphology.

In the present work we investigate surface effects arising from the two-step film casting procedure as a common practice in many polymer thin film studies. Specifically, we show that annealing a polymer film on mica results in a difference between the air/polymer interface relative to the air/mica interface (termed i-aPS and i-mPS in the following). The difference between i-aPS and i-mPS is elucidated through the study of the solid/liquid boundary condition of the film after transfer to a hydrophobic substrate. A schematic representation of the sample preparation protocol is shown in Figure 6.1. Mechanisms contributing to the observed differences may include short-chain surface segregation and ordering of polymer chains (or their segments) that can cause conformational or compositional heterogeneities along the film thickness, and importantly, near the solid-liquid interface after transfer. The investigations were undertaken by observing, with optical microscopy, the growth of nucleated holes in polymer films with undisturbed thicknesses  $150 < h_0 < 200$  nm. Quantitative information about the slip boundary condition was obtained by recording the profiles of the rims formed ahead of the dewetting fronts with atomic force microscopy (AFM).

## 6.2. Materials and Experiments

We used polystyrene, PS (Polymer Source Inc.) with number-averaged molecular weights  $M_n = 10, 27, 51, 130$  and  $465$  kg/mol and polydispersity indices below 1.05; we refer to these as the monodisperse polymers, and use, for example, the shorthand notation PS(465k). These monodisperse polymers were dissolved in toluene with various concentrations in order to obtain undisturbed film thicknesses  $150 < h_0 < 200$  nm when spin coated onto freshly cleaved mica. Bidisperse solutions of PS(465k), with weight fraction  $\phi$ , and PS(27k), with weight fraction  $1-\phi$ , in toluene were also prepared. Total polymer mass fractions in the toluene solutions were chosen in order to obtain the same range of film thicknesses as for the monodisperse films. These film thicknesses were at least 8 times the unperturbed polymer size (radius of gyration) of the polymers used here [133].

PS films on mica were cut into several smaller pieces, roughly 7 mm × 7mm, using a scalpel blade. In cases where the comparison between as-cast and pre-annealed films were made, half of the pieces examined were floated and transferred to hydrophobic substrates (see below) and the remainder were pre-annealed. Films were pre-annealed in air using a Linkam heating stage at 95, 110, 130 and 150 °C for 1 hr for molecular weights 10, 51, 130 and 465 kg/mol. Bidisperse films were all pre-annealed at 150 °C for 1 hr. All raw data (i.e. optical or atomic force microscopy) compared to each other in a given figure therefore has the same preparation history on mica aside from the pre-annealing procedure, and comes from the same film on mica.

All films were floated onto the surface of an ultra-clean water bath (TKA-GenPure, 18.2 MΩ cm, total organic carbon content < 5ppb) and picked up using hydrophobized Si wafers (Si-Mat Silicon Materials, (100) crystal orientation). Silicon wafers were hydrophobized in two ways. The first was to use dodecyltrichlorosilane (DTS, Sigma-Aldrich) self-assembled monolayers (SAMs), with the details of the silanization procedure found in [134]. Monodisperse films dewetted from these SAMs. Second, we used a fluoropolymer AF 2400 (Poly[4,5-difluoro-2,2-bis(trifluoromethyl)-1,3-dioxido-co-tetrafluoro-ethylene], Sigma-Aldrich) which was used for the dewetting of bidisperse films. General conclusions drawn in this study are not affected by the choice of the substrate, and we note that similar effects have also been observed using monodisperse 173 kg/mol poly(methyl-methacrylate) dewetting from DTS.

We selectively picked up the floating films from the top or bottom surface as schematically depicted in Figure 6.1. In films picked up from the top surface, the polymer/air interface is placed onto the DTS. When the film is picked up from the bottom surface, its polymer/water interface – previously in contact with mica - is placed onto the DTS. Therefore, we categorize polymer films on DTS according to their previous contact with air (denoted as i-aPS) or mica (denoted as i-mPS). Before picking up the polymer/air interface, the hydrophobized substrate was first inserted into the water. This allows us to ensure that the substrate contact with water, as occurs in case of the polymer/mica interface (Figure 6.1d), is not the source of any potential discrepancy in results.

Samples were heated to above the glass transition  $T_g \leq 100$  °C to start dewetting by nucleation and growth of holes. Optical microscopy (Leitz) and atomic force microscopy AFM (Multimode) were used to capture the flow dynamics and morphology of the dewetting rim. In all experiments on as-cast and annealed samples, dewetting was captured only for holes nucleated with at least 10 min delay after the dewetting temperature was reached. This can be considered as additional pre-annealing on the dewetting substrate. The pre-annealing is vital to ensure that dewetting is least affected by spin coating-induced frozen-in stresses, which are likely the highest in case of as-cast films [135].

### 6.3. Results and Discussion

Figures 6.2a) and 6.2b) show optical microscopy images of PS(465k) films ( $h_0 \approx 175$  nm) dewetting from DTS. Between a) and b), the only difference in film preparation was whether or not the sample was of the pre-annealed i-aPS or i-mPS type (see Figure 6.1 for nomenclature definitions); the identical film on mica was used, sections of which were floated onto pieces of the same DTS coated Si wafer, and the films were dewetted at the same temperature. Figure 6.2c) shows the temporal evolution of the contact line radius,  $R(t)$ , of similarly prepared PS films dewetting from DTS. The results in Figure 6.2 show that with the pre-annealed i-mPS in contact with DTS, dewetting is slower compared to all other experimentally accessed possibilities. That is, the disparity between i-aPS and i-mPS type samples is dependent on pre-annealing. Furthermore, an as-cast (not pre-annealed) i-mPS sample dewets similarly to i-aPS, regardless of the annealing history of i-aPS type samples.

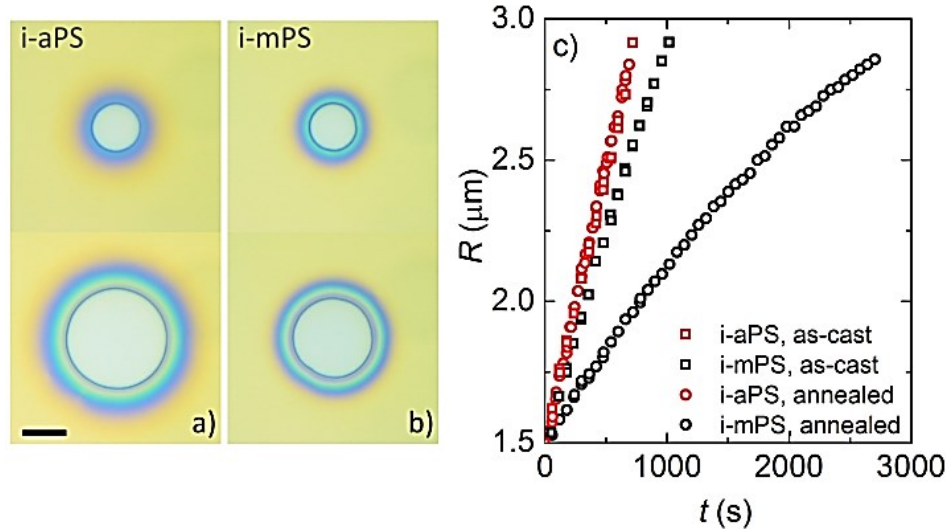


Figure 6.2. (a) Optical microscopy of dewetting PS(465k) films (yellow online) with annealed i-aPS in contact with DTS (white) and (b) with annealed i-mPS in contact with DTS. The initial radii (top row) are the same, and the time interval between top and bottom rows are the same. (c) For similar films, contact line radius,  $R$ , as a function of time. For comparison, unannealed i-aPS and i-mPS data sets are shown, which, within the expected variance, are consistent with the annealed i-aPS dewetting sample.

The height profiles, obtained using AFM, of the dewetting films represented in Figure 6.2c) are shown in Figure 6.3a). Consistent with the varying dynamics seen in Figure 6.2 the rim morphologies of i-aPS samples and pre-annealed i-mPS samples are also different, suggesting an altered hydrodynamic slip boundary condition. Specifically, the pre-annealed i-mPS sample exhibits a much shorter decay length compared to the i-aPS sample and the two samples that were not pre-annealed.

Only the interfaces in contact with the DTS are different in comparing different data sets in Figure 6.2. We therefore turn our attention to the evaluation of the slip hydrodynamic boundary condition. The slip hydrodynamic boundary condition can be characterized by the linear Navier slip length,  $b$ ,  $b = \eta/k_f$ , where  $\eta$  is the fluid viscosity and  $k_f$  is the friction coefficient. There are various methods of evaluating the slip length in dewetting films [93,127,132]. In the following, however, we use the most reliable method, which is the characterization of the form of the dewetting front [93,127]. Specifically, the relaxation of the front into the undisturbed portion of the film is characterized with one or two relaxation length scales, from which the slip length is derived.

To summarize the ideas detailed in [93,127] a sufficiently strong slip boundary condition at the polymer/solid interface results in a rim with a long decay length and a monotonic decay, whereas the no-slip boundary condition results in a shorter decay length with an oscillatory decay profile. At a particular dimensionless dewetting speed (i.e., the capillary number  $Ca$ ) and slip length to film thickness ratio, a transition between oscillatory and monotonic decays can be observed [93,127,132]. Therefore the rim profile of holes of the same contact line radius and film thickness (conservation of volume) can quickly be used to compare relative slip lengths between films: profiles of such holes with oscillations of largest amplitude have the lowest slip length, while those with the longest monotonic decay length have the largest slip length. In making this comparison, care must be taken to ensure that the conditions of Newtonian flow are satisfied (e.g. no visco-elasticity or shear thinning/thickening effects), as is the case here [45].

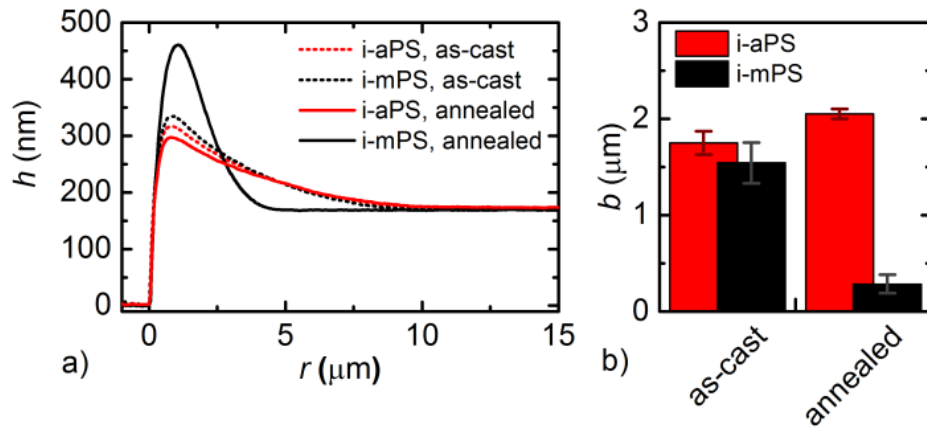


Figure 6.3. (a) Rim profiles of PS(465k) dewetting from DTS at similar hole radius, cf. Figure 6.1b). (b) Slip length of PS(465K) on DTS at  $T_d = 150 \text{ }^\circ\text{C}$  for the profiles shown in (a), from rim profile analysis as described in [127].

Fig. 3b) shows the slip lengths obtained from evaluations of the rim profiles shown in Fig. 3a). The data clearly confirms the disparity between the two interfaces: The slip length of PS(465k) on DTS at  $150 \text{ }^\circ\text{C}$  drops by about an order of magnitude: from  $2 \mu\text{m}$  for the annealed PS/air interface to  $\sim 300 \text{ nm}$  in case of the i-mPS sample. This observation suggests a significant change in the composition or conformation of the PS chains located at the interfacial layer between PS and mica. Furthermore, it is confirmed that without pre-

annealing, there are no differences observable from the present dewetting experiments, between i-aPS and i-mPS.

In order to understand the effect of polymer chain length on the observed slip length disparity, we examine in addition to PS(465k) the dewetting of PS(10k), PS(51k) and PS(130k) on DTS as shown in Figure 6.4a). Dewetting was performed at different dewetting temperatures  $T_d$  as indicated in the caption of Figure 6.4. It is evident that the disparity between the two interfaces is present over a wide range of molecular weights, and that the disparity is molecular weight dependent. We note that obtaining an exact dependence of the extent of disparity between pre-annealed i-aPS and i-mPS samples on  $M$  is difficult since (i) slip of PS on DTS is temperature dependent [93] and (ii) the choice of the dewetting temperature is experimentally limited by the range of viscosities (at least four orders of magnitude at a given temperature) presented by the range of molecular weights. Nevertheless, the extent of slip disparity on DTS decreases with decreasing  $M$ , almost disappearing in the case of PS(10k). Therefore, chain entanglements and/or chain end density may significantly contribute to the observed disparity.

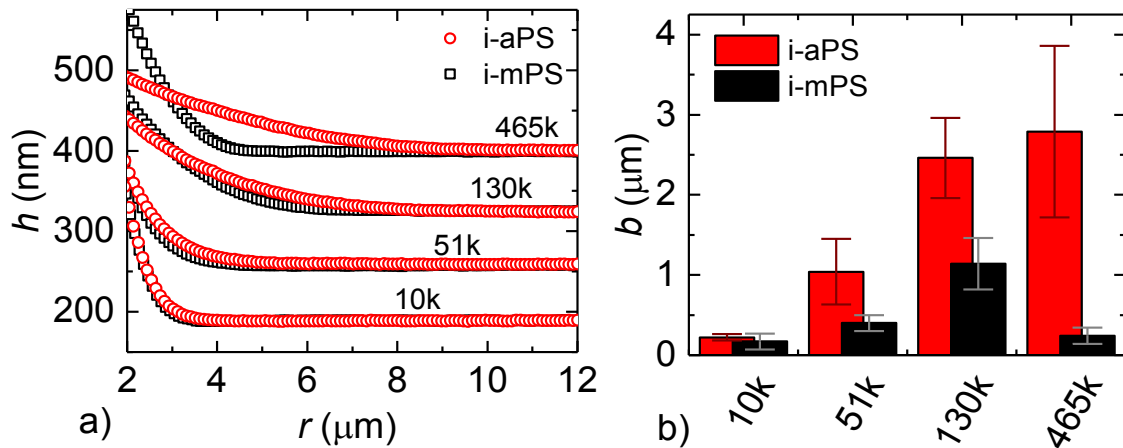


Figure 6.4. (a) Height profiles of PS rims formed during dewetting from DTS: PS(10k) at dewetting temperature  $T_d = 105$  °C; PS(51k) at  $T_d = 120$  °C with vertical profile shifts of 100 nm; and PS(130k) at  $T_d = 140$  °C, 140 nm shift; PS(465k) at  $T_d = 150$  °C, 230 nm shift. All films were annealed on mica prior to transfer (see text for details). (b) Slip lengths extracted from the rim profiles shown in a) for i-aPS and i-mPS (cf. Fig. 1).

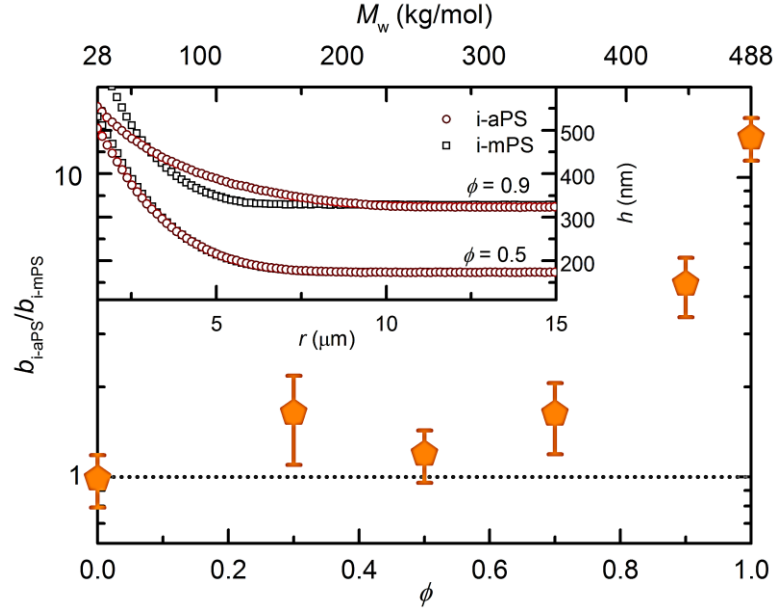


Figure 6.5. Slip length ratios obtained for bidisperse dewetting PS films composed of weight fraction,  $\phi$ , of  $M_w = 488$  kg/mol PS and weight fraction,  $1-\phi$ , of  $M_w = 28$  kg/mol. Inset: height profiles of PS rims formed during dewetting from AF 2400. Profiles for  $\phi = 0.9$  are vertically shifted by 150 nm for clarity.

To assess the relative importance of chain length and chain ends on the annealing effects discussed above, we investigate the slip length disparity between i-aPS and i-mPS in bidisperse polymer films dewetting from AF 2400. PS(465k) and PS(27k) were used to prepare the bidisperse films. As before, the two different interfaces (i-aPS and i-mPS) from the same pre-annealed polymer film in contact with the AF 2400 surface are compared in dewetting experiments. The inset of Figure 6.5 shows height profiles of dewetting films for two compositions. For  $\phi = 0.5$  there is little change in the rim formation arising from the occurrence of either i-aPS or i-mPS in contact with AF 2400; however, the disparity of rim shapes between i-aPS and i-mPS samples is significant for  $\phi = 0.9$ . While the details of the slip lengths obtained from other bi- and tri-disperse polymer melts will be the topic of another work, in the main part of Figure 6.5 we show the ratio of slip lengths between the air and mica interfaces,  $b_{i-aPS}/b_{i-mPS}$ , as a function of blend composition -- since a linear relationship exists between  $\phi$  and the weight averaged molecular weight [136], we show  $M_w$  of the blends for comparison on the top axis of Figure 6.5. For  $\phi \leq 0.5$  no slip length

disparity is observable, while it increases monotonously for  $\phi > 0.5$ . The extent of the disparity on AF 2400 is within error identical to that observed on DTS for the pure PS(465) (i.e.,  $\phi = 1$ ). We also note that  $b_{i\text{-aPS}}/b_{i\text{-mPS}} = 1$  for low molecular weights, i.e. PS(10k) and PS(27k), on both substrates. Thus the effect is not specific to our choice of nonwetting substrates.

In comparing the data sets between Figure 6.4b) and Figure 6.5, we note an apparent contradiction between the onset of slip length disparity for monodisperse and bidisperse molecular weight distributions. For the monodisperse case, we see that a resolvable slip length disparity first appears for  $M_w = 53$  kg/mol. In contrast, the disparity is only observed beyond  $M_w = 260$  kg/mol ( $\phi = 0.5$ ) for the bidisperse blends. Considering instead the number averaged molecular weight,  $M_n$ , this apparent contradiction does not arise.  $M_n$  for a bidisperse blend is computed according to [136]  $M_n = [\phi/M_1 + (1-\phi)/M_2]^{-1}$  where for the films studied here  $M_1 = 465$  kg/mol and  $M_2 = 27$  kg/mol. Accordingly,  $M_n = 51$  kg/mol for  $\phi = 0.5$ , which brings the onset of slip length disparity for the blends in line with the monodisperse observations. Furthermore, this molecular weight is somewhat larger than the critical molecular weight for entanglements ( $M_c = 35$  kg/mol for PS [136]), which coincides as well with the molecular weight at which slip becomes significant for polymer films dewetting from a similar fluoropolymer coating to that which was used here [45,113].

Differences between the liquid/vapour and solid/liquid interfaces of polymer films have been studied both experimentally, theoretically and in simulations. Experimentally for example, Gautam and coworkers [137] used well entangled, monodisperse, PS and studied interfacial phenyl ring ordering using sum frequency generation. They concluded that phenyl rings in PS chains orient differently in contact with air as compared to the orientations present at the solid sapphire interface, the latter being a high-energy surface. Such an ordering discrepancy was also observed in molecular dynamics simulations [138] using PS films surrounded by air and an unstructured, total wetting substrate. With respect to the slip boundary condition, a different orientation of phenyl rings at the solid/PS interface can contribute to a change of the boundary condition for low molecular weight PS [127,139]. If phenyl ring ordering were the dominating effect in these experiments,

however, no influence due to a variation of molecular weight would be expected, which is yet at variance with our observations.

A further disparity can arise from surface segregation of short chains or chain ends to the interface. There have been many experimental and theoretical studies on surface segregation of polymer melts [114-116,50,69,71,76,79,118,119]. Even while a deuterated species preferentially segregates to both solid/liquid and liquid/vapour interfaces [118], Kajiyama and coworkers reported on the enrichment of hydrogenated chain ends at the liquid/vapour interface in monodisperse films of otherwise deuterated PS [114]. The surface enrichment of shorter chains was as well demonstrated by Hariharan and coworkers in further neutron reflectivity studies [119]. What is critical in the present study is to understand how the extent of chain end or short chain segregation at the polymer/air interface may differ from that at the polymer/mica interface; such a difference was reported in [118] for PS on Si. Molecular dynamics (MD) simulations from Daoulas and coworkers [140] furthermore showed that polyethylene chain ends segregate to the liquid/vapour interface to a larger extent than at the solid/liquid interface. Furthermore, Zhou and coworkers studied the hydrodynamic slip boundary condition of polycarbonate on nickel using MD, and found that the slip length was a non-trivial, non-monotonic function of the chain end composition [120,121]. Nickel is a high energy surface and the slip mechanism is different from that in our studies on nonwetting surfaces.

Aside from surface segregation of short chains or end segments, statistical polymer melt properties may also differ significantly between the solid/liquid and liquid/vapour interfaces. Atomistic MD simulations [138,140] indeed show large differences in the density profiles normal to the two interfaces. Such density profile variations are accompanied by differences in polymer chain statistical properties such as orientational bond order and projections of the linear chain end-to-end vector. Since transport properties (*e.g.* viscosity) [136] are governed by such chain statistics, it is reasonable to expect that these differences may have an impact on the experimentally observed slip boundary condition after transfer of the solid/liquid or liquid/vapour interface to an identical substrate.

Clearly, there are several mechanisms by which i-aPS and i-mPS may obtain their apparent differences as observed in the dewetting experiments presented here. Whatever the mechanism for the observed slip length disparity between i-aPS and i-mPS, the outcome of the present work is of crucial importance in surface studies of high molecular weight polymers. Evidently, surface transport properties such as the slip length of thin polymer films may strongly vary from the air to the buried interface, and the compositional and/or conformational arrangement across the film thickness inherited from the annealing procedure on mica persists through the substrate exchange (mica to DTS or AF 2400). These observations have important implications in thin film surface studies involving the two-step film preparation procedure where the choice of the interface may affect the final film properties. Care must be taken to find the appropriate annealing protocol for a given experiment rather than taking published results that may have been achieved on a different substrate [123-126]. As a consequence, differences in compositional or conformational arrangements between the air and buried surfaces have to be carefully addressed when examining surface or bulk properties of thin polymer films when the films are composed of highly entangled polymers.

#### **6.4. Conclusion**

In the present work using dewetting experiments, we showed that annealed polymer/mica and polymer/air interfaces can show significant differences in terms of molecular composition and/or conformation even in the case of monodisperse linear polymers. We showed that the dewetting dynamics and rim morphology of the dewetting hole of annealed polymer films on hydrophobized substrates depend on whether the polymer has been previously in contact with air or mica, and whether the film has been pre-annealed. We find also that the effect is molecular weight dependent, with a larger disparity for well-entangled as compared to unentangled polymers. We showed that these effects induced by specific polymer casting history can be long lasting, i.e., the compositional or conformational arrangements formed during casting may not be undone by the change of substrate and further annealing.

## 7. CHAPTER 7

### Effect of Short Chains on Slip of Thin Polystyrene Films on Non-wetting Substrates <sup>1,2</sup>

S. Mostafa Sabzevari †, Joshua D. McGraw ‡, Karin Jacobs ‡, Paula Wood-Adams †

† *Department of Mechanical and Industrial Engineering, Concordia University, Montreal, Canada*

‡ *Department of Experimental Physics, Saarland University, Saarbrücken, Germany*

#### Abstract

We investigate the effect of short chains on slip of highly entangled polystyrenes (PS) during thin film dewetting from nonwetting fluorinated surfaces. Binary and ternary mixtures were prepared from monodisperse PS with weight average molecular weights  $5 < M_w < 490$  kg/mol. Flow dynamics and rim morphology of dewetting holes were captured using optical and atomic force microscopy. Slip properties are assessed in the framework of hydrodynamic models describing the rim height profile of dewetting holes. We show that short chains with  $M_w$  below the polymer critical molecular weight,  $M_c$ , play an important role in slip of highly entangled polymers. Among mixtures of the same  $M_w$  those containing chains with  $M < M_c$  exhibit larger slip lengths as the number average molecular weight,  $M_n$  decreases. The slip enhancement effect is only applicable when chains with  $M < M_c$  are mixed with highly entangled chains in a lower proportion -- the content of the long chain component,  $\phi_L$ , has to be dominant ( $\phi_L > 0.5$ ). Results show that short chains affect slip of highly entangled polymers due to the physical/chemical disparities of end

---

<sup>1</sup> This chapter is under preparation to be submitted for journal publication as: “Effect of Short Chains on Slip of Highly Entangled Polystyrenes during Thin Film Dewetting”, S. Mostafa Sabzevari, Joshua D. McGraw, Karin Jacobs, Paula Wood-Adams.

<sup>2</sup> Additional information is given in Appendix C.

groups as compared to the backbone units. The enhanced slip in this regard is attributed to the effect of chain end groups on the interfacial friction coefficient. Accordingly, for PS, a higher concentration of end groups at the interface results in a lower friction coefficient which consequently enhances the slip length.

## 7.1. Introduction

In contrast to the common no-slip boundary condition of small molecule fluids, polymer melts exhibit different boundary conditions from no-slip to strong slip, the extent depending on a variety of factors including the substrate surface chemistry and polymer chain size. Highly entangled polymer melts as an example exhibit a great deal of slip during flow on low surface energy substrates, however, the slip length is significantly reduced if highly adsorbing substrates are used instead [1]. Thorough understanding of the extent of polymer slip is critical due to extensive practical importance. Knowledge of slip properties allows for the correct measurement and characterization of material properties such as viscosity [141]. It also allows for improving manufacturing processes [18,20], spreading of paints and coatings [142], and surface finishes of polymeric products [2]. Such knowledge is also vital for developing more accurate slip theories for better model predictions [29,39].

In polymer flow, slip can be due to cohesive and/or adhesive failure, the failure mode is mainly governed by the substrate surface energy and shear rate [2,29,39]. On a high surface energy substrate such as glass or steel, some polymer chains adsorb onto the solid wall forming an adsorbed layer above the interface while others move with the bulk flow above them. During flow, the polymer starts to slip away on the adsorbed layer due to cohesive failure; slip in this case is called apparent slip. At high shear rates, the slip mechanism may change to adhesive failure if desorption occurs [26]. Dynamics of slip on high surface energy substrates is controlled by the density of adsorbed chains, their bonding energy to the wall, and number of entanglements between adsorbed and mobile chains [19,102,103].

On smooth and non-adsorbing surfaces [26], with supposedly very low surface energies, slip is due to adhesive failure and mobile chains are directly in contact with the solid surface. Polymer slip on non-adsorbing walls, called true slip, is shear stress independent and controlled by the chain-wall friction coefficient and polymer viscosity [29,93].

The slip behavior of monodisperse polymers on high surface energy [1,19] and low surface energy substrates [45,93] has been studied extensively in the past. Industrial polymers are however polydisperse [57]. The polydispersity effect on apparent slip has previously been explored [57,64,65,102,103]. It has been shown that the polymer slip on adsorbing walls may significantly be affected by the size and content of short chains in the system. Weakly entangled chains are in particular of significant importance in enhancing slip of highly entangled polymers [102,103]. The enhanced slip was partly attributed to the enrichment of short chains at the slip plane which reduces the number of entanglements between the adsorbed and mobile chains [63,104].

The effect of polydispersity on slip near low surface energy substrates has not yet been fully explored. Theoretical [26,29,30] and experimental [45] studies on slip of polymers on low energy substrates have been focused on monodisperse samples. Polydisperse polymers with large polydispersity indices are rich in the number of end groups that is likely affecting surface/interfacial properties [116]. Other polydispersity related phenomena such as end group surface localization [77,79] and short chain surface segregation [50] can also significantly influence surface properties including the slip length.

A simple tool to study the effect of polydispersity on slip of polymers near low surface energy substrates is the dewetting experiment [48]. Recent theoretical and experimental studies on the morphology of the dewetting hole/front on nanoscale thin polymer films showed that the boundary condition at the polymer-wall interface directly governs the rim morphology of the dewetting hole/front [92,93]. Specifically, the relaxation of the front into the undisturbed portion of the film is characterized with one or two relaxation length scales, from which the slip length is derived. Hydrodynamics equations along with the

Navier's slip boundary condition were used to model the front portion of the dewetting rim. The rim profile analysis technique is a reliable method of slip length determination using dewetting experiments.

In the present work, we investigate the effect of short chains on slip of highly entangled polystyrene (PS) mixtures near fluorinated substrates as the first step towards understanding the more complex subject of polydispersity. To this end, dewetting of thin PS films on fluoropolymer (AF 2400) coated Si wafers are examined. Binary and ternary mixtures of long and short chains with different compositions are studied in a systematic manner. Results show that short chains of molecular weights,  $M$ , below the polymer critical molecular weight,  $M_c$ , play an important role in slip of polymer mixtures near low energy surfaces. Among mixtures of the same weight average molecular weight,  $M_w$ , (given the longest chains are the same among all mixtures), mixtures containing chains of  $M < M_c$  exhibit larger slip lengths than those containing short chains of  $M > M_c$ . This is attributed to physical/chemical disparities between end groups and backbone units implying that PS end groups on fluorinated surfaces exhibit lower friction coefficient than backbone units. Therefore, a higher concentration of end groups at the polymer-solid interface gives a larger slip length. The end group surface localization can also be considered as an important contributing factor to the enhanced slip.

## 7.2. Materials and Experiments

We used atactic polystyrene (Polymer Source Inc.) with  $M_w = 5.4, 28.4, 53.3, 86.4, 135.8$  and  $490$  kg/mol and polydispersity indices below 1.05. In the following, these polymers are referred to as monodisperse polystyrenes with short-hand notations, e.g., PS(5k). Binary and ternary mixtures of different weight fractions were prepared from monodisperse samples.

In all our mixtures, PS(490k) was used as the primary high molecular weight component (HMW); other polymers were treated as the low molecular weight components (LMW). Several sample sets were examined (Table 7.1): monodisperse PS samples (set#1); binary and ternary mixtures of a fixed  $M_w \cong 318 \pm 2$  kg/mol and varying number average

molecular weight,  $M_n$  (set#2); binary mixtures of a fixed amount of HMW ( $\phi_{PS(490k)} = 90$  wt%) and varying LMW component - this sample set denoted by PS(LMW)-PS(490k) also has a fixed  $M_w \cong 447 \pm 5$  kg/mol (set#3:); binary mixtures of PS(28k) and PS(490k) of different compositions - denoted PS(28k)-PS(490k) (set#4); and binary mixtures of PS(86k) and PS(490k) with different compositions - denoted PS(86k)-PS(490k) (set#5).

To obtain homogeneous solutions for spin coating, samples were dissolved in toluene: the solution was stirred for one day at room temperature and remained on the shelf for two additional days to ensure homogeneity. The polymer concentration in toluene for each sample was different depending on the molecular weight (max.  $\sim 25$  mg/ml) in order for obtaining films of thicknesses,  $h_0$ , in the range of 120 – 200 nm when solutions were spin coated on freshly cleaved mica sheets.

All films spin coated on mica were pre-annealed in air (Linkam) at 150 °C for 1 hr. Films were next floated onto the surface of water in an ultra-clean water bath (TKA-GenPure, 18.2 M $\Omega$  cm, total organic carbon content < 5 ppb) after which they were picked up from the air-PS surface [143] using the hydrophobized Si wafers (Si-Mat Silicon Materials, 100 crystal orientation). Hydrophobization was accomplished using a fluoropolymer: AF 2400 (Poly[4,5-difluoro-2,2-bis(trifluoromethyl)-1,3-dioxido-co-tetrafluoro-ethylene], Sigma-Aldrich) with coating thickness of  $h_0 \sim 15$  nm.

Samples were heated to above their glass transition temperature,  $T_g$ , (for PS:  $T_g \leq 100$  °C) to start dewetting by the nucleation and growth mechanism. Optical microscopy (Leitz) and AFM (Multimode) were used to capture flow dynamics and rim morphology of the dewetting holes. In *all* experiments, only holes growing with, at least, a 10 min delay after the dewetting temperature,  $T_d$ , was reached were examined. This can be considered as annealing of films on the hydrophobized substrate allowing films to be less affected by frozen-in-stresses [89].

Table 7.1. Polymer mixtures and dewetting temperatures examined in this work\*

Sample set	Sym.	$T_d(^{\circ}\text{C})$	$\phi_{5k}$	$\phi_{28k}$	$\phi_{53k}$	$\phi_{86k}$	$\phi_{136k}$	$\phi_{490k}$	$M_n$	$M_w$
Set#1: monodisperse PSs	PS(5k)	110	1	-	-	-	-	-	4.7	5.4
	PS(28k)	120	-	1	-	-	-	-	27	28.4
	PS(53k)	140	-	-	1	-	-	-	51	53.3
	PS(86k)	140	-	-	-	1	-	-	85	86.4
	PS(136k)	140	-	-	-	-	1	-	130	135.8
	PS(490k)	150	-	-	-	-	-	1	465	490
Set#2: $M_w \cong 318 \pm 2$ kg/mol and varying $M_n$	$M_n_{20k}$	130/140/150	0.22	-	-	-	0.19	0.59	20	316
	$M_n_{86k}$	130/140/150	-	0.25	-	-	0.14	0.60	86	320
	$M_n_{206k}$	130/140/150	-	-	-	-	0.49	0.51	206	316
Set#3: PS(LMW)-PS(490k) $\phi_{PS(490k)} = 0.90$	PS(5k)-PS(490k)	150	0.10	-	-	-	-	0.90	43	442
	PS(28k)-PS(490k)	150	-	0.10	-	-	-	0.90	177	444
	PS(53k)-PS(490k)	150	-	-	0.10	-	-	0.90	257	446
	PS(86k)-PS(490k)	150	-	-	-	0.10	-	0.90	322	450
	PS(136k)-PS(490k)	150	-	-	-	-	0.10	0.90	370	455
Set#4: PS(28k)-PS(490k)	PS(28k)-PS(490k) 70-30	130	-	0.70	-	-	-	0.30	167	38
	PS(28k)-PS(490k) 50-50	130	-	0.50	-	-	-	0.50	259	51
	PS(28k)-PS(490k) 30-70	140	-	0.30	-	-	-	0.70	352	79
	PS(28k)-PS(490k) 10-90	150	-	0.10	-	-	-	0.90	444	177
Set#5: PS(86k)-PS(490k)	PS(86k)-PS(490k) 70-30	140	-	-	-	0.70	-	0.30	208	113
	PS(86k)-PS(490k) 50-50	140	-	-	-	0.50	-	0.50	288	144
	PS(86k)-PS(490k) 30-70	140	-	-	-	0.30	-	0.70	369	199
	PS(86k)-PS(490k) 10-90	150	-	-	-	0.10	-	0.90	450	322

\* Unit of  $\phi$  is [wt%], and  $M_w$  and  $M_n$  is [kg/mol].

### 7.3. Results and Discussion

Characterization of the slip length,  $b$ , using the rim profile analysis of dewetting front/holes has previously been well established [93]. Here, we use the third-order Taylor expansion of the full Stokes model of Fetzer *et al.* to extract the slip length [93].

An example of the fitting procedure using the rim profile analysis for two monodisperse samples PS(28k) and PS(490k) is shown in Figure 7.1. The normalized height profiles, obtained using AFM, of the dewetting films are represented in Figure 7.1a). In this figure, the rim height in the vertical axis is normalized by the film thickness and the horizontal axis representing the distance to the contact line,  $\xi$ , is normalized by the hole radius,  $R$ . Figures 7.1b) and 7.1c) show the portion of the height profile used for curve fitting as well as the best fit to the experimental data of PS(28k) and PS(490k), respectively. As seen in this figure, PS(490k) exhibits a monotonic decay with a long decay length indicating a strong slip boundary condition at the polymer-solid interface with  $b = 4.49 \pm 0.66 \mu\text{m}$ , whereas PS(28k) exhibits a shorter decay length and an oscillatory decay profile indicating a weak slip boundary condition with  $b = 15 \pm 2 \text{ nm}$ .

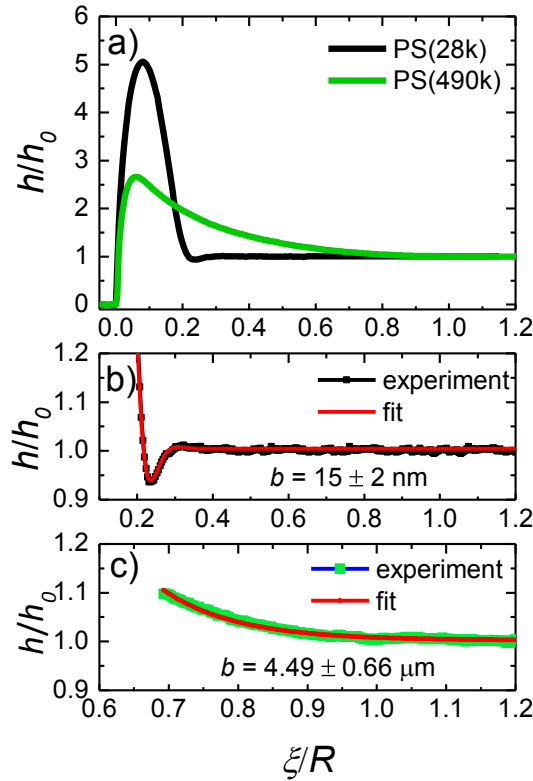


Figure 7.1. a) Normalized height profiles of PS dewetting rim on AF 2400: PS(28k) with  $h_0 = 120 \text{ nm}$ , hole radius  $R = 5.9 \mu\text{m}$  and  $T_d = 120 \text{ }^\circ\text{C}$ , and PS(490k) with  $h_0 = 172 \text{ nm}$ , hole radius  $R = 6.8 \mu\text{m}$  and  $T_d = 150 \text{ }^\circ\text{C}$ ; b) the best fit to experimental data for PS(28k); and c) the best fit to experimental data for PS(490k).

We first examine the slip length of monodisperse PS as shown in Figure 7.2. The molecular weight dependence of the slip length of PS on AF 1600 has previously been investigated [45]; PS on AF 2400 exhibits the same slip behavior as it did on AF 1600. For monodisperse PS, samples with molecular weights below the critical molecular weight:  $M \leq M_c$  ( $M_c \approx 35$  kg/mol for PS [136]) exhibit weak slip with almost a constant value of slip length on the order of a few nanometers. Slip length of samples of  $M > M_c$  show a power law dependence close to the theoretical power law value of 3 [26]. Slight deviation may be the result of the non-ideal conditions and extreme sensitivity of the friction coefficient of thin films to atomistic differences in the substrate composition, as shown in ref [93]. Also, it can be seen in this figure that PS(490k) is the only sample with slip length deviating from the power of 3. This may also indicate that the theoretical model might not be suitable for detecting the slip length of highly entangled polymers.

In the Navier slip model, the slip length is defined as the ratio of melt viscosity,  $\eta$ , to the friction coefficient,  $\kappa$ , i.e.,  $b = \eta/\kappa$ , which is obtained by balancing the stress at the fluid-solid interface [26]. In the dewetting experiments, the Weissenberg number is very small ( $Wi < 0.2$ ) [45] and therefore non-Newtonian behavior such as shear thinning can be safely excluded; the polymer flows within the linear viscoelastic (LVE) regime. The melt viscosity in the LVE region can be represented by the zero shear viscosity,  $\eta_0$ , which only depends on the value of  $M_w$  [141]. However, what can be critical in slip of polydisperse polymers is the value of  $M_n$  – sensitive to the content of short chains – which can affect the polymer slip behavior via the friction coefficient. We therefore start examining mixtures of a fixed  $M_w$  and varying  $M_n$ . Sample set#2 (as shown in Table 7.1) contains three samples with  $M_w \cong 318 \pm 2$  kg/mol and  $M_n$  values ranging from 20 to 206 kg/mol.

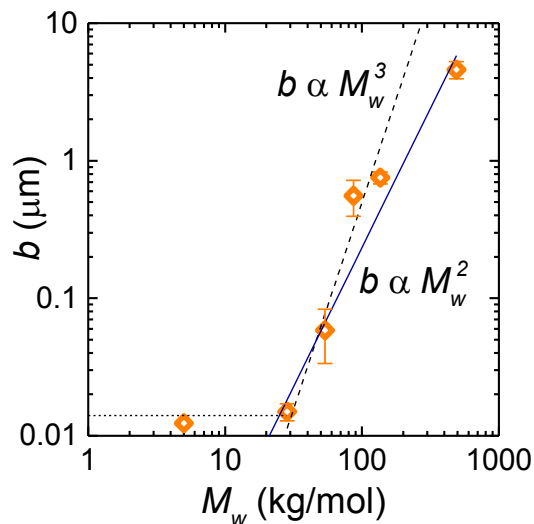


Figure 7.2. Slip length versus molecular weight of monodisperse PSs on AF 2400. The solid line represents the best fit:  $b \propto M_w^2$  in contrast to the theoretical  $b \propto M_w^3$  shown by the dashed line. The dotted line drawn at  $M < M_c \sim 35$  kg/mol is a guide to eye representing the constant slip length at the weak slip regime.

The temporal evolution of the dewetting holes of the  $M_w$ -fixed mixtures on AF 2400 at  $T_d = 150$  °C are shown in Figure 7.3. As seen, the growth rate of the dewetting holes significantly increases when  $M_n$  is decreased. This indicates that flow dynamics of polydisperse polymers can be extremely sensitive to its value of  $M_n$ . The enhanced growth rate of dewetting holes with lower  $M_n$  is likely due to the lower viscosity and/or slip length. Regarding the viscosity, we note that although  $M_w$  is approximately the same among these samples, the  $T_g$  can however be different among these samples depending on their compositions. For PS, the  $T_g$  starts to dramatically drop at molecular weights below  $M_c$  [114] meaning that samples containing chains of  $M < M_c$  may possess a lower  $T_g$  and thus a lower viscosity [141]. The faster dynamics of the low  $M_n$  samples can hence be due to their lower viscosity and no conclusion on their slip behavior can be made from their dynamics alone. We thus investigate the slip behavior of these samples through their rim profiles.

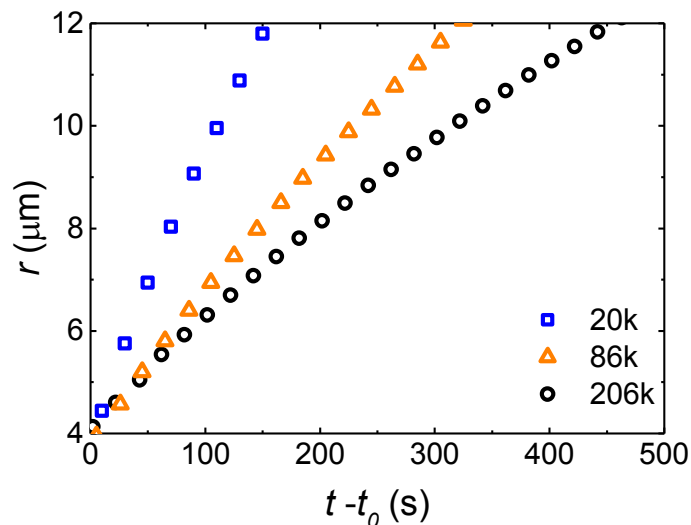


Figure 7.3. Temporal evolution of dewetting holes in thin films ( $\sim 150$  nm) of  $M_w$ -fixed mixtures (set#2) on AF 2400 at  $T_d = 150$  °C. The legend indicates the value of  $M_n$ .

Figure 7.4 shows the slip length of the same PS samples in Figure 7.3 along with data at two other dewetting temperatures: 140 °C and 130 °C. In this figure, all samples of the same  $M_n$  examined at different dewetting temperatures were prepared from the same film and thus have the same preparation and pre-annealing history. It can be seen in Figure 7.4 that the slip length of PS mixtures of the same  $M_w$  is larger with lower  $M_n$ , an effect consistent in all dewetting temperatures. In this graph, the sample with  $M_n = 20$  kg/mol shows the largest slip length, significantly higher than that of the sample with  $M_n = 206$  kg/mol, in accord with the observed behavior in Figure 7.3.

Furthermore, the decrease of the dewetting temperature has little or no effect on the value of the slip length of a certain sample. According to the WLF equation [144], the decrease of the polymer melt temperature results in an exponential increase in the film viscosity. With the exponential increase in the melt viscosity, the slip length might be expected to increase. However, consistent with Bäumchen *et al.* for the slip of PS on AF 1600 [45], we observe that the slip length data in Figure 7.4 are insensitive to the change of the dewetting temperature. This is perhaps due to the simultaneous change of the friction coefficient at the PS-PTFE interface along with the PS bulk viscosity. As a result, the change of the dewetting temperature has little or no influence on the slip length.

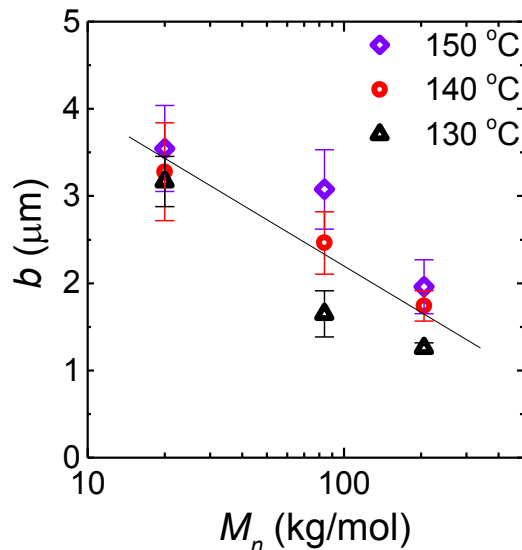


Figure 7.4. Slip length of  $M_w$ -fixed mixtures (set#2) on AF 2400 as a function of  $M_n$  at different dewetting temperatures. The solid line is to guide the reader's eye.

The enhanced slip of the low  $M_n$  samples in Figure 7.4 signifies the crucial effect of short chains on slip of polydisperse polymers on low surface energy substrates. Since the highest slip length in this graph corresponds to the sample containing the shortest chains as listed in Table 7.1, it is interesting to further investigate the effect of the size of short chains.

To this end, we examine binary mixtures of long and short chains in which the size and content of the HMW component is fixed while the size of LMW component varies (set#3). Figure 7.5a) shows the slip length of sample set#3 as a function of the molecular weight of the LMW component denoted by  $M_{LMW}$ . All dewetting experiments were done on AF 2400 at  $T_d = 150$  °C. The slip length of pure PS(490k) is added to this graph for comparison. We note that PS(490k) has a significantly higher  $M_w$  in contrast to an average of  $M_w \cong 447 \pm 5$  kg/mol for binary mixtures. This causes a difference in the slip length of pure PS(490k) versus binary samples: mixtures exhibit a lower slip length due to their lower  $M_w$ . However, as seen in Figure 7.5, the slip length decrease due to the lower  $M_w$  is only seen for certain binary mixtures. In contrast, binary mixtures containing short chains of  $M < M_c$  (samples: PS(5k)-PS(490k) and PS(28k)-PS(490k)) exhibit enhanced slip.

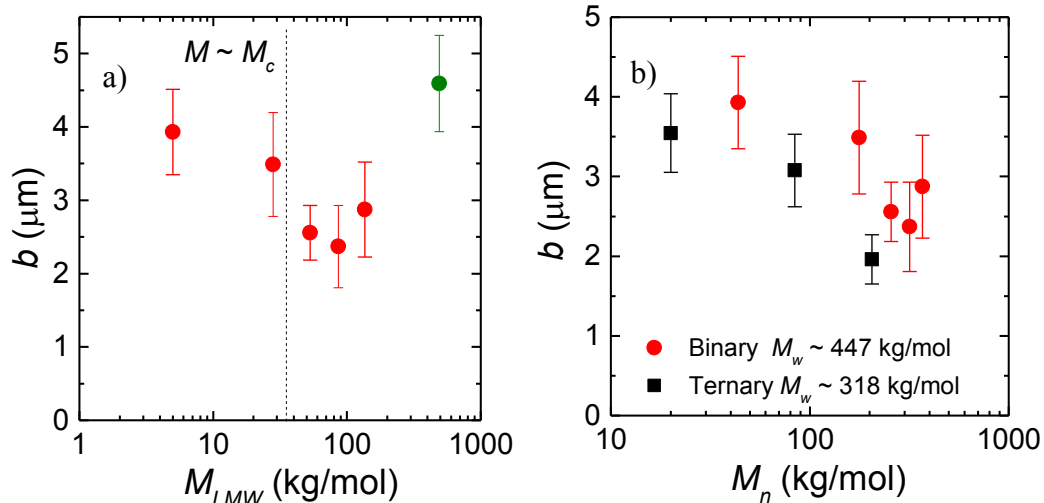


Figure 7.5. a) Slip length of set #3, PS(LMW)-PS(490k) binary mixtures ( $\phi_{PS(490k)} = 0.90$  in all samples) on AF 2400 versus the molecular weight of the LMW component,  $M_{LMW}$ ; the dotted line shows  $M = M_c$ . b) Slip length versus  $M_n$  for two sets of fixed  $M_w$  mixtures.

The slip lengths of the two previous sample sets, i.e., mixtures of  $M_w \cong 318 \pm 2$  kg/mol ( $T_d = 150$  °C) and PS(LMW)-PS(490k) binary mixtures with  $M_w \cong 447 \pm 5$  kg/mol are compared in Figure 7.5b) as a function of  $M_n$ . As can be seen, there is a general trend of an increase in the slip length with a decrease in  $M_n$ . These results suggest that among mixtures of the same  $M_w$  those with a higher content of short chains of  $M < M_c$  are likely to exhibit larger slip lengths.

To investigate this hypothesis rigorously, we study the effect of the content of short chains in binary mixtures. Two sets of binary mixtures: set#4) PS(28k)-PS(490k) and set#5) PS(86k)-PS(490k) with different compositions were examined. The choice of PS(28k):  $M < M_c$  versus PS(86k):  $M > M_c$  is made based on their slip behavior in Figure 7.5a) and the fact that their molecular weights fall right below and above  $M_c$ , respectively. Figure 7.6 shows the slip length of set#4 and set#5 as a function of the content of PS(490k),  $\phi_{PS(490k)}$ . In this graph,  $\phi_{PS(490k)} = 1$  represents the slip lengths of pure PS(490k) and  $\phi_{PS(490k)} = 0$  represents the slip length of pure PS(28k) and PS(86k).

Interestingly, the slip behavior of the two sample sets relative to one another is divided into two different regions with respect to  $\phi_{PS(490k)} = 0.5$ . For samples in which

$\phi_{PS(490k)} \leq 0.5$ , the slip length of mixtures changes in accord with their corresponding  $M_w$ , i.e., binary mixtures containing PS(86k) exhibit equal or larger slip length than those containing PS(28k) because of their higher  $M_w$ . For samples with  $\phi_{PS(490k)} > 0.5$ , the slip length is significantly dependent on the size and content of short chains. Binary mixtures containing 10 and 30 wt% PS(28k) exhibit larger slip lengths than those containing 10 and 30 wt% PS(86k). In particular, it is very interesting that the sample PS(28k)-PS(490k)/30-70 with  $M_w \cong 352$  kg/mol and  $M_n \cong 79$  kg/mol exhibits as large a slip length as pure PS(490k).

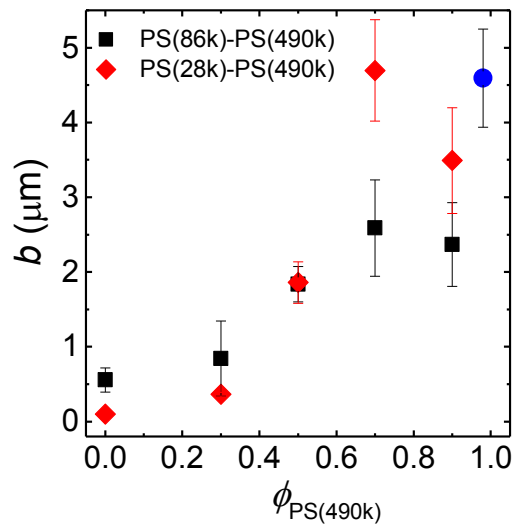


Figure 7.6. Slip length  $b$  versus  $\phi_{PS(490k)}$  for two sets of binary mixtures: PS(28k)-PS(490k) and PS(86k)-PS(490k) on AF 2400. Pure PS(490k) is distinguished with a different symbol.

The slip behavior of binary mixtures in Figure 7.6 indicates that both size and content of short chains are important factors in slip of polymer mixtures on low energy surfaces. In this regard, chains of  $M < M_c$  are of specific importance when mixed with highly entangled polymers at lower proportions.

As shown by Brochard and de Gennes in their slip theory [26], the polymer slip length – defined as the ratio of melt viscosity to the friction coefficient at the slip plane – shows a strong molecular weight dependence,  $b \propto M^3$ . The molecular weight dependence of  $b$

in the Brochard and de Gennes relation comes from that of the viscosity, i.e.,  $\eta \propto M^3$  [26], while the friction coefficient in this relation has been considered a constant:  $k_f = k_{f0}$ , where  $k_{f0}$  is that of the flow of monomers, and therefore independent of  $M$ .

The slip mechanism of polymers on low energy surfaces is believed to be due to adhesive failure in which the slip plane is located at the polymer-solid interface. The friction coefficient at the polymer-solid interface can thus be molecular weight dependent due to the change in the content of species (end groups versus backbone units) coming into contact with the solid surface as  $M$  varies. Alike surface tension [145], the friction coefficient is a surface/interface property and may hence depend on the chemistry of monomers present at the surface/interface. Moreover, the friction coefficient has been shown [92, 144] to be strongly dependent on physical characteristics of monomers present at the surface/interface. At small values of  $M$ , as a result, we expect that the friction coefficient to be dominantly governed by end group properties whereas backbone properties become dominant as  $M$  increases.

The disparities between backbone units and end groups are specifically important in polydisperse polymers of broad molecular weight distributions. For instance, polydisperse samples of the same  $M_w$  may significantly differ in the end group to backbone ratio depending on their  $M_n$  values. Accordingly, polydisperse polymers with large polydispersity indices are rich in the number of end groups that likely affects their surface/interfacial properties. As we observe in the present work, short chains of  $M < M_c$  can significantly enhance the slip length of highly entangled PS mixtures on AF 2400. This can evidently be due to the presence of end groups at the PS-solid interface via the incorporation of short chains into the sample. As a result, the friction coefficient which is dominated by the backbone characteristics in case of pure PS(490k) becomes influenced by characteristics of end groups in binary mixtures. We can therefore infer that, for PS, a higher concentration of end groups at the interface results in a lower friction coefficient which consequently enhances the slip length.

The extent of the presence of end groups at the surface/interface can also be significantly higher than that in the bulk. There have been many experimental and

theoretical studies on surface enrichment of end groups at the surface/interface [50,77,79,116]. Molecular dynamics (MD) simulations from Daoulas and coworkers [140] showed that polyethylene chain ends segregate to both liquid/vapour and solid/liquid interface. Matsen and Mahmoudi using self-consistent field theory showed that chain ends segregate to a narrow region next to the surface due to entropic effects [115]. In case of polystyrene, Kajiyama *et al.* [77] reported that thin films of PS with  $M < 30$  kg/mol spin coated on silicon wafer show enhanced mobility at the air-PS interface even at room temperature attributed to the surface localization of chain end groups. They also showed that surfaces of binary and ternary mixtures of monodisperse PSs show enhanced mobility when a component with  $M < 30$  kg/mol is present [79]. The slip length enhancing effect we observe in our binary and ternary mixtures containing short chains of  $M < M_c$  can therefore be as well influenced by the surface enrichment of chain end groups.

#### 7.4. Conclusion

The slip length of monodisperse PSs and their binary and ternary mixtures was examined on AF 2400, a low energy surface, using dewetting experiments. It was shown that chains of  $M < M_c$  can significantly enhance the slip length of highly entangled PS mixtures on AF 2400: among mixtures of the same  $M_w$  those containing chains of  $M < M_c$  exhibit larger slip lengths, which is consistent with a lower value of  $M_n$ . The slip enhancement effect of chains of  $M < M_c$  in their binary mixtures with highly entangled chains is only applicable when the content of the long chain component,  $\phi_L$ , is dominant ( $\phi_L > 0.5$ ). In particular, we showed that a binary mixture of PS(490k) and PS(28k) containing 30 wt% PS(28k) exhibits as large slip length as pure PS(490k); the slip length reduced to almost half its value when PS(28k) was replaced with PS(86k).

Our results in the present work suggests that the effect of short chains of  $M < M_c$  on slip of highly entangled PSs on AF 2400 is due to the presence of chain end groups at the interface. It can therefore be concluded that, for PS, a higher concentration of end groups at the interface results in a lower friction coefficient which consequently enhances the slip

length. In this regard, the observed slip behavior can be significantly influenced by the surface segregation mechanisms enriching the chain end groups at the interface.

## 8. CHAPTER 8

### Conclusions and Contributions

#### 8.1. Conclusions

In the present work, we examined the effect of molecular weight distribution on steady state slip of linear polymer melts on solid substrates. Our model polymers include polybutadiene and polystyrene both available with a wide variety of well-characterized narrowly-distributed molecular weights. We used substrates of different surface energies: silicon wafer and stainless steel as high energy surfaces and fluorinated and silanized surfaces as low surface energy substrates.

Polydispersity was introduced by mixing appropriate weight fractions of narrowly-distributed samples instead of using actual broad polydisperse samples. This gives us a discrete molecular weight distribution allowing us to systematically vary certain controlling parameters such as  $M_w$  or  $M_n$ . The disadvantage is that use of discrete molecular weight distributions may not reveal exact features of the slip of samples with broad continuous MWDs.

We used a combination of different experimental techniques including i) confocal microscopy and particle image velocimetry, ii) sliding plate rheometry and gel permeation chromatography, and iii) dewetting and atomic force microscopy in the slip studies.

In Chapters 3 and 4, we examined steady state slip of PBD mixtures on silicon wafer under simple shear in a displacement-controlled geometry. In Chapter 5, we investigated the surface enrichment of short chains of different PBD mixtures under steady shear using a strain-controlled sliding plate rheometer. All measurements on PBD in Chapters 3 to 5 were done at room temperature. In Chapters 6 and 7, slip of PS on Teflon coated (AF 2400) and DTS coated silicon wafers was examined under Poiseuille flow during dewetting at elevated temperatures above the glass transition temperature.

We showed that, under simple shear, highly entangled monodisperse linear PBDs can undergo significant slip on silicon wafer when mixed with a small amount of weakly entangled chains. Examination of binary mixtures composed of a highly entangled PBD ( $M_w = 195$  kg/mol) and short chains of different sizes revealed that slip is significantly affected in mixtures of  $G_r > 1$ . The addition of a small amount ( $\sim 10$  wt%) of weakly entangled chains with  $M \sim M_c \sim 3M_e$  to a monodisperse PBD of sufficiently long chains (e.g.  $M \sim 118M_e$ ) significantly reduces the friction coefficient in the strong slip regime. The apparent slip as a result is perceptibly enhanced in certain binary mixtures of long and short chains compared to moderate/weak slip of pure constituents within the same experimental window.

Surprisingly for binary mixtures with the enhanced slip, the slip length in the strong slip regime scales with the content of long chains as  $b_\infty \propto \phi^{2.2}$ , a relationship similar to that established between binary mixtures plateau modulus  $G_N$  and  $\phi$  as  $G_N \propto \phi^{2.2}$ . While the weak slip friction coefficient seems to scale well with bulk rheology and entanglement density of chains, the strong slip friction coefficient seems to be a more complex factor of the disentangled chain-chain and chain-wall interactions at the interface in addition to rheological properties. We also found that the critical shear stress  $\sigma^*$  for the onset of the transition to strong slip regime in binary PBD mixtures scales with  $\eta_0$ . As a result,  $\sigma^*$  reduces to lower values when the content of short chains in the binary mixture of long and short chains increases.

These findings have important implications in polymer processing. For example, we showed that while monodisperse PBDs with  $M$  up to 195 kg/mol may not exhibit strong slip, their mixtures with weakly entangled chains reduces the onset of strong slip to weight average molecular weights as low as 62 kg/mol. In polymer processing when the use of highly entangled polymers is limited due to high pressures required for polymer flow, perhaps addition of a small amount of weakly entangled chains can facilitate processing to some significant extent without sacrificing the end-use mechanical properties.

The role of short chains in polymer slip on high energy surfaces was further revealed in experiments using ternary mixtures. We showed that apparent slip of tridisperse PBDs

with fixed  $M_w$  and varying  $M_n$  on a silicon wafer is very sensitive to the content and size of short chains. We found that within our experimental window weakly entangled and unentangled chains influence PBD apparent slip differently: ternary mixtures containing moderate amounts of weakly entangled chains exhibit enhanced slip compared to equivalent systems containing unentangled chains.

Particular to ternary mixtures containing weakly entangled chains, the apparent slip in samples of fixed  $M_w = 143$  kg/mol strongly depends on their  $M_n$ . Over our experimental window of shear stress, the high- $M_n$  samples were within their weak slip regime while the low- $M_n$  samples were in the process of transitioning to the strong slip regime. The key differences among these samples are their critical shear stresses  $\sigma^*$  at the onset of the transitional regime and the slopes in the transition. Since the differences become more pronounced at lower values of  $M_n$ , it is evident that slip is favored in binary mixtures with two distinct molar modes in contrast to ternary samples containing a third middle-size constituent. As a result, polydisperse polymers with low  $M_n$  may not necessarily show the same enhanced slip behavior as our ternary samples did.

The difference in the slip behavior of samples containing weakly entangled and unentangled chains can be explained using the tube dilation theory and Brochard and de Gennes disentanglement slip mechanism. The slip behavior depends on the amount of viscous force transferred to surface adsorbed coils and the coil stiffness in the two cases which determines the critical coil diameter for the onset of the transition regime. The slip behavior is different in these two cases since the force balance between the mobile and adsorbed chains changes through the reduced entanglement density and coil stiffness due to the incorporation of short chains. In conclusion, both size and content of short chains are of critical importance when apparent slip of polydisperse polymers is to be addressed.

The surface enrichment of short chains of mixtures of monodisperse linear PBDs after strong slip under simple shear was also examined. In a sliding plate rheometer equipped with stainless steel plates, at small gaps ( $\sim 0.7$  mm), a hazy debris remains on the substrate after the sample undergoes strong slip. We believe that this debris represents the interfacial

layer of polymer melt below the slip plane. We collected samples from the debris and bulk and characterized their MWD using gel permeation chromatography.

We found that the MWD of all debris samples are significantly richer in short chain species than those predicted by thermodynamic segregation theories. We proposed a simple disentanglement induced enrichment mechanism in accord with the Brochard and de Gennes slip model. In flow of a polydisperse polymer melt over adsorbing surfaces after disentanglement occurs, some mobile chains become trapped among the adsorbed chains and some are pulled out. In our proposed mechanism, we make the following assumptions: i) the slip plane is located at about one radius of gyration of the longest chains from the interface, and ii) a portion of chains within half their radius of gyration is pulled out from the interfacial layer by bulk flow. Our model closely conforms to the observed experimental data. We believe that the proposed model can adequately describe the MWD of the interfacial layer of polydisperse polymer melts after strong slip. The disentanglement induced enrichment mechanisms has important implications in understanding several common polymer processing instabilities including wall slip, melt fracture, and the die drool phenomenon.

On the slip of polymers on low energy surfaces, we showed that slip of thin polymer films on nonwetting substrates strongly depends on the film preparation history on a sacrificial mica substrate. As a common practice in the preparation of thin polymer films on nonwetting substrates or free-standing films, the polymer film is first spin coated onto a freshly cleaved sheet of mica and then transferred to the desired substrate by floating onto the surface of water in an ultraclean water bath. Using dewetting experiments of PS on hydrophobized silicon wafers, we found that there is a significant difference in flow dynamics and rim morphology of dewetting holes depending on whether the film was previously in contact with air or mica. The difference is consistent with reduced slip in case of the surface previously in contact with mica and interestingly, pre-annealing on mica results in a larger difference. The observed behavior is attributed to long-lasting compositional/conformational arrangements due to the surface segregation and/or surface ordering of chains or their segments.

We finally examined wall slip of binary and ternary mixtures of PS on fluorinated silicon wafers using dewetting experiments. We showed that among mixtures of the same  $M_w$  those with a higher content of short chains of  $M < M_c$  are likely to exhibit larger slip lengths. The slip enhancement effect of short chains is only applicable in mixtures with higher proportion of long chains ( $\phi_L > 0.5$ ). Our results suggest that the effect of short chains of  $M < M_c$  on slip of highly entangled PSs on AF 2400 is due to the presence of chain end groups at the interface. Therefore for our PS samples, a higher concentration of end groups at the interface results in a lower friction coefficient which consequently enhances the slip length. Surface segregation mechanisms, in this regard, can play an important role in the extent of surface enrichment of end groups at the interface.

## 8.2. Contributions

This thesis allows for better understanding of the liquid-solid boundary conditions in flow of linear molten polymers. The knowledge produced from this work has significant practical importance with key implications in polymer processing and slip models. Specific areas of interest may include shear mixing, lubrication, paints and coatings, and extrusion of polymers and biopolymers. In particular in extrusion process, our results can be useful in describing phenomena such as wall slip, melt fracture, and die drool.

The main contributions are as follows: i) we showed that short chains play a crucial role in wall slip of highly entangled linear polymers, ii) we proposed a disentanglement induced surface enrichment mechanism that significantly impact our understanding of many polymer flow related phenomena including wall slip, die drool, and extrudate surface instabilities, and iii) compositional/conformational arrangements of polymer chains near a solid significantly impacts its liquid-solid boundary condition specifically in thin polymer films.

In detail, the new knowledge created in the present work is:

- ❖ Incorporation of short chains into the entanglement structure of long linear polymer chains promotes slip on both low and high surface energy substrates: specific size and content criteria apply to the different cases.

- ❖ Among mixtures of the same  $M_w$  those with a higher content of short chains are likely to exhibit larger slip lengths; as a result, binary mixtures of long and short chains of two distinct molar modes exhibit higher slip lengths than polydisperse polymers of the same  $M_w$ .
- ❖ On high surface energy substrates such as stainless steel, glass, and silicon wafer, a small amount of weakly entangled chains of  $M \sim M_c$  can significantly affect the dynamics of the transition from the weak slip regime to the strong slip within the range of shear rates over which only weak slip was observed for the pure long chains.
- ❖ On low surface energy substrates such as fluorinated or silanized surfaces, binary mixtures of long and short chains of two distinct molar modes exhibit promoted slip if i) the long chain component is dominant in content ii) short chains have molecular weights of  $M < M_c$ .
- ❖ Surface enrichment plays a crucial role in polymer slip on solid substrates:
  - On high energy surfaces, significant surface enrichment of short chains is observed in flow of binary and ternary mixtures of long and short linear chains after strong slip under simple shear.
  - On low energy surfaces, significant surface enrichment of short chains is inferred when binary and ternary mixtures of long and short linear polymer chains are examined in dewetting experiments.
- ❖ Although slip mechanisms of highly entangled polymers on substrates of different surface energies are believed to be different – disentanglement versus detachment – the consequence of the incorporation of short chains is similar, i.e., polymer wall slip is promoted.
- ❖ Highly entangled thin polymer films prepared in the two-step film preparation procedure involving sacrificial mica and pre-annealed on mica are sensitive to the choice of interface when dewetting a nonwetting substrate: buried interface exhibits significantly lower slip length than air interface.

## References

1. Archer, L. A. In *Polymer processing instabilities control and understanding*, Hatzikiriakos, S. G.; Migler, K. B., Eds.; (Marcel Dekker, New York, **2005**).
2. Denn, M. M. *Annu. Rev. Fluid Mech.* **2001**, 33, 265-287.
3. Archer, L. A.; Larson, R. G.; Chen, Y. L. *J. Fluid Mech.* **1995**, 301, 133-151.
4. Kalika, D. S.; Denn, M. M. *J. Rheol.* **1987**, 31, 815-834.
5. Park, H. E.; Lim, S. T.; Smillo, F.; Dealy, J. M.; Robertson, C. G. *J. Rheol.* **2008**, 52, 1201-39.
6. Wang, S. Q.; Drda, P. A. *Rheol. Acta* **1997**, 36, 128-128.
7. Ramamurthy, A. V. *J. Rheol.* **1986**, 30, 337-357.
8. Piau, J. M.; Kissi, N.; Mezghani, A. *J. Non-Newtonian Fluid Mech.* **1995**, 59, 11-30.
9. Wang, S. Q.; Drda, P. A. *Macromolecules* **1996**, 29, 2627-2632.
10. Wang, S. Q.; Drda, P. A. *Macromolecules* **1996**, 29, 4115-4119.
11. Yang, X.; Wang, S.; Halasa, A.; Ishida, H. *Rheol. Acta* **1998**, 37, 415-23.
12. Yang, X.; Wang, S.; Halasa, A.; Ishida, H. *Rheol. Acta* **1998**, 37, 424-9.
13. Vinogradov, G. V.; Protasov, V. P.; Dreval, V. E. *Rheol. Acta* **1984**, 23, 46-61.
14. Dao, T. T.; Archer, L. A. *Langmuir* **2002**, 18, 2616-2624.
15. Hatzikiriakos, S. G.; Dealy, J. M. *J. Rheol.* **1991**, 35, 497-523.
16. Mhetar, V.; Archer, L. A. *Macromolecules* **1998**, 31, 8607-8616.
17. Sanchez-Reyes, J.; Archer, L. A. *Langmuir* **2003**, 19, 3304-3312.
18. Ghanta, V. G.; Riise, B. L.; Denn, M. M. *J. Rheol.* **1999**, 43, 435-442.
19. Leger, L.; Hervet, H.; Massey, G.; Durliat, E. *J. Phys. Condens. Matter* **1997**, 9, 7719-7740.
20. Legrand, F.; Piau, J. M.; Hervet, H. *J. Rheol.* **1998**, 42, 1389-402.
21. Migler, K. B.; Hervet, H.; Leger, L. *Phys. Rev. Lett.* **1993**, 70, 287-90.
22. Shidara, H.; Denn, M. M. *J. Non-Newtonian Fluid Mech.* **1993**, 48, 101-110.
23. El Kissi, N.; Piau, J. M.; Toussaint, F. *J. Non-Newtonian Fluid Mech.* **1997**, 68, 271-290.
24. Mhetar, V.; Archer, L. A. *Macromolecules* **1998**, 31, 8617-8622.
25. Baumchen, O.; Jacobs, K. *J. Phys.: Condens. Matter* **2010**, 22, 033102.
26. Brochard-Wyart, F.; de Gennes, P. G.; Hervet, H.; Redon, C. *Langmuir* **1994**, 10, 1566-1572.
27. Hill, D. A.; Hasegawa, T.; Denn, M. M. *J. Rheol.* **1990**, 34, 891-918.
28. Anastasiadis, S. H.; Hatzikiriakos, S. G. *J. Rheol.* **1998**, 42, 795-812.
29. Brochard, F.; de Gennes, P. G. *Langmuir* **1992**, 8, 3033-3037.
30. Brochard-Wyart, F.; Gay, C.; de Gennes, P. G. *Macromolecules* **1996**, 29, 377-377.
31. Brochard-Wyart, F.; Gennes, P.-G. d.; Pincus, P. A. *Acad. Sci.* **1992**, 314, 873-878.
32. Ajdari, A.; Brochard-Wyart, F.; de Gennes, P. G.; Leibler, L.; Viovy, J. L.; Rubinstein, M. *Physica A* **1994**, 204, 17-17.

33. Gay, C. *J. phys. II* **1996**, 6, 335-353.
34. Gay, C. *Eur. Phys. J. B* **1999**, 7, 251-262.
35. Joshi Y. M.; Lele, A. K.; Mashelkar, R. A. *J. Non-Newtonian Fluid Mech.* **2000**, 94, 135–149
36. Esperidiao, M. C. A. *Ind. Eng. Chem. Res.* **2003**, 42, 5819-5826.
37. Joshi, Y. M.; Lele, A. K.; Mashelkar, R.A. *J. Non-Newtonian Fluid Mech.* **2000**, 89, 303-335.
38. Joshi, Y. M.; Lele, A. K.; Mashelkar, R.A. *Macromolecules* **2001**, 34, 3412-3420
39. Tchesnokov, M. A.; Molenaar, J.; Slot, J. J.; Stepanyan, R. *J. Chem. Phys.* **2005**, 122, 214711.
40. Bergem, N. ‘Visualization studies of polymer melt flow anomalies in extrusion’, In *7th International Congress on Rheology*, Gothenburg, Sweden, **1976**, 50–54.
41. Mhetar, V.; Archer, L. A. *Macromolecules* **1998**, 31, 6639-6649.
42. Malkus, D.S.; Nohel, J.A.; Plohr, B.J. *J. Comp. Phys.* **1990**, 87, 464–487.
43. Mcleish, T.C.B. Ball, R.C. *J. Polym. Sci. Polym. Phys. Ed.* **1986**, 24, 1735–1745.
44. Lin, Y.H. *J. Rheol.* **1985**, 29, 605–637.
45. Baumchen, O.; et al. *J. Phys.: Condens. Matter* **2012**, 24, 325102.
46. Durliat, E.; Hervet, H.; Leger, L. *Europhys. Lett.* **1997**, 38, 383-8.
47. Niavarani, A.; Priezjev, N. V. *J. Chem. Phys.* **2008**, 129, 144902.
48. de Gennes, P. G.; Brochard-Wyart, F.; Quere, D. *Capillarity and Wetting Phenomena, Drops, Bubbles, Pearls, Waves* (Springer, New York, **2004**).
49. Hayes, K. A.; Buckley, M. R.; Cohen, I.; Archer, L. A. *Phys. Rev. Lett.* **2008**, 101, 218301.
50. Minnikanti, V. S.; Qian, Z.; Archer, L.A. *J. Chem. Phys.* **2007**, 126, 144905.
51. Dee G. T.; Sauer, B. B. *Macromolecules* **1993**, 26, 2771- 2778.
52. Colby, R. H.; Fetters, L. J.; Graessley, W. W. *Macromolecules* **1987**, 20, 2226–2237.
53. Kazatchkov, I. B.; Bohnet, N.; Goyal, S. K.; Hatzikiriakos, S. G. *Polym. Eng. Sci.* **1999**, 39, 804-815.
54. Myerholtz, R. W. *J. Appl. Polym. Sci.* **1967**, 11, 687-698.
55. Ansari, M.; Hatzikiriakos, S. G.; Sukhadia, A. M.; Rohlfing, D. C. *Polym. Eng. Sci.* **2011**, 52, 795-804.
56. Blyler, L. L.; Hart, A. C. *Polym. Eng. Sci.* **1970**, 10, 193–203
57. Hatzikiriakos, S. G. *Prog. Polym. Sci.* **2012**, 37, 624-643.
58. Wang, S.; Wang, S. Q.; Halasa, A.; Hsu, W.-L. *Macromolecules* **2003**, 36, 5355–5371
59. Park, S. J.; Larson, R. G. *Macromolecules* **2004**, 37, 597–604.
60. Struglinski, M. J.; Graessley, W. W. *Macromolecules* **1985**, 18, 2630–2642.
61. Watanabe, H.; et al. *Macromolecules* **2004**, 37, 6619–6631.
62. Schreiber, H. P. *J. Polym. Sci., Part B: Polym. Lett.* **1969**, 7, 851–860.
63. Inn, Y. W. *J. Rheol.* **2013**, 57, 393–406.
64. Ansari, M.; et al. *Polym.* **2012**, 53, 4195–4201.

65. Ansari, M.; Hatzikiriakos, S. G.; Mitsoulis, E. *J. Non-Newtonian Fluid Mech.* **2012**, 167-168, 18–29.
66. Ansari, M.; Hatzikiriakos, S. G. ‘Wall slip of linear polymers (HDPEs)’, In *Novel Trends in Rheology V*, American Institute of Physics: College Park, MD, **2013**.
67. Ansari, M.; et al. *J. Rheol.* **2013**, 57, 927–948.
68. Minnikanti, V. S.; Archer, L. A. *J. Chem. Phys.* **2005**, 122, 084904.
69. van der Gucht, J.; Besseling, N. A. M.; Fleer, G. J. *Macromolecules* **2002**, 35, 6732–6738.
70. Hariharan, A.; Kumar, S. K.; Russell, T. P. *Macromolecules* **1990**, 23, 3584–3592.
71. Hariharan, A.; Kumar, S. K.; Russell, T. P. *Macromolecules* **1991**, 24, 4909–4917.
72. Gander, J. D.; Giacomini, A. *J. Polym. Eng. Sci.* **1997**, 37, 1113–1126.
73. Musil, J.; Zatloukal, M. *Chem. Eng. Sci.* **2012**, 81, 146–156
74. Schmalzer, A. M.; Giacomini, A. *J. Polym. Eng.* **2013**, 33, 1–18.
75. Shelby, M.D.; Caflisch, G.B. *Polym. Eng. Sci.* **2004**, 44, 1283–1294
76. Stark, R.; Kappl, M.; Butt, H. *Macromolecules* **2007**, 40, 4088–4091
77. Tanaka, K.; Takahara, A.; Kajiyama, T. *Macromolecules* **1997**, 30, 6626–6632
78. Jones, R. A. L.; Richards, R. W. *Polymers at Surfaces and Interfaces* (Cambridge University Press, Cambridge, **1999**).
79. Tanaka, K.; Kajiyama, T.; Takahara, A.; Tasaki, S. *Macromolecules* **2002**, 35, 4702–4706
80. de Gennes, P.-G. *Scaling Concepts in Polymer Physics* (Cornell University Press, Ithaca, **1979**)
81. Redon, C.; Brochard-Wyart, F.; Ronledez, F. *Phys. Rev. Lett.* **1991**, 66, 715.
82. Brochard-Wyart F.; Dilliant, J. *Can. J. Phys.* **1990**, 68, 1084–1088.
83. Bertrand, E.; Blake, T. D.; De Coninck, J. *Colloids Surf. A* **2010**, 369, 141–147.
84. Redon, C.; Brzoska, J. B.; Brochard-Wyart, F. *Macromolecules* **1994**, 27, 468–471.
85. Reiter, G.; Khanna, R. *Langmuir* **2000**, 16, 6351–6357.
86. Xu, L.; Sharma, A.; Joo, S. W. *Macromolecules* **2010**, 43, 7759–7762.
87. Henn, G.; Bucknall, D. G.; Stamm, M.; Vanhoorne, P.; Jerome, R. *Macromolecules* **1996**, 29, 4305–4313.
88. Jacobs, K.; Seemann, R.; Schatz, G.; Herminghaus, S. *Langmuir* **1998**, 14, 4961–4963.
89. Reiter, G. In *Glass Transition, Dynamics and Heterogeneity of Polymer Thin Films*, Kanaya, T., Ed.; (Springer, Berlin, Heidelberg, **2013**).
90. Baumchen, O.; McGraw, J. D.; Forrest, J. A.; Dalnoki-Veress, K. *Phys. Rev. Lett.* **2012**, 109, 055701.
91. McGraw, J. D.; et al. *Adv. Colloid Interface Sci.* **2014**, 210, 13–20.
92. Fetzer, R.; et al. *Phys. Rev. Lett.* **2005**, 95, 127801.
93. Fetzer, R.; et al. *Langmuir* **2007**, 23, 10559–10566.
94. Milner, S. T.; McLeish, T. C. B. *Macromolecules* **1997**, 30, 2159–2166.
95. Milner, S. T.; McLeish, T. C. B.; Likhtman, A. E. *J. Rheol.* **2001**, 45, 539–563.

96. Park, S. J.; Larson, R. G. *J. Rheol.* **2006**, 50, 21–39.
97. Liu, C.; et al. *Polym.* **2006**, 47, 4461–4479.
98. Hayes, K. A.; et al. *Macromolecules* **2010**, 43, 4412–4417.
99. Lim, F. J.; Schowalter, W. R. *J. Rheol.* **1989**, 33, 1359–1382.
100. Nigen, S.; El Kissi, N.; Piau J. M.; Sadum, S. *J. Non-Newtonian Fluid Mech.* **2003**, 112, 177–202.
101. Perez-Gonzalez, J.; Denn, M. M. *Ind. Eng. Chem. Res.* **2001**, 40, 4309–4316.
102. Sabzevari, S. M.; Cohen, I.; Wood-Adams, P. M. *Macromolecules* **2014**, 47, 3154–3160.
103. Sabzevari, S. M.; Cohen, I.; Wood-Adams, P. M. *Macromolecules* **2014**, 47, 8033–8040.
104. Sabzevari, S. M.; Strandman, S.; Wood-Adams, P. M. ‘Slip of polydisperse polymers: molecular weight distribution above and below the plane of slip’, In *Novel Trends in Rheology VI*, American Institute of Physics: College Park, MD, **2015**.
105. Tsui, O.; Russell, T., Eds.; *Polymer Thin Films* (World Scientific, Singapore, **2008**).
106. Keddie, J.L.; Jones, R.A.L.; Cory, R.A. *Europhys. Lett.* **1994**, 27, 59–64.
107. Herminghaus, S.; Jacobs, K.; Seemann, R. *Eur. Phys. J. E.* **2001**, 5, 531–538.
108. Bodiguel, H.; Fretigny, C. *Phys. Rev. Lett.* **2006**, 97, 266105.
109. Napolitano, S.; Cangialosi, D. *Macromolecules* **2013**, 46, 8051–8053.
110. Silberberg, A. *J. Colloid Interface Sci.* **1982**, 90, 86–91.
111. Brown, H.R.; Russell, T.P. *Macromolecules* **1996**, 29, 798–800.
112. Si, L.; Massa, M.V.; Dalnoki-Veress, K.; Brown, H.R.; Jones, R.A.L. *Phys. Rev. Lett.* **2005**, 94, 127801.
113. Bäumchen, O.; Fetzer, R.; Jacobs, K. *Phys. Rev. Lett.* **2009**, 103, 247801.
114. Kajiyama, T.; Tanaka, K.; Takahara, A. *Macromolecules* **1997**, 30, 280–285.
115. Matsen, M.W.; Mahmoudi, P. *Eur. Phys. J. E.* **2014**, 37, 78.
116. Wu, D.T.; Fredrickson, G.H.; Carton, J.-P.; Ajdari, A.; Leibler, L. *J. Polym. Sci. Part B: Polym. Phys.* **1995**, 33, 2373–2389.
117. Cohen, Y.; Reich, S. *J. Polym. Sci. Part B: Polym. Phys.* **1981**, 19, 599–608.
118. Hariharan, A.; et al. *J. Chem. Phys.* **1993**, 99, 656–663.
119. Hariharan, A.; Kumar, S.K.; Russell, T.P. *J. Chem. Phys.* **1993**, 98, 4163–4173.
120. Zhou, X.; Andrienko, D.; Delle Site, L.; Kremer, K. *Europhys. Lett.* **2005**, 70, 264–270.
121. Zhou, X.; Andrienko, D.; Delle Site, L.; Kremer, K. *J. Chem. Phys.* **2005**, 123, 104904.
122. Napolitano, S.; Wübbenhorst, M. *Nat. Commun.* **2011**, 2, 260.
123. Chowdhury, M.; Freyberg, P.; Ziebert, F.; Yang, A.C.M.; Steiner, U.; Reiter, G. *Phys. Rev. Lett.* **2012**, 109, 136102.
124. Barbero, D.; Steiner, U. *Phys. Rev. Lett.* **2009**, 109, 248303.
125. Thomas, K.R.; Chenneviere, A.; Reiter, G.; Steiner, U. *Phys. Rev. E.* **2011**, 83, 021804.

126. McGraw, J.D.; Fowler, P.D.; Ferrari, M.L.; Dalnoki-Veress, K. *Eur. Phys. J. E.* **2013**, 36, 7.
127. McGraw, J.D.; et al. *Adv. Colloid Interface Sci.* **2014**, 210, 13-20.
128. Wang, J.; McKenna, G.B. *J. Polym. Sci. Part B: Polym. Phys.* **2013**, 51, 1343-1349.
129. Heedong, Y.; McKenna, G.B. *Macromolecules* **2014**, 47, 8808–8818.
130. Roth, C.B.; McNerny, K.L.; Jager, W.F.; Torkelson, J.M. *Macromolecules* **2007**, 40, 2568-2574.
131. Roth, C.B.; Dutcher, J.R. *J. Polym. Sci. Part B: Polym. Phys.* **2006**, 44, 3011-3021.
132. Blossey, R. *Thin Liquid Films: Dewetting and Polymer Flow* (Springer, Dordrecht, **2012**).
133. Cotton, J.P.; et al. *Macromolecules* **1974**, 7, 863-872.
134. Lessel, M.; et al. *Surf. Interface Anal.* **2015**, 47, 557-564.
135. Reiter, G.; et al. *Nat. Mater.* **2005**, 4, 754-758.
136. Rubinstein, M.; Colby, R. *Polymer Physics*, **2003**, Oxford University Press.
137. Gautam, K.S.; et al. *Phys. Rev. Lett.* **2000**, 85, 3854-3857.
138. Hudzynskyy, D.; Lyulin, A.V. *Model. Simul. Mater. Sci. Eng.* **2011**, 17, 074007.
139. Gutfreund, P.; et al. *Phys. Rev. E.* **2013**, 87, 012306.
140. Daoulas, K.Ch.; Harmandaris, V.A.; Mavrantas, V.G. *Macromolecules* **2005**, 28, 5780-5795.
141. Faith A. Morrison, *Understanding Rheology*, (Oxford University Press, **2001**).
142. de Gennes, P. G. *Rev. Mod. Phys. Part I*, **1985**, 57, 828-862.
143. Sabzevari, S. M.; McGraw, J. D.; Jacobs, K.; Wood-Adams P. M., *submitted*.
144. Williams, M. L.; Landel, R. F.; Ferry, J. D. *J. Am. Chem. Soc.* **1955**, 77, 3701-3707.
145. Jalbert, C.; Koberstein, J. T.; Yilgor, I.; Gallagher, P.; Krukoni, V. *Macromolecules*, **1993**, 26, 3069–3074.

## Appendix A

Appendix A contains additional information regarding the experimental technique used in Chapters 3 and 4. In these chapters, we performed a microfluidic study of the slip velocity of polybutadiene (PBD) on silicon wafer under simple shear using confocal microscopy and particle image velocimetry.

### A.1. Plane parallelism in Couette flow shear cell

In our experimental set up as shown in Figure A.1, the two plates after sample placement are initially installed at a safe distance at which they are not touching one another. The adjusting screws are then used to adjust the gap and make the two plates parallel. To do this, the initial gap is firstly measured using the top and bottom interfaces at the four corners of the bottom plate. Then the adjusting screws are repeatedly used to adjust the gap and plane parallelism.

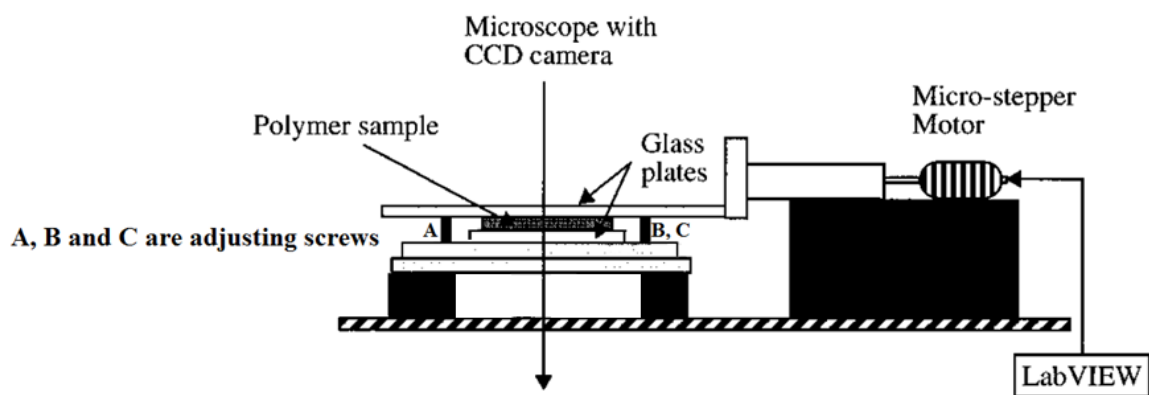
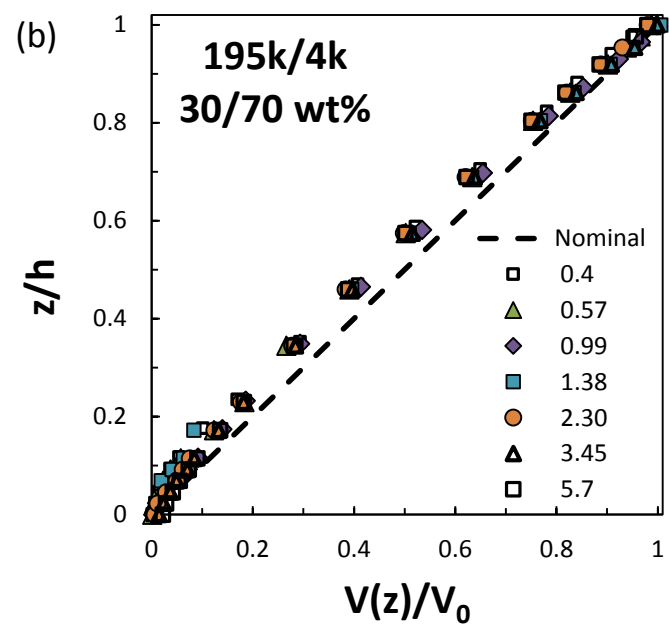
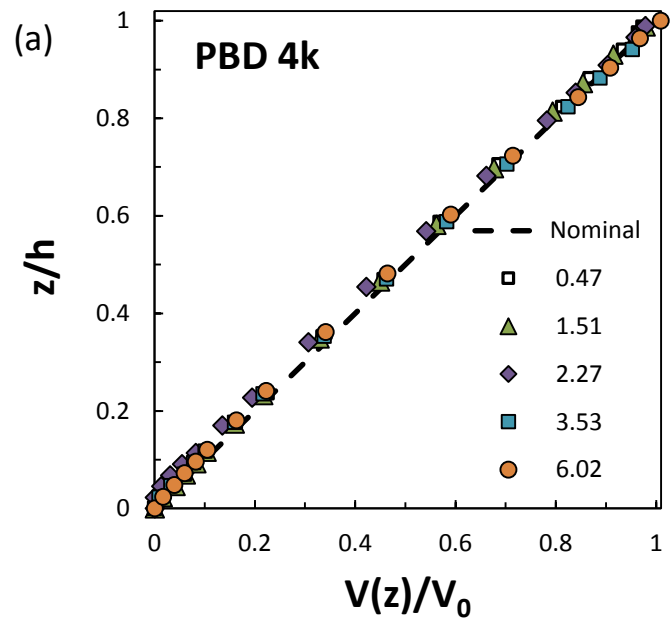
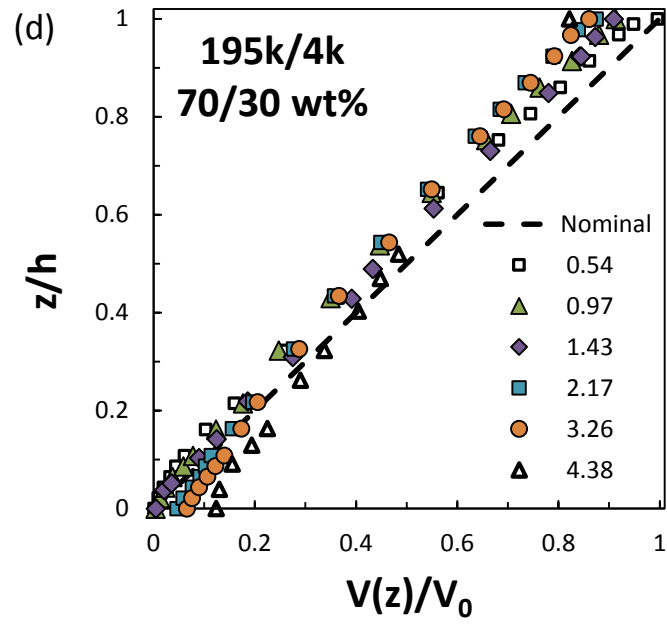
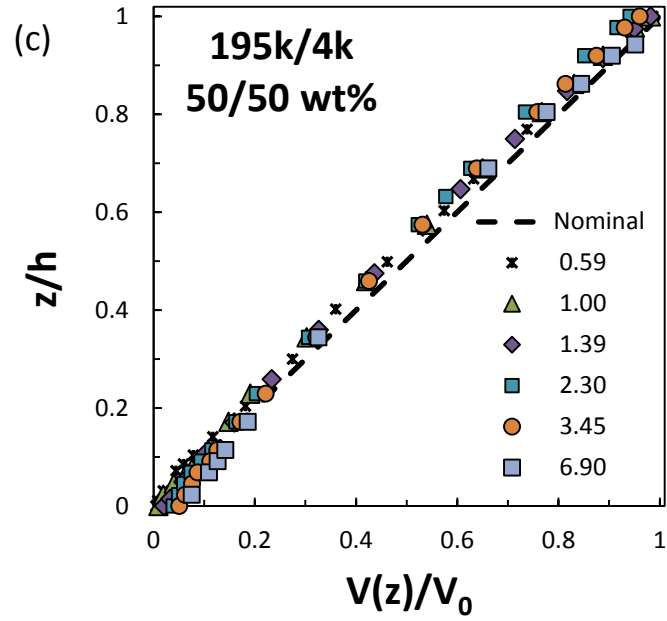


Figure A.1. Schematic of Couette flow shear cell used for slip velocity measurements [16].

### A.2. Velocity profiles of PBD mixtures at different shear rates

In the following, we present normalized velocity profiles of binary and ternary mixtures of PBD(4k), PBD(88k) and PBD(195k). For each sample, velocity profile measurements were carried out at different shear rates ( $\dot{\gamma}_n = V_0/h$ ) as labeled.





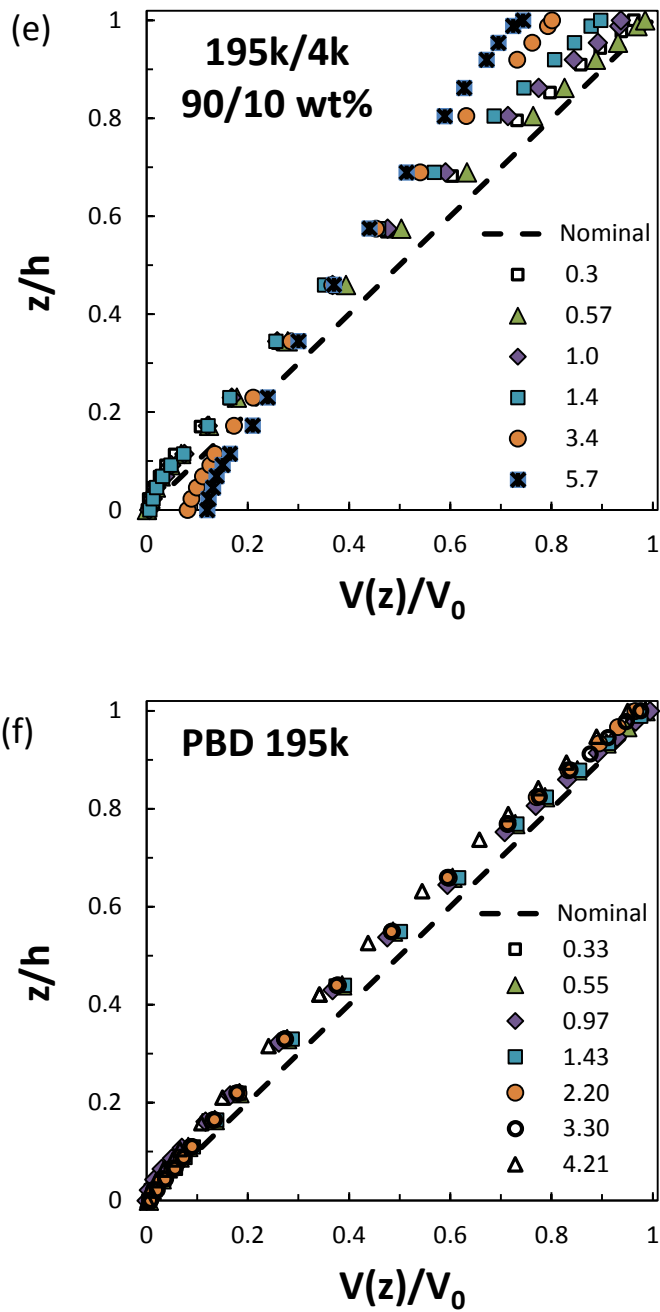
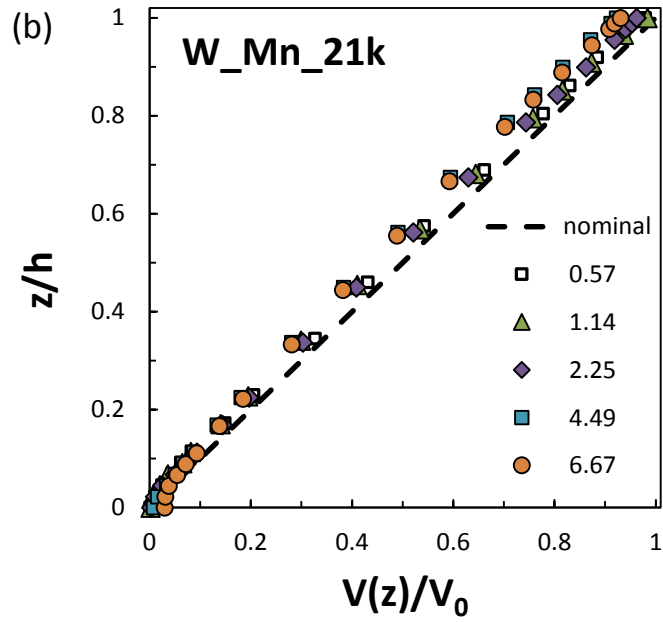
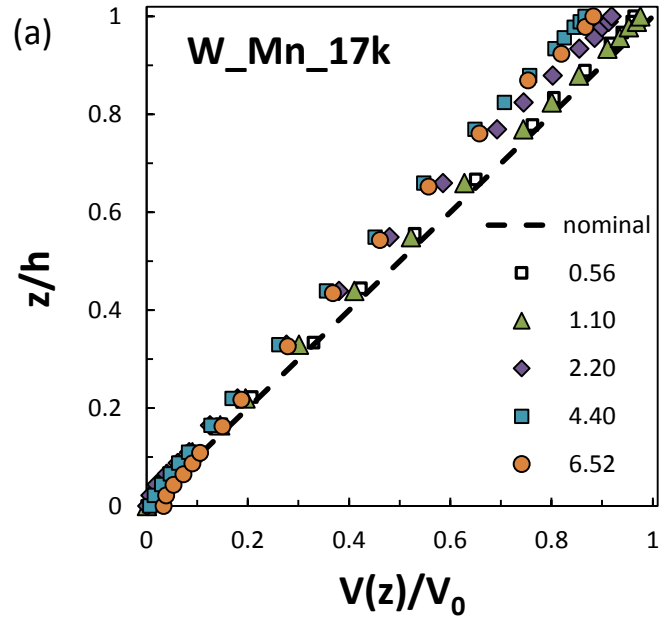


Figure A.2. Normalized velocity profiles of PBD 4k, PBD 195k and their binary mixtures: (a)-(f). For each sample, velocity profile measurements were carried out at different shear rates ( $\dot{\gamma}_n = V_0/h$ ) as labeled. Shear rate unit is ( $s^{-1}$ ). The dashed line in all graphs represents the nominal velocity profile according to the theory for simple shear.



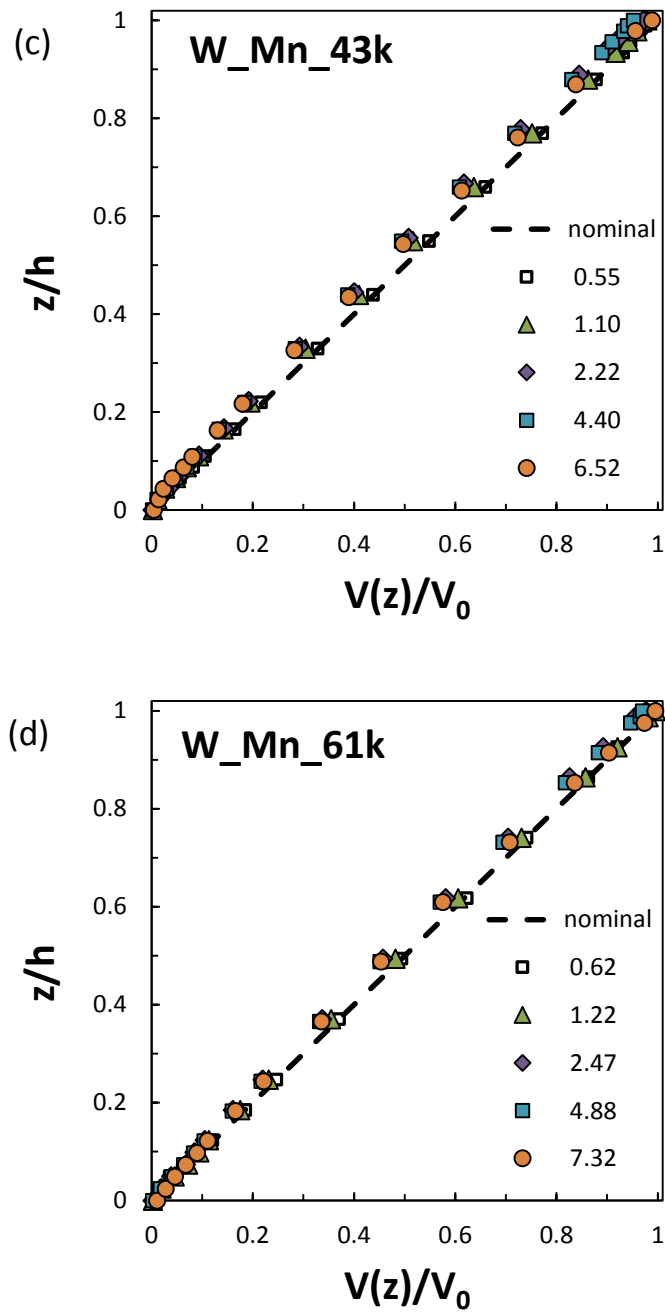
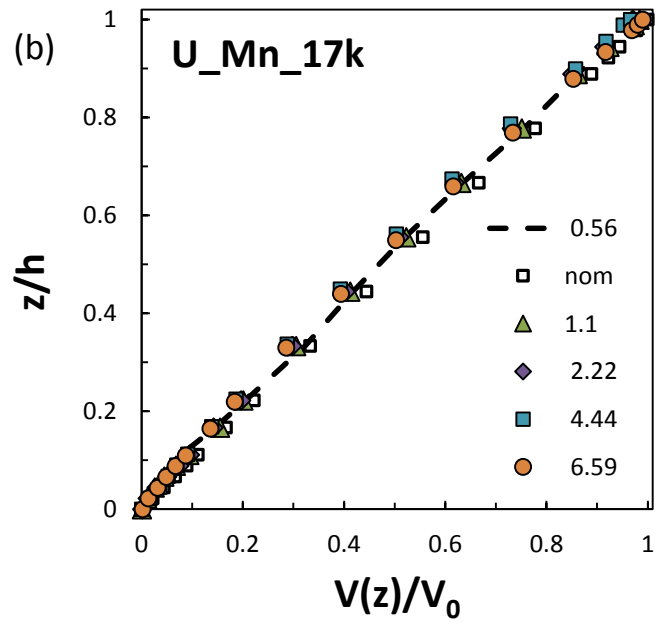
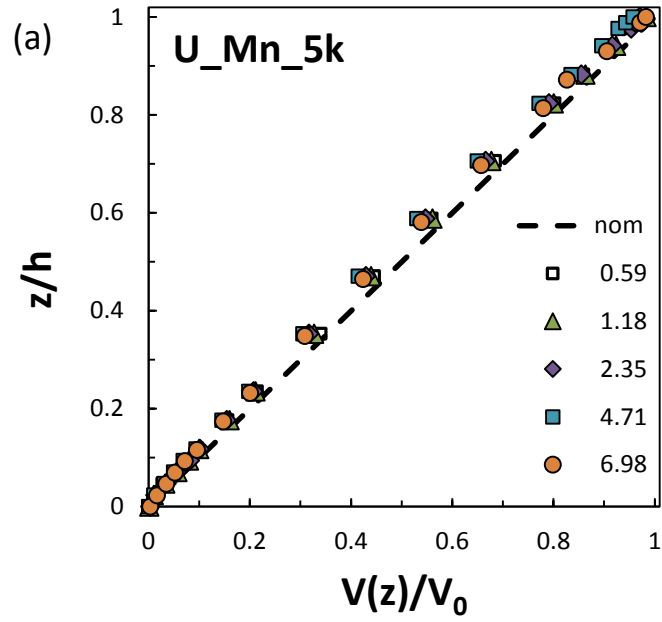


Figure A.3. Normalized velocity profiles of ternary mixtures with a fixed  $M_w = 143.5$  kg/mol and varying  $M_n$  (set W in Chapter 4) containing PBD 4k, 88k and 195k: (a)  $M_n = 17$  kg/mol, b)  $M_n = 21$  kg/mol, (c)  $M_n = 43$  kg/mol, (d)  $M_n = 61$  kg/mol. For each sample, velocity profile measurements were carried out at different shear rates ( $\dot{\gamma}_n = V_0/h$ ) as

labeled. Shear rate unit is ( $s^{-1}$ ). The dashed line in all graphs represents the nominal velocity profile according to the theory for simple shear.



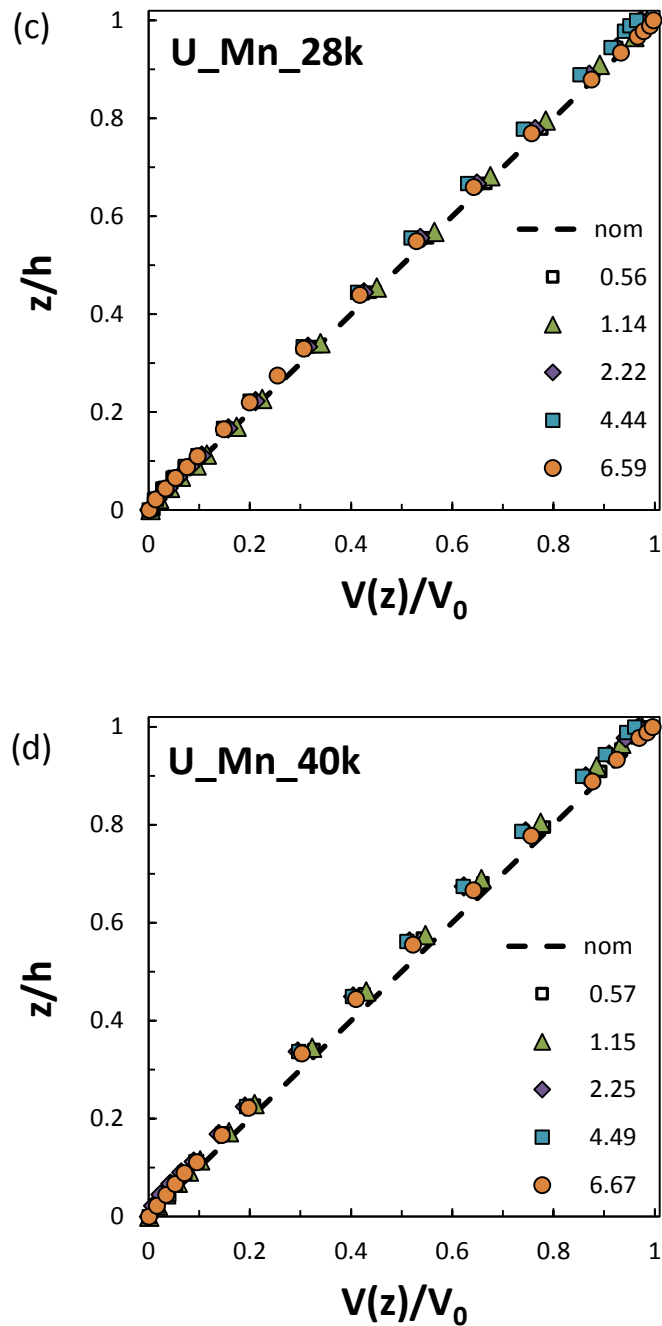


Figure A.4. Normalized velocity profiles of ternary mixtures with fixed  $M_w = 143.5$  kg/mol and varying  $M_n$  (set U in Chapter 4) containing PBD 1k, 88k and 195k: (a)  $M_n = 5$  kg/mol, (b)  $M_n = 17$  kg/mol, (c)  $M_n = 28$  kg/mol, (d)  $M_n = 40$  kg/mol. For each sample, velocity profile measurements were carried out at different shear rates ( $\dot{\gamma}_n = V_0/h$ ) as labeled.

Shear rate unit is ( $s^{-1}$ ). The dashed line in all graphs represents the nominal velocity profile according to the theory for simple shear.

## **Appendix B**

Appendix B presents additional information and data for Chapter 5 in the study of the molecular weight distribution of the bulk and debris samples in the sliding plate rheometer.

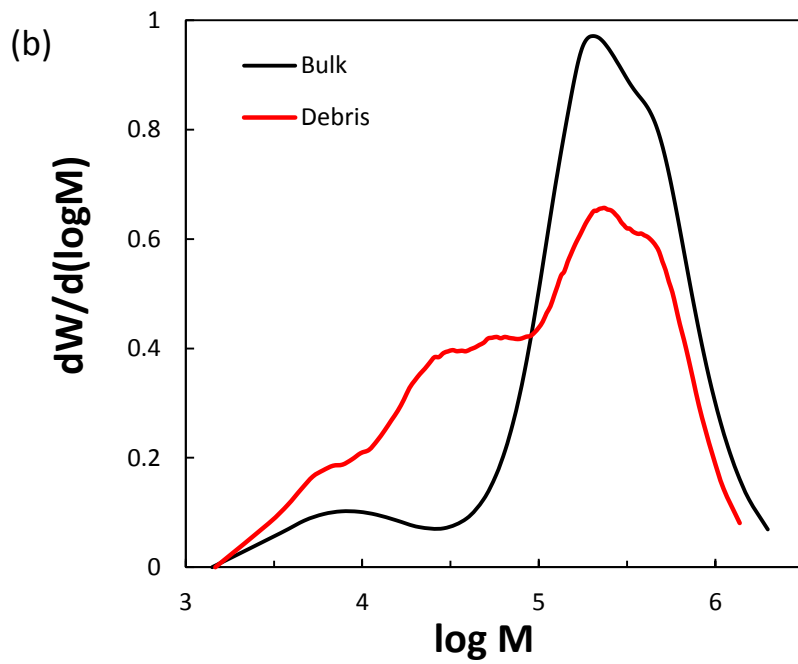
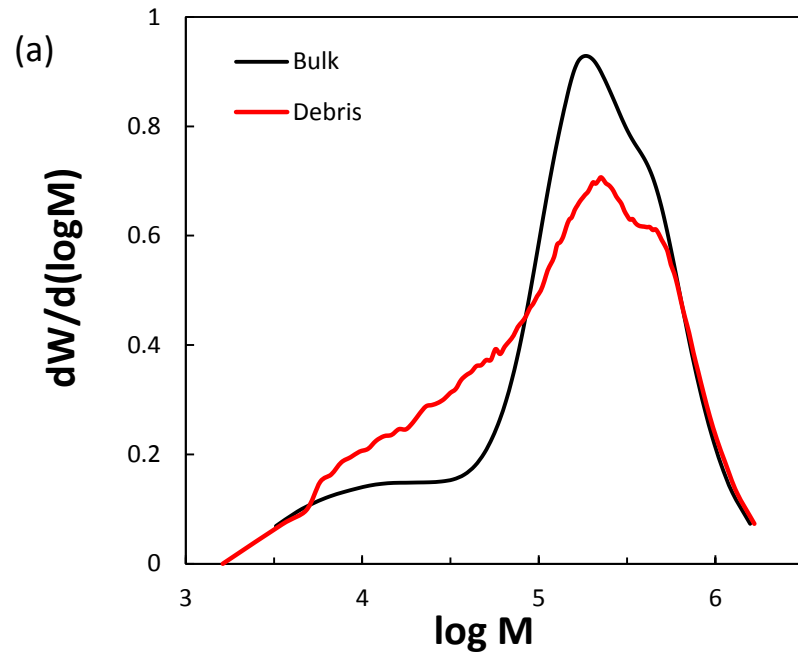
### **B.1. Debris collection**

In our sliding plate rheometer using PBD on stainless steel plates (mirror polished) at small gaps ( $\sim 1$  mm), a hazy debris remains on the substrate (steel) after the sample undergoes shear at shear rates above the critical shear rate for the onset of the strong slip. We collected the debris after each experiment using tetrahydrofuran (THF). This was done with small drops of THF on the debris using a glass pipette (1 ml) and plastic bulb to place and retrieve the THF. The debris collection is a repetitive procedure involving 3 steps: i) by compressing the bulb, a drop of THF is placed on the debris to wet an area of the size of a dime, ii) 2 to 3 seconds is given to the solvent to dissolve the polymer, and iii) the solution is sucked back into the glass pipette by decompressing the bulb. This is repeated 3 times on the same area. The same procedure is done all over the central portion of the debris to collect enough polymer for the GPC measurements.

### **B.2. Additional examples of the molecular weight distribution (MWD) of the debris versus bulk samples for bimodal mixtures of PBD(19k) and PBD(277k)**

In addition to the PBD samples used in Chapter 5, we also examined two polydisperse PBD samples i) PBD(19k) with  $M_w = 19$  kg/mol and  $PI = 2.82$  and PBD(277k) with  $M_w = 277$  kg/mol and  $PI = 2.22$  (purchased from Sigma Aldrich). For bimodal mixtures of PBD(19k) and PBD(277k), the GPC results revealed that some of the samples have undergone strong slip by surface rupture of the polymer as seen in the distribution of polymer chains of the debris samples. These results come in the following:

B.2.1. PBD samples undergoing strong slip by surface rupture



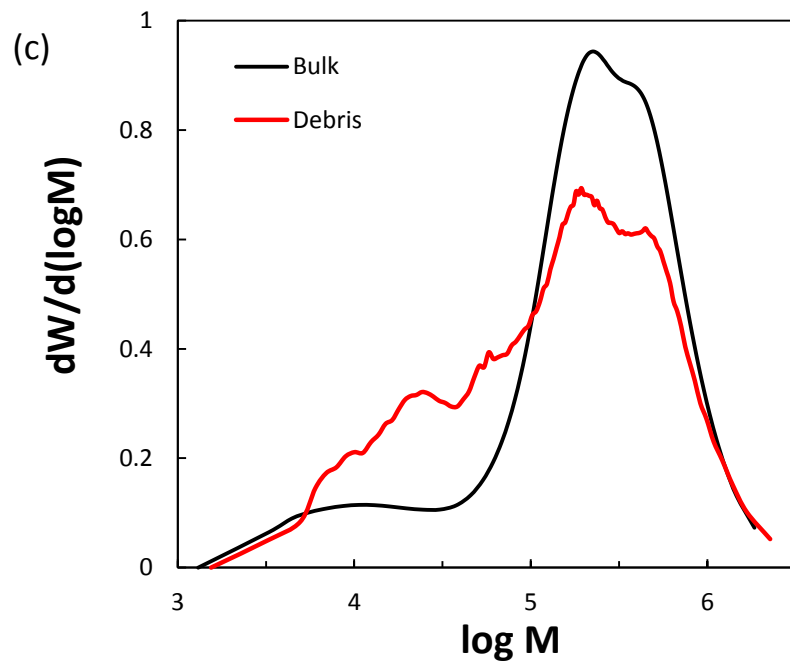
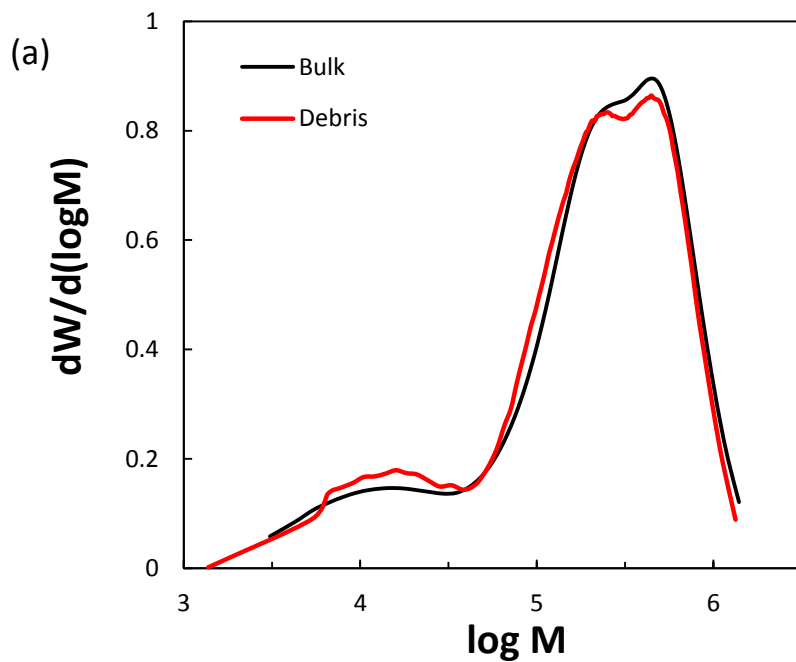


Figure B.1. MWD of bulk versus debris samples for 3 bimodal mixtures of PBD(19k) and PBD(277k): (a)-(c).

### B.2.2. PBD samples undergoing strong slip by the disentanglement mechanism



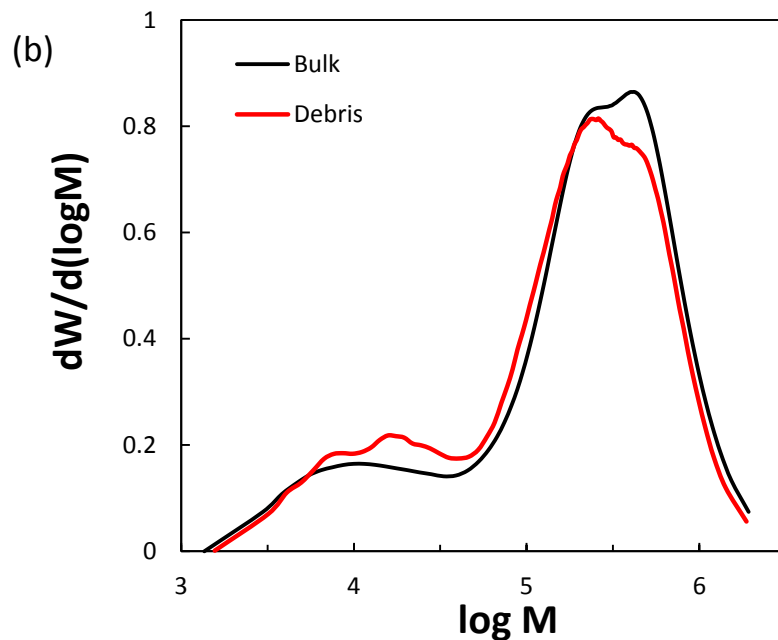


Figure B.2. MWD of bulk versus debris samples for 2 bimodal mixtures of PBD(19k) and PBD(277k): (a) and (b).

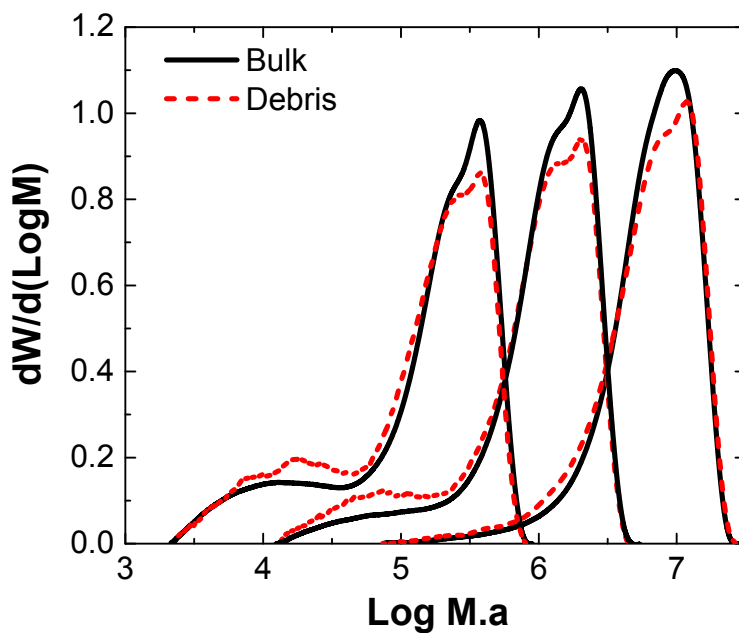


Figure B.3. MWD of bulk and debris samples of pure PBD(277k) and its mixtures with 10 and 20 wt% of PBD(19k). In this graph, results of pure PBD(277k) and PBD(277k)-PBD(19k)/(90-10 wt%) are shifted by  $\text{Log } a = 1.5$ , and  $0.75$ , respectively.

## Appendix C

Appendix C includes additional information for the dewetting experiments in Chapters 6 and 7.

### C.1. Fitting models for calculation of $b$

The fitting procedure for calculation of  $b$  is well documented in Refs [25, 127]. In our dewetting experiments in Chapter 7, we used fitting models of oscillatory or monotonic decay as shown in Table C.1.

The following applies to the data in Table C.1:

- i) Data highlighted in yellow were analyzed with the oscillatory rim profile fitting model.
- ii) Data highlighted in orange could be analyzed with both oscillatory and monotonic fitting models. I used results from oscillatory model since it gives a better fit.
- iii) The rest of the samples were analyzed with the monotonic fitting model using only one decay length.

Table C.1. List of dewetting experiments used in Chapter 7. Highlights show different fitting models used for each sample.

Sample set	Sym.	$T_d(^{\circ}\text{C})$	$\phi_{5k}$	$\phi_{28k}$	$\phi_{53k}$	$\phi_{86k}$	$\phi_{136k}$	$\phi_{490k}$	$M_n$	$M_w$
Set#1: monodisperse PSs	PS(5k)	110	1	-	-	-	-	-	4.7	5.4
	PS(28k)	120	-	1	-	-	-	-	27	28.4
	PS(53k)	140	-	-	1	-	-	-	51	53.3
	PS(86k)	140	-	-	-	1	-	-	85.5	86.4
	PS(136k)	140	-	-	-	-	1	-	130	135.8
	PS(490k)	150	-	-	-	-	-	1	465	490
Set#2: $M_n$ xx $M_w \cong 318 \pm 2$ kg/mol and varying $M_n$	$M_n$ _20k	130/140/150	0.22	-	-	-	0.19	0.59	20	316
	$M_n$ _86k	130/140/150	-	0.25	-	-	0.14	0.60	86	320
	$M_n$ _206k	130/140/150	-	-	-	-	0.49	0.51	206	316
Set#3: PS(LMW)- PS(490k) $\phi_{PS(490k)} = 0.90$	PS(5k)-PS(490k)/10-90	150	0.10	-	-	-	-	0.90	43	442
	PS(28k)-PS(490k)/10-90	150	-	0.10	-	-	-	0.90	177	444
	PS(53k)-PS(490k)/10-90	150	-	-	0.10	-	-	0.90	257	446
	PS(86k)-PS(490k)/10-90	150	-	-	-	0.10	-	0.90	322	450
	PS(136k)-PS(490k)/10-90	150	-	-	-	-	0.10	0.90	370	455
Set#4: PS(28k)-PS(490k)	PS(28k)-PS(490k)/70-30	130	-	0.70	-	-	-	0.30	38	167
	PS(28k)-PS(490k)/50-50	130	-	0.50	-	-	-	0.50	51	259
	PS(28k)-PS(490k)/30-70	140	-	0.30	-	-	-	0.70	79	352
	PS(28k)-PS(490k)/10-90	150	-	0.10	-	-	-	0.90	177	444
Set#5: PS(86k)-PS(490k)	PS(86k)-PS(490k)/70-30	140	-	-	-	0.70	-	0.30	113	208
	PS(86k)-PS(490k)/50-50	140	-	-	-	0.50	-	0.50	144	288
	PS(86k)-PS(490k)/30-70	140	-	-	-	0.30	-	0.70	199	369
	PS(86k)-PS(490k)/10-90	150	-	-	-	0.10	-	0.90	322	450

## C.2. Additional evidence of discrepancies between the air and buried interfaces for high molecular weight polymers

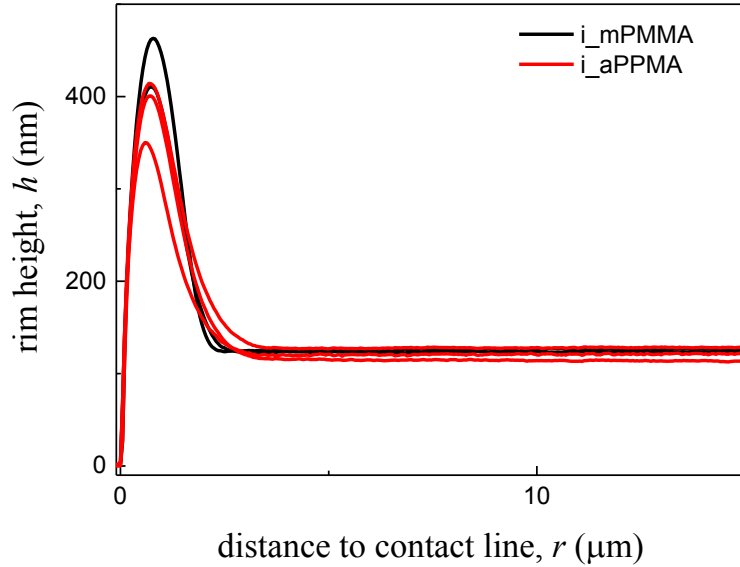


Figure C.1. Rim profiles of dewetting holes for thin films of PMMA ( $M = 173$  kg/mol) on DTS for  $6\ \mu\text{m}$ -diameter holes. The dewetting temperature is  $190\ ^\circ\text{C}$ . Before dewetting, all samples were annealed on mica at  $150\ ^\circ\text{C}$  for 2 h.

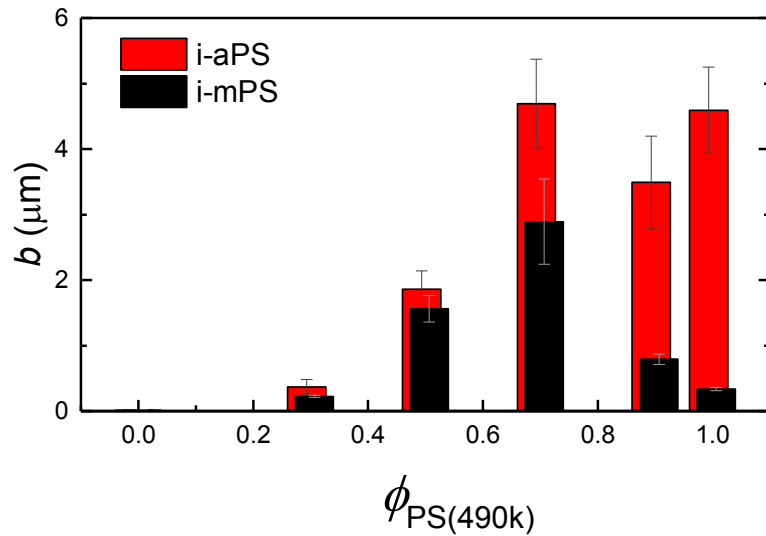


Figure C.2. Slip length as a function of the content of long chains for binary mixtures of PS 28k-490k on AF 2400. Thin films are pre-annealed on mica and dewetting was done using air (i-aPS) and buried (i\_mPS) interfaces as explained in Chapter 6.

### C.3. Rim profiles of ternary PS mixtures examined in Chapter 7

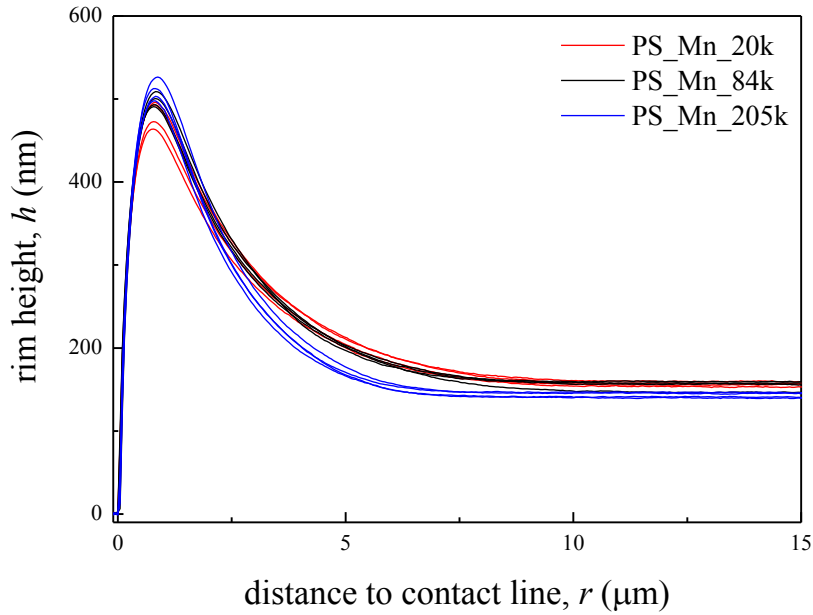


Figure C.3. Rim profiles of dewetting holes for thin films of PS mixtures with a fixed  $M_w = 315$  kg/mol and varying  $M_n$  (as labeled) on AF 2400.

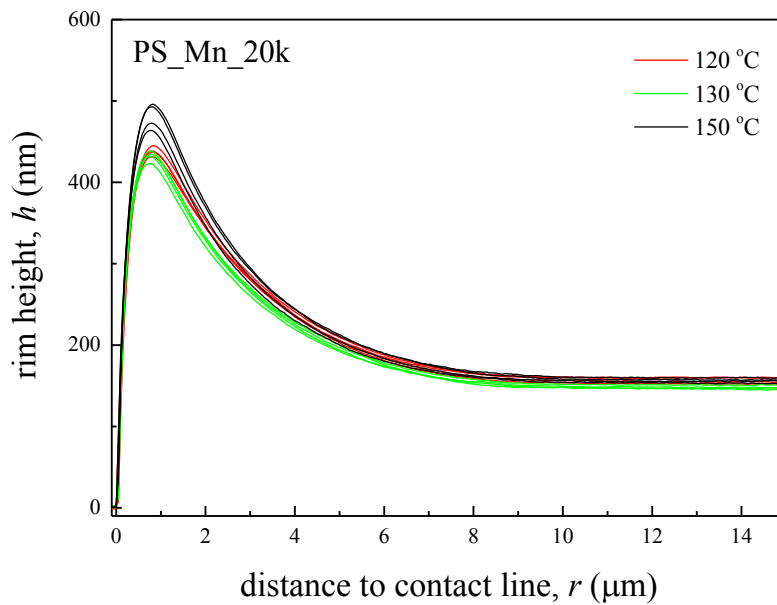


Figure C.4. Rim profiles of dewetting holes for thin films of a PS mixture with  $M_w = 315$  kg/mol and  $M_n = 20$  kg/mol on AF 2400 at three different dewetting temperatures.